Faculty of Science and Engineering

WASM: Minerals, Energy and Chemical Engineering

Investigate the influence of the hydrodynamics on the photobioreactor performance: Effect of configuration and gas distributor

Ahmed Abdul Aziz Ibrahim Arkoazi

This thesis is presented for the degree of
Doctor of Philosophy
of
Curtin University

June 2020

Declaration

To the best of my knowledge and belief this thesis contains no material previously published by any other person except where due acknowledgment has been made. This thesis contains no material which has been accepted for the award of any other degree or diploma in any university.

Name*: Ahmed Abdul Aziz Arkoazi*

Signature*:*

Date*: 02/06/2020*

Acknowledgements

Dedication

To God, Allah

To my Mother

To my wife, Fatimah
and our kids, Abody and Jilan

Abstract

Microalgae are rapidly cultivable photosynthetic microorganisms that have received considerable interest in many industrial applications such as wastewater treatments and biofuel production. Algal cells can grow in open systems (raceway ponds) or in closed systems (bubble columns, airlifts, and flat plates). However, the cultivation of microalgae in closed systems faces many challenges such as the high cost of production, photobioreactor design, and scale-up. The main challenge in the design and scale-up of photobioreactors is light availability and its distribution inside the reactor. It has been reported that mixing performance and hydrodynamics can greatly improve light intensity distribution inside the photobioreactor which leads to enhanced productivity of biomass. The mixing and hydrodynamics of photobioreactors are greatly impacted by the type of gas sparger, photobioreactor geometry, and operating conditions.

The performance of photobioreactors is strongly affected by hydrodynamics (sparger type), light intensity and its distribution, gas-liquid mass transfer, and bioreactor configuration. The type and number of orifices in the gas distributor greatly impact the mixing during the liquid phase due to their significant impact on the gas holdup, bubble velocity, and bubble size distribution. In addition, the interaction between photobioreactor hydrodynamics and microalgae cultivation has not been fully investigated.

Therefore, the overall objectives of this study were to understand the role of gas sparger type in algal photobioreactors and thus their performance in terms of CO_2 biofixation, biomass productivity, nutrients (TN and TP) removal, and lipid formation. A further objective was to develop a fundamental modelling approach for evaluating photobioreactor performance.

To investigate the impact of hydrodynamics on the bubble column and airlift reactor in a two-phase system (air-water), an optical fibre probe technique was used to study the effect of sparger design on local and overall gas holdup, and the properties of bubble dynamics such as bubble passage frequency, chord length distribution, and interfacial area in an air-water system in a bubble column photobioreactor. Experiments were conducted to investigate the effect of gas sparger type on the hydrodynamics of the bubble column (10 cm in diameter and 100 cm in height) at superficial gas velocities of 0.48, 0.96, 1.44, 2.4, and 4.8 cm s^{-1}. Three sparger types were used: perforated plate sparger, cross sparger, and ring sparger. The radial and axial profiles of these parameters were measured at r/R: 0, $\pm$ 0.575, and $\pm$ 0.787, while *H/D* were 2, 3, and 5, respectively. It was observed that gas holdup (ε_G), interfacial area (*a*), and chord

length (l_c) are linearly related to superficial gas velocity (U_g). The perforated plate sparger was the preferred type to produce the highest gas holdup and interfacial area, as well as a broad distribution of mean chord length at all ranges of gas velocity (0.48 – 4.8 cm s^{-1}).

To expand the study, the way in which the hydrodynamics and sparger type influence the performance of photobioreactors in a real system were investigated. In this study, the effect of sparger geometry (perforated plate sparger, cross sparger, and ring sparger) on the hydrodynamics (gas holdup, and mass transfer coefficient), CO_2 biofixation, and light intensity distribution inside a bubble column photobioreactor using *Chlorella vulgaris* were investigated. When comparisons were made, the results indicated that the perforated plate sparger was the most effective geometry for CO_2 biofixation and biomass production. The rates of CO_2 fixation at 200 µmol m^{-2} s^{-1} light intensity for the three geometries of gas sparger were 0.51, 0.314, and 0.264 g L^{-1} d^{-1} respectively. In addition, CO_2 removal efficiency was 70.1% for the perforated plate sparger, 57.2% for the cross sparger and 50.1% for the ring sparger.

For a better understanding of the interaction of gas-liquid inside a photobioreactor and the influence of gas sparger type on its hydrodynamics, which could make wastewater treatment using microalgae economically viable, additional investigations were undertaken. *Chlorella vulgaris* was cultivated in primary wastewater using a draft tube airlift photobioreactor to study the influence of gas sparger on the hydrodynamics (gas holdup, bubble arrival frequency, and mass transfer coefficient) at different superficial velocities (0. 24, 0. 48, 0. 96, 1.44, and 1.92 cm s^{-1}) and the capability of microalgae to remove nutrients. Over a 10-day cultivation period, the highest cell density of 61.5×10^6 was attained using the perforated plate sparger. Also, total nitrogen (TN), total phosphorus (TP), and chemical oxygen demand (COD) removal efficiency were 84%, 99.4%, and 85.25%, respectively. As a comparison, the perforated plate sparger showed the best results for hydrodynamics, microalgae growth, and nutrient removal compared to the other two types. In addition, for better simulating the microalgae cultivation in photobioreactors, it is crucial to apply an accurate kinetic model that considers the influence of light intensity and bubble dynamics. A model was proposed based on the Monod model to describe algae growth in an airlift photobioreactor. Biomass concentration in the photobioreactor was calculated by solving mass balance equations. The model was validated with experimental data from cultivation of *Chlorella vulgaris* in a batch mode. The influence of four limiting factors (total nitrogen TN 30.6 mgL^{-1}, total phosphorous TP = 6.6 mgL^{-1}, CO_2 concentration 2%, and light intensity $I = 200$ µmol m^{-2} s^{-1}) on algae growth were also examined.

There were no significant differences between model simulation and experimental data for biomass concentration, nutrients (TN and TP) uptake, and light distribution profile. Therefore, the proposed kinetic model could be a useful tool for optimization, and scale-up, in addition to predicting *Chlorella vulgaris* growth and nutrient (P and N) uptake.

Lastly, based on the above results, *Chlorella vulgaris* was cultivated in a draft airlift photobioreactor using a perforated plate sparger to study the synergistic effects and to optimize the most effective parameters (gas flow rate, CO_2 concentration, and light intensity) on CO_2 biofixation rate and total nitrogen (TN and TP) removal efficiencies. Microalgae were cultivated under different conditions of gas flow rate (1-8 L min^{-1}), CO_2 concentration (0.03-7%), and light intensity (150-400 µmol m^{-2} s^{-1}) using primary wastewater as a medium. The response Surface Methodology and Box-Behnken (experimental) Design was used to find optimum values of gas flow rate, CO_2 concentration, and light intensity that have significant effects on CO_2 biofixation rate, and TN and total TP removal efficiencies. The optimum values of the three independent variables (gas flow rate, CO_2 concentration, and light intensity) and desirability were 7.5 L min^{-1}, 3.5%, 400 µmol m^{-2} s^{-1}, and 0.904, respectively. The maximum biomass produced, CO_2 biofixation rate, total nitrogen, and total phosphorus removal efficiencies at optimum conditions were 5.7 g L^{-1}, 1.23 g L^{-1}d^{-1}, 83.9% and 100%, respectively. The synergistic impact between gas flow rate and CO_2 concentration, and between gas flow rate and light intensity was considerable for all three responses, while the influence between CO_2 concentration and light intensity was less considerable on CO_2 biofixation rate. The results of this study could be very useful when using microalgae for CO_2 biofixation and nutrient removal from wastewater treatment.

Publications

Journal Papers

- Arkoazi, A., Znad, H., & Utikar, R. (2019). Synergistic Impacts and Optimization of Gas Flow Rate, Concentration of CO2, and Light Intensity on CO2 Biofixation in Wastewater Medium by Chlorella vulgaris. *International Journal of Biotechnology and Bioengineering*, *13*(10), 260-266.

- Arkoazi, A., & Znad, H., Influence of Gas Sparger Type on the Hydrodynamics of Bubble Column in Bubbly Flow. Submitted to Chemical Engineering science Journal in 2020.

- Arkoazi, A., & Znad, H., Influence of gas sparger geometry on Carbon Dioxide (CO_2) biofixation by *Chlorella vulgaris* and light intensity distribution inside photo-bioreactor Submitted to Biomass and Bioenergy Journal in 2019.

- Arkoazi, A., & Znad, H., Influence of gas sparger on *Chlorella vulgaris* performance for nutrients removal from wastewater in a draft tube airlift photobioreactor and kinetic modelling and simulation. Submitted to Bioresource Technology Journal in 2020.

International Conference papers

- Arkoazi, A., Znad, H., & Utikar, R, Influence of the gas sparger geometry on the microalgae (*Chlorella v.*) performance in a bubble column photo-bioreactor. *IWAlgae2019- 1st - 2nd July 2019 Valladolid (Spain).*

- Arkoazi, A., Znad, H., & Utikar, R. (2019). Synergistic Impacts and Optimization of Gas Flow Rate, Concentration of CO2, and Light Intensity on CO2 Biofixation in Wastewater Medium by Chlorella vulgaris. IVBB: International Conference on Biotechnology and Bioengineering. Paris, France, October 29-30 2019.

Table of Contents

Contents

List of Figures

List of Tables

List of Symbols and Abbreviations

Symbol	*Description and Units*
PIV	particle image velocimetry
COD	chemical oxygen demand
$NADPH_2$	nicotinamide adenine dinucleotide hydrogen phosphate
ATP	adenosine triphosphate
U_G	superficial gas velocity (cm s^{-1})
I	local light intensity (μmol m^{-2} s^{-1})
Io	incident light intensity (μmol m^{-2} s^{-1})
β	extinction coefficient (m^{-1})
z	light path (m)
a	interfacial area (m^{-1})
ε_g	gas holdup
d_b	bubble diameter (m)
K_a	light absorption coefficient of microalgae (m^{-1})
μ	growth rate (day $^{-1}$)
El	activation energy (J mole^{-1})
R	gas constant (L atm mol^{-1} K^{-1})
T	temperature (°K)
μ_{max}	maximum growth rate (day $^{-1}$)
S	concentration of limiting substrate (g L^{-1})
K_S	half-saturation constant (g L^{-1})
d_o	sparger orifice diameter (mm)
TN	total nitrogen
TP	total phosphorous
A_d	downcomer area (m^2)
A_r	riser area (m^2)
υ_B	bubble rise velocity (m s^{-1})
L_S	probe sensing length (mm)
t_R	signal rise time (s)
C_B	bubble chord length (mm)

$K_L a_L$	overall mass transfer coefficient (m s^{-1})
$k_G a_L$	volumetric mass transfer coefficient of gas phase (m s^{-1})
$k_L a_L$	volumetric mass transfer coefficient of liquid phase (m s^{-1})
H	Henry's constant (mol m^{-3} Pa $^{-1}$)
D_{O_2}	diffusivity of oxygen (m^2 s^{-1})
D_{CO_2}	diffusivity of carbon dioxide (m^2 s^{-1})
DO	dissolved oxygen
C^*	DO concentration at saturation condition (kg m^{-3})
C_o	initial DO concentration (kg m^{-3})
t_o	initial time (s)
Tm	mixing time (s)
OD	Optical density
X	Biomass concentration (g L^{-1})
X_o	Initial biomass concentration (g L^{-1})
X_t	final biomass concentration (g L^{-1})
t	cultivation time (day)
P	biomass productivity (g L^{-1} day^{-1})
MW_{CO_2}	molecular weight of carbon dioxide
MW_c	molecular weight of carbon
BBD	Box-Behnken Design
DDF	Derringer's desired function
Rc	input rate of CO_2 from the air in bubbles
Cs	liquid-phase concentration of CO_2 in equilibrium with air in bubble (mg L^{-1})
S_C	concentration of inorganic carbon (mg L^{-1})
V	the reactor volume (L)
H	Henry's law constant

Chapter One
Introduction

1.1   Background and Motivation

Bubble column reactors are broadly used in many gas/liquid or gas/liquid/solid processes, such as hydrogenation, oxidation, aerobic fermentation, chlorination, coal liquefaction, and wastewater treatment [1-5]. Bubble column reactors are more favourable than other multiphase reactors (packed towers, trickle bed reactors, stirred vessels, etc.) due to their simple construction, low maintenance, high heat transfer rate, easy temperature control, and good mass transfer rates at low input energy. In addition, studying the bubble properties such as gas holdup (ε_G), gas-liquid interfacial area (a), and bubble size (l_c) is essential for appropriate design and operation of bubble column reactors.

Microalgae are unicellular organisms that convert light energy, CO_2, and nutrients (nitrates and phosphates) into organic substances (sugar, lipids, protein, and etc.…) through a photosynthesis process. They consume minimal amounts of nutrients and higher amounts of CO_2 compared to terrestrial plants. CO_2 concentration increases in the atmosphere as a result of higher consumption of fossil fuels, which is an essential cause of global warming [6]. Therefore, microalgae are important for biofuel production as a biofuel third generation and fixation of atmospheric CO_2. In addition, they diminish water pollution problems through their capability of uptake of nitrates and phosphates in wastewater.

Several techniques have been used for CO_2 sequestration such as chemical, physical, and biological techniques. The most effective and productive method for utilization and fixation of CO_2 is a biological technique through microalgae cultivation and terrestrial plants [7]; however, microalgae are more efficient due to biomass production and faster growth, and their CO_2 fixation efficiency is 50 times better than terrestrial plants [8]. Microalgae biomass comprises around 50% carbon which is derived from CO_2. For example, Razzak et al. [9] stated that microalgae biomass of 1 kg fixes approximately 1.83 kg of CO_2.

Microalgae cells have the ability to grow in different types of wastewater such as municipal, industrial, and petroleum wastewater. Therefore, they are a significant bioremediation agent through their capability to absorb most forms of nitrogen [9], assimilate and store phosphorous [10], and remove heavy metals. The utilization of microalgae has attracted great attention in recent years due to their strength in removing CO_2 and other compounds during their growth. Thus, an incorporation of CO_2 sequestration, wastewater treatment, and biofuel production is a promising process to mitigate CO_2 and alternative source for energy.

Open systems, such as lakes and natural ponds, and closed system such as bubble columns, flat plate reactors, airlift reactors, and stirred tank reactors, are the major design systems for microalgae cultivation [11]. The selection of cultivation system relies on different parameters like availability of light energy, nutrients, and optimal gas-liquid mass transfer rate. The main advantages of closed systems over open systems include limited space, efficient gas-liquid mass transfer, and minimum contamination risk [12]. Algal growth is strongly affected by environmental factors, such as light, pH, CO_2 concentration, and nutrient availability, and operational factors such as reactor geometry, mixing rate, and intensity of light inside the reactor [13].

Light is one of the most effective parameters that influences microalgae growth. Sufficient light intensity is very important to keep the culture healthy. Excess or limited light leads to photo-inhibition or photo-limitation. Therefore, appropriate light intensity distribution through the culture is required to prevent mutual shading especially in dense culture and to aid the cells to receive adequate light for their growth. These obstacles can be overcome by efficient mixing that facilitates suitable cell movement between dark and light zones.

Flow hydrodynamics, such as gas holdup, gas-liquid interfacial area, and bubble size, and mass transfer coefficient are crucial factors that impact the mixing, productivity and efficiency of the photosynthesis process [14]. Low rate of mixing will cause cells to settle inside the reactor and decrease the gas-liquid mass transfer [15] while maximum stress of hydrodynamics on algal cells leads to cell wall rupturing. Merchuk and Mukmenev [16], reported that microalgae growth was enhanced by increasing turbulence as a result of improved supply of light and CO_2 and the growth decreased sharply with increased superficial gas velocity above an optimum level as a result of cell damage. Consequently, better understanding of hydrodynamics and its effects are important for optimization of biomass production and photobioreactor scale-up.

The type and configuration of gas sparger have a significant influence on the hydrodynamics of the reactor. The sparger plays an essential role in enhancing photobioreactor performance since it is responsible for the mixing in pneumatic photobioreactors. Proper mixing improves the distribution of light and nutrients inside photobioreactors. Li et al. [17] reported that a gas sparger has a considerable impact on gas-liquid mass transfer rate by directly influencing bubble size in the photobioreactor. In addition, a gas sparger enhances the photobioreactor performance through improving both mass transfer rate and mixing [18, 19]. Generally, the gas sparger plays an essential role in the hydrodynamics parameters of a photobioreactor [20, 21].

Both intrusive techniques, such as conductivity and optical probes, and non-intrusive techniques, such as particle image velocimetry (PIV), visualization techniques, and X-ray tomography, are used for bubble hydrodynamics measurement. The disadvantages of non-intrusive techniques are that they cannot be used in dense culture and in high pressure and high temperature operating conditions. For intrusive techniques, an optical probe is more favourable due to higher sensitivity and less signal to noise ratio compared with a conductivity probe [22]. The performance of a photobioreactor is strongly influenced by the efficiency of the gas sparging system. Therefore, the effectiveness of a sparging system must be properly investigated to overcome limitation of light, poor mixing, and distribution of nutrients inside the photobioreactor. In order to enhance the performance of the photobioreactor, the current study focused on the effect of sparger geometry on hydrodynamics and light intensity distribution in a two-phase system, using a standard medium and a real system that used wastewater.

1.2 Research objectives

The main objective of this thesis was to understand how photobioreactor design (configuration, gas distributor) can impact the overall performance of the photobioreactor. Specifically, the objectives were to:

- Investigate the influence of different types of gas sparger, such as perforated plate sparger, cross sparger, and ring sparger, and different photobioreactor configurations, bubble column and airlift, on hydrodynamics and light intensity distribution inside the photobioreactor,

- Understand the relationship between hydrodynamics and light intensity and how this relationship impacts photobioreactor performance and productivity,

- Employ the most promising gas sparger and photobioreactor for wastewater treatment, CO_2 bio-fixation, and lipid formation, and

- Propose and suggest a kinetic model that links hydrodynamics, light intensity, and photobioreactor configuration with its productivity.

1.3 Significance

- A gas sparger is essential for bubble column photobioreactors as it has a significant impact on their hydrodynamics which leads to enhanced photobioreactor performance (specific growth rate, productivity, lipid content…. etc). However, the selection of the best type of gas sparger is lacking in the literature.

- Previous studies investigated the influence of gas sparger on bioreactor hydrodynamics in a two-phase system. To the best of our knowledge, no study has investigated the impact of gas sparger on the performance of photobioreactors using a real system, and further, of the available studies investigated, the effect of gas sparger in wastewater treatment process.

- Another innovative component of this study was developing a model that relates the biomass concentration to light intensity and its distribution with bubble dynamics for analysis and optimization purposes.

1.4 Structure of the thesis

This thesis consists of eight chapters as explained below and also demonstrated in Figure 1.1:

- **Chapter One** presents the motivation, research objectives, significance, and the structure of the thesis.

- **Chapter Two** relates the relevant literature to this work.

- **Chapter Three** describes the methodology applied, including a detailed description of the preparation of samples, the experimental setup and the analytical methods involved.

- **Chapter Four** reports the results obtained from investigating the influence of sparger type on local and overall gas holdup, gas-liquid interfacial area, bubble arrival frequency, and bubble chord length distribution in bubble columns for a two-phase system.

- **Chapter Five** reports the impact of different spargers in a bubble column using a standard culture medium on microalgae growth, CO_2 biofixation rate, CO_2 removal efficiency, mixing time, overall volumetric gas-liquid mass transfer coefficient, overall gas holdup, and light intensity distribution inside the photobioreactor.

- **Chapter Six** reports the influence of different spargers in a draft-tube airlift column using wastewater as a culture medium on microalgae growth, mixing time, nutrient removal (total nitrogen, total phosphorous, and COD), overall volumetric gas-liquid mass transfer coefficient, and overall gas holdup. In addition, a kinetic model based on Monod model was

proposed, which considered the influence of light intensities, bubbles dynamics on the microalgae growth and nutrient removal, under various cultivation conditions of light intensity and CO_2 gas concentration in a batch system.
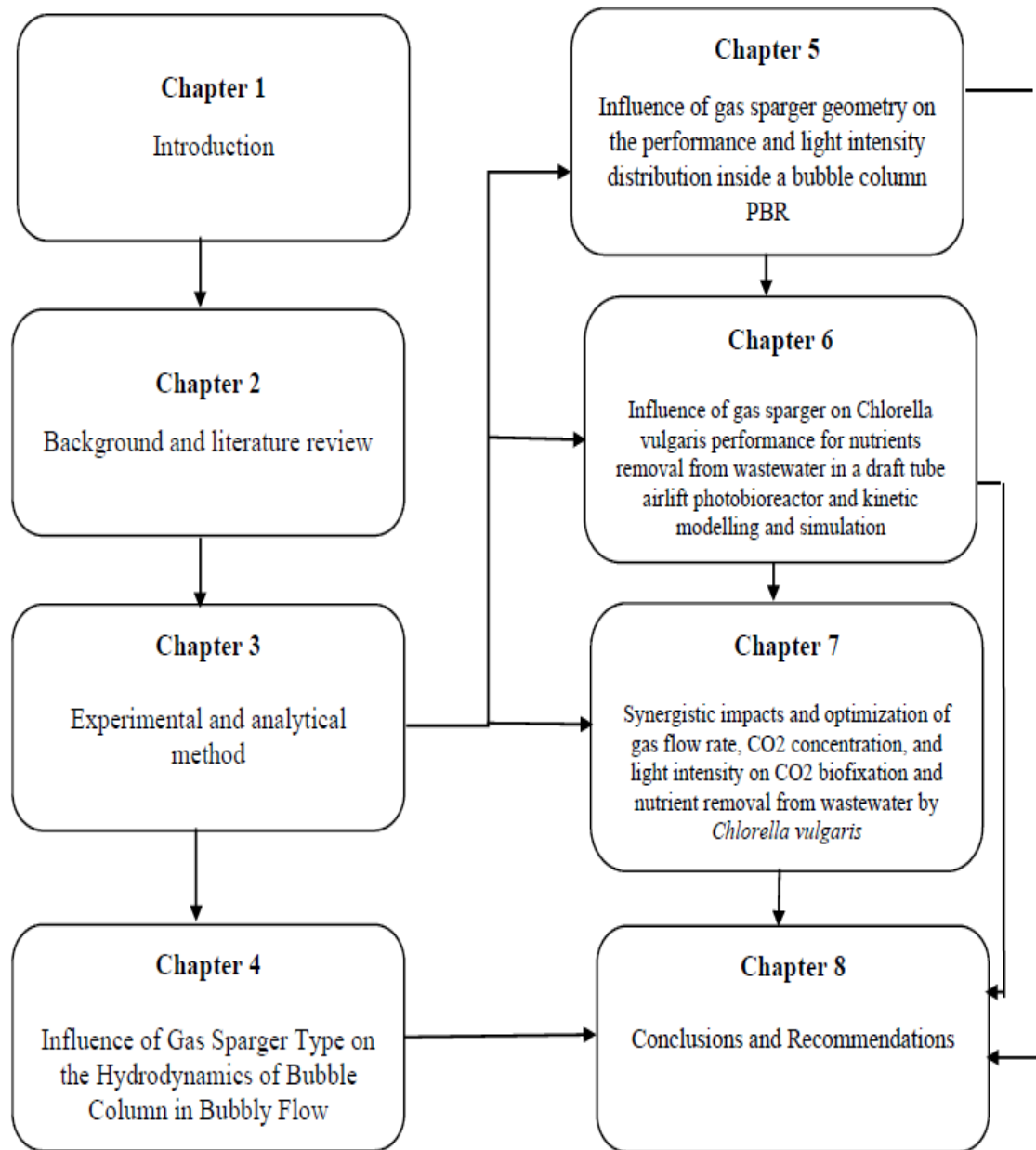
Figure 1. 1 Thesis structure

Chapter Two
Background and literature reviews

2.1 Microalgae culture technology (MCT)

Microalgae culture technology (MCT) combines CO_2 mitigation and nutrient removal (TN and TP) from wastewater to produce valuable products, such as biofuel. In general, the culture system is categorized into open systems and closed systems. An open system is an outdoor facility, such channels, ponds, shallow circulating units, and lagoons, while a closed system (photobioreactors) is tubes or vessels with walls made of transparent materials for light penetration [23]. Closed systems could be located outdoors to utilize sunlight as a light source or indoors using an artificial light. As a result of technical complications, photobioreactors are considered to provide advantageous technology for algal cultivation [9, 24]. Therefore, a photobioreactor is practically more favourable than an open system for CO_2 mitigation and wastewater treatment process [25-27].

Photobioreactor design faces many challenges that have to be considered, such as difficulties in scale-up, oxygen accumulation, sufficient light, and cell damage due to high shear stress rate [13]. To overcome these drawbacks, it needs to use the proper photobioreactor geometry and gas sparger type. Choosing the most appropriate sparger can have a significant positive impact on the mixing inside the photobioreactor, which in turn leads to enhanced light intensity distribution inside. Also, it impacts the photobioreactor hydrodynamics which can reduce shear stress rate on algal cells and consequently enhance its productivity [28].

Microalgae are small unicellular microorganisms that have the ability to transform CO_2 and light into energy (lipids and carbohydrates) stored as a carbon source [29]. In the photobioreactor, the microalgae utilize CO_2, nutrients, and natural or artificial light to produce biomass which is then used to produce biofuel. Furthermore, microalgae can capture waste CO_2, nutrients in many types of wastewater and sunlight to produce biomass as shown in Fig. 2.1. Therefore, these photosynthetic microorganisms are used in many bioremediation processes such as CO_2 mitigation and wastewater treatment.

The microalgae biomass produced could then be used to produce many useful products such as biodiesel, bio-hydrogen, polymers, and animal feed. In oxygenic photosynthetic processes, the microalgae capture the light in a certain wavelength via their pigments and chlorophyll and CO_2 and water convert into oxygen and carbohydrates. The process is a redox reaction divided into light reaction and dark reaction. In a light reaction, the energy of light transforms into
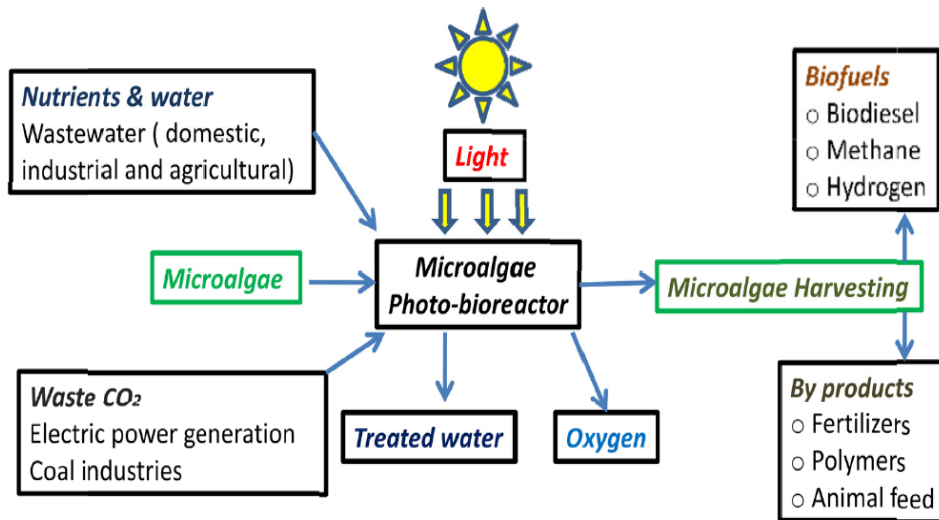
Figure 2. 1 Microalgae photo-bioreactors application [30]

NADPH$_2$ (nicotinamide adenine dinucleotide hydrogen phosphate) and ATP (adenosine triphosphate). In a dark reaction, the NADPH$_2$ and ATP are used in CO$_2$ reduction to carbohydrates[31].

Photosynthesis is a biological process through which plants and microorganisms transform light and CO$_2$ as a carbon source into chemical energy which is kept in bonds of organic molecules (e.g. sugars)[32]. In this process, CO$_2$ is mitigated to produce carbohydrates and water to generate oxygen as a by-product. Almost all the oxygen in the atmosphere is produced via the photosynthetic process and in doing so fixes 10^{11} tons of carbon in CO$_2$ into sugar. The photosynthetic process is represented by:

$$nCO_2 + nH_2O \xrightarrow{Light} (CH_2O)n + nO_2 \qquad (2.1)$$

The photosynthesis process relies on light intensity (irradiance or the incident light on a surface). It consists of two stages of reactions: a light phase, which occurs when cells are subjected to a light source, and a dark phase, which takes place in the absence of light [33]. In the light phase reactions, light energy is converted into a form of NADPH$_2$ and ATP, which can be utilised in metabolic processes. The light-independent reactions include the utilization of the NADPH$_2$ and ATP molecules generated via the light-dependent reactions[34].

2.2 Microalgae Cultivation

Growth characteristics and chemical composition of microalgae are known to rely on cultivation conditions [35]. Cultivation conditions of microalgae are categorised as: photoautotrophic, heterotrophic, mixotrophic and photoheterotrophic cultivation [35]. Table 2.1 summarizes the characteristics of each cultivation condition.

Table 2. 1 Characteristics of different state of microalgae cultivation [35]

Cultivation state	Source of Energy	Source of Carbon	Reactor type	Cost	Disadvantages
Phototrophic	Light	Inorganic	Open pond or photobioreactor	Low	• Low cell density • High condensation cost
Heterotrophic	Organic	Organic	Conventional fermenter	Medium	• Contamination • High substrate cost
Mixotrophic	Light and organic	Inorganic and organic	photobioreactor	High	• Contamination • High equipment cost • High substrate cost
Photoheterotrophic	Light	Organic	photobioreactor	High	• Contamination • High equipment cost • High substrate cost

2.3 Cultivation system

The cultivation systems of microalgae can be categorized into two main types: an open system and a closed system.

2.3.1 Open system

An open raceway pond is the simplest and oldest system for cultivation of microalgae. It is usually constructed by containing the water within poured concrete walls or into the ground

and lining the raceway with a plastic liner. The depth of a raceway pond is about 20-50 cm [29, 36] but its width and length vary depending on design and scale. Pumps and paddle-wheels are used for water circulation and to keep the algal cells suspended in the pond [37, 38] as shown in Fig. 2.2.

A raceway pond has low capital costs, it is easily cleaned, and it is effective for mass cultivation of algae, but it is difficult to control the operating conditions such as light intensity and temperature, and it has a low mass transfer rate due to poor mixing, resulting in low productivity [39]. A raceway pond suffers from contamination or predatory behaviour of algal cultures by other organisms [40, 41].
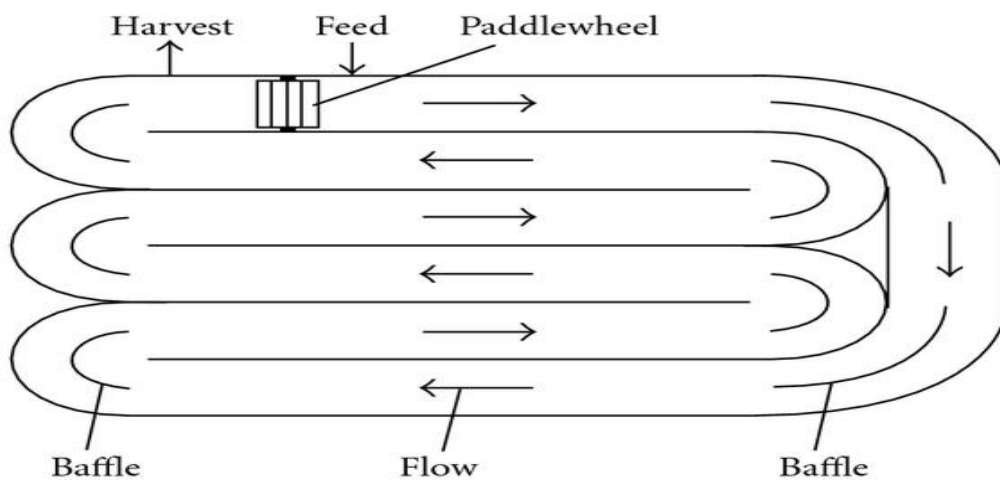
Figure 2. 2 schematic of open raceway pond [29]

2.3.2 Closed photobioreactor (PBR)

Algal photobioreactors have different geometries, such as bubble column, flat plate, horizontal tubular and airlift[29, 42]. The design limitations for closed photobioreactors are light distribution, aeration, pH, temperature, sterility, and mixing. Light distribution is more dependent on reactor geometry and aeration, while pH and temperature are dependent on operating conditions [29, 39, 43]. An efficient photobioreactor design should achieve the following: 1) have a high biomass productivity and selectivity, 2) show efficient utilization of photosynthetically active radiation (PAR) and nutrients; 3) demonstrate precise control of operational conditions and growth parameters such as temperature, pH, O_2, and CO_2 [44], and 4) minimize capital and operational costs.

Light transport and distribution into algae photobioreactors are considered to be the main barriers to improved productivity [43, 45, 46]. According to the Beer-Lambert law, the light intensity decays when it penetrates through the suspended algal culture, which leads to large

dark zones inside the photobioreactor and subsequent negative impact on reactor productivity. Recently, several approaches have been carried out to reduce dark zones inside the reactor by making the reactor thinner, enhancing mixing, or using internal light sources [47-49]. Temperature and pH are significant factors for algal cultivation since they influence the highest rate of growth of algal cells. The typical temperature for algal cultivation ranges from 10-30ºC [29]while the optimum pH ranges from 7-9, despite the fact that some algal species could tolerate higher values of pH [50]. Therefore, the closed system or the algal photobioreactors are more favourable than the open system, as discussed above. This thesis focused on the closed cultivation system (photobioreactor).

Table 2. 2 Comparison between the open and closed systems used for microalgae cultivation [51]

Parameters	Open systems	Closed systems
Efficiency of light	Quite good	Better
Mass transfer	Weak	Better
Hydrodynamic stress on algal cells	Low	Very high
Sterility	None	Attainable for short time
Scale up cost	Low	High
Temperature control	None	Some
Surface/volume ratio	Average	High
Productivity	Low	High
Oxygen produced	High	Higher
Control species	Challenging	Attainable

2.4 Types of algal photobioreactors (PBRs)

2.4.1 Flat-plate photobioreactors

Flat plate photobioreactors have an elevated surface area to volume ratio (S/V), which can provide high algal productivity due to their highly illuminated surface area. Generally, these

photobioreactors are composed of flat plastic or glass panels bonded to plates as shown in Fig. 2.3. The recommended photobioreactor height is up to 150 cm and the width up to 10 cm due to cost considerations [52]. Also, the thickness of the photobioreactor material is also significant, where maximum algal cell density and high biomass productivity is achieved using thinner sheet material to enable a minimum light path [53, 54]. One significant advantage of the photobioreactor design is its geometry which can be inclined and angled to maximise utilization of incident light and achieve high productivity [52]. However, the growth of algal cells in the flat-plate reactors suffers from a common issue of biofouling on the inside wall of the reactor which decreases the light penetration [55]. There are two types of flat-plate reactors depending on the mixing type used: (i) pump-driven where the turbulence and the direct mixing are provided by liquid pumping, and (ii) airlift, where the turbulence and buoyancy-driven mixing are provided by aeration [41].
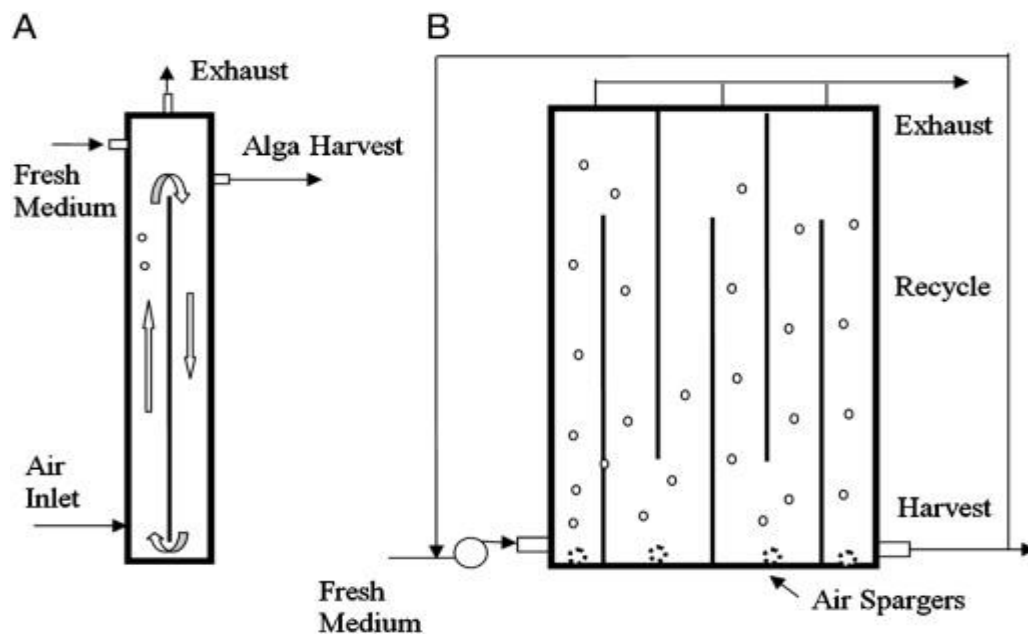
Figure 2. 3 Schematic diagram of (A) side view of airlift type and (B) front view of pump driven type [41].

2.4.2 Vertical Tubular photobioreactors

Vertical tubular photobioreactors are made of glass or flexible plastic transparent tubes to maximize light penetration. These photobioreactors are appropriate for indoor and outdoor biomass cultivation due to their high surface area. The medium of algal growth is circulated via an air pump or airlift system. Vertical tubular photobioreactors are low-cost, simple to operate, compact, and easy to construct[56]. The vertical orientation of the reactors allows the

gas to be introduced at a lower level inside the reactor and rise towards the top. The gas rapidly moves upwards to the top of the photobioreactor and disperses when it arrives at the photobioreactor surface, allowing the liquid to be circulated in the whole column [57]. Vertical tubular photobioreactors can be classified on the basis of the mode of liquid flow into bubble column and airlift reactors.

2.5.2.1 Bubble columns

Bubble column photobioreactors are pneumatic reactors, in which the mixing and agitation are achieved by the sparging of gas into the bottom of the reactor. This process provides a simple and cheap procedure to mix and contact different phases [58]. Bubble columns are widely utilized in many processes such as biochemical, chemical, pharmaceutical, petrochemical, food, and wastewater treatment [59]. The photobioreactor design is simple, with a high aspect ratio ($H/D_R > 2$) (Fig. 2.4). Its height is a very important variable, mostly for batch and semi-batch modes due to its impact on process and residence times [60]. The hydrodynamics and mass transfer rate of the photobioreactor are totally dependent on the behaviour of the gas bubbles released from the gas sparger [55].
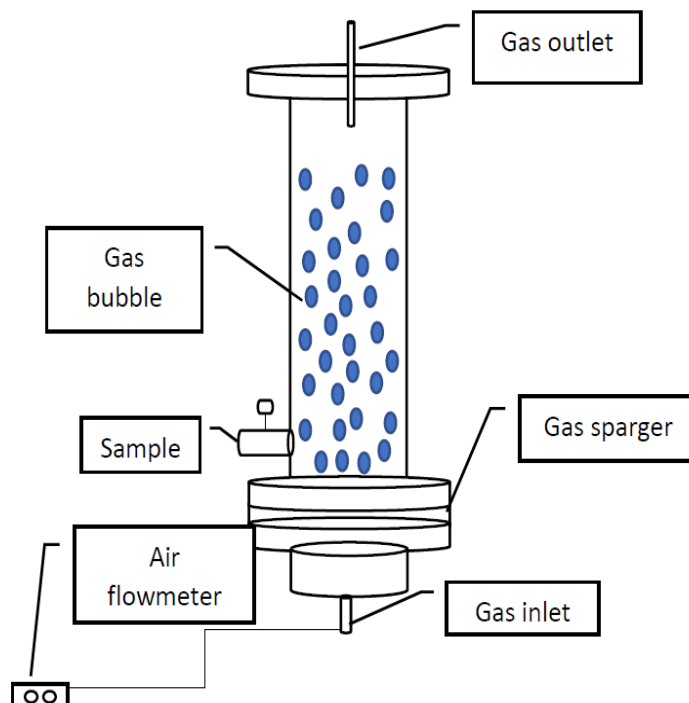
Figure 2. 4 Schematic diagram of a bubble column reactor

Different flow regimes occur in the photobioreactor depending on the superficial gas velocity (U_G) as shown in Fig. 2.5. In this figure, the first line (a) is when gas holdup is still increased to a local maximum value within the transition flow regime, while line (b) occurs rapidly, which is specified by a continued increase in gas holdup. Line (c) is a pure heterogeneous flow regime that occurs with viscous liquids, large orifices of gas sparger, and/or small reactor diameters.

Homogeneous or bubbly flow develops at low U_G, when bubbles are small in size and uniformly distributed across the radial direction and there is minimum or zero gas phase back-mixing. The gas sparger is the most effective design variable for the size of the bubbles in a homogeneous flow regime. A heterogeneous flow regime occurs when increasing U_G as the bubbles and liquid have a tendency to ascend towards the photobioreactor's centre and the liquid flows down near the reactor walls. Back-mixing happens as a result of bubbles being dragged by liquid circulation.
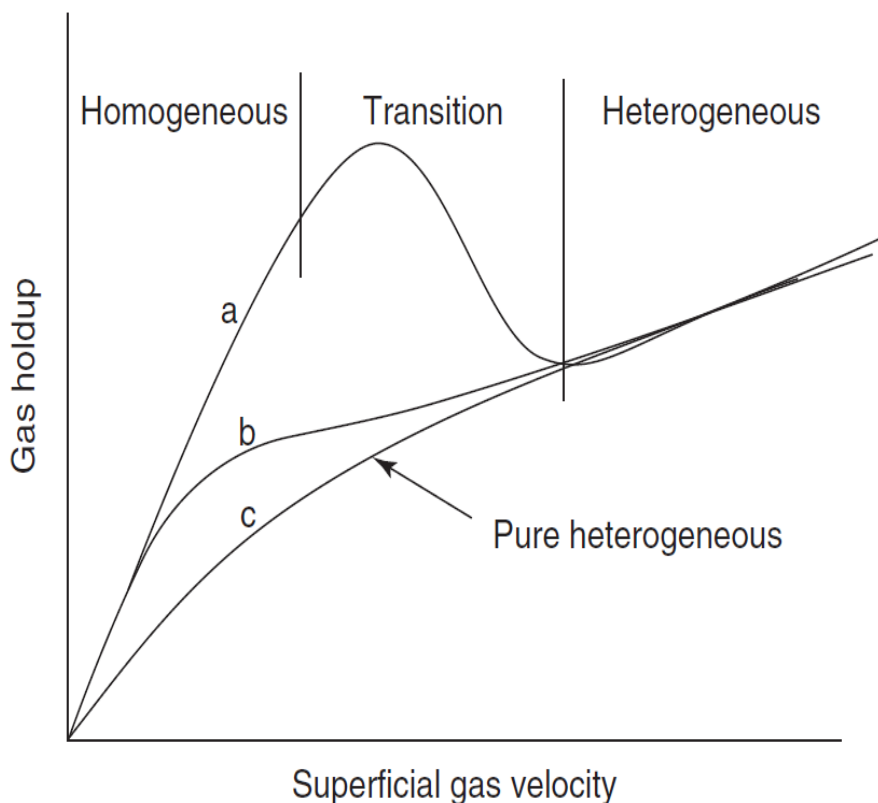
Figure 2. 5 Progression of flow regimes [61]

As the light energy is supplied externally in bubble photobioreactors, the efficiency of the photosynthetic process is highly dependent on gas flow rate [62]. The advantages of bubble column reactors include a high ratio of surface area to volume, low construction cost, non-

moving parts, a high rate of heat and mass transfer, and highly effective release of residual gas mixtures and oxygen.

2.4.2.2 Airlift photobioreactors

Algal airlift photobioreactor is characterised by two main sections: the riser (up-flowing) and the downcomer (down-flowing) streams (Fig. 2.6). Gas is injected through the riser section, which causes gas holdup, which leads to a decrease in the density of the fluid and upward movement in the riser. At the top of the vessel, when gas bubbles are released from the liquid, larger bubbles are left to recirculate through the downcomer. Hence, the circulation of liquid inside the airlift photobioreactors is caused by the difference in density between the riser and downcomer [63]. An airlift photobioreactor has the advantage of generating a circular mixing pattern, resulting in the culture flowing continuously through dark and light zones which gives the effect of flashing light to algal cells [62].

The configuration of airlift photobioreactors can be divided into two common designs: internal loop and external loop. In one type of internal loop photobioreactor (Fig. 2.6a), the riser and downcomer are divided by an internal separator. While the other type of internal loop (Fig. 2.6b), the riser, where gas is sparged, and the downcomer are separated by a draught tube causing liquid circulation between the dark zone (riser) and the light zone (downcomer). In external loop reactors (Fig. 2.6c), individual vertical tubes are linked by small horizontal pieces at both ends of the photobioreactor. As the riser and the downcomer are at a greater distance from each other, disengagement of the gas is more effective. Consequently, mixing in external loop reactors is usually more effective than in internal loop reactors [63].
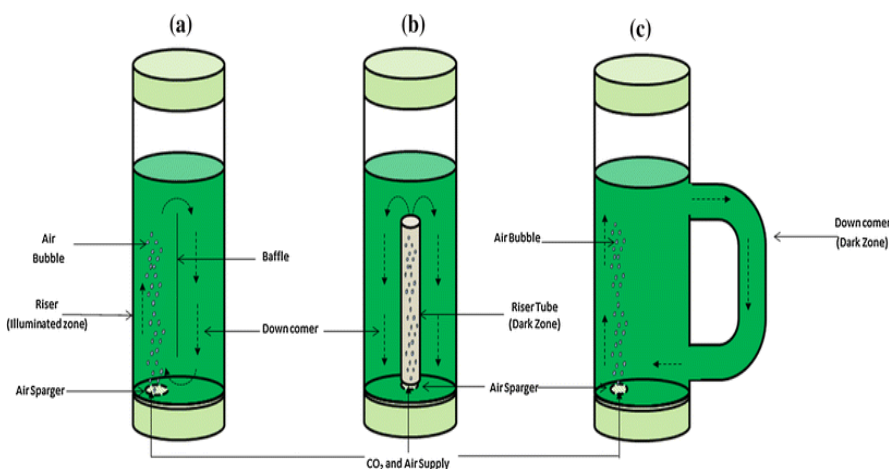
Figure 2. 6 Schematics of an airlift photobioreactor (a) internal loop, (b) internal loop concentric, and (c) external loop [55]

2.5.3 Horizontal Tubular photobioreactors

The most common closed systems are horizontal tubular photobioreactors. These rectors are unlike the vertical tubular reactors in regard to their *S/V* ratio, the volume of gas in dispersion, the characteristics of the mass transfer between gas-liquid phases, the movement fluid nature and the light intensity inside the photobioreactor [64]. All horizontal tubular photobioreactors basically work in the same way (Fig. 2.7), but they are comprised of multiple tubes positioned in numerous varying orientations, such as inclined, horizontal, helicoidal, spiral, and their modified versions. They also differ with respect to their tube length, circulation system, flow velocity and geometric structure of the light receiver. Usually, the diameters of these tubes range from 1cm to 6cm, and their lengths up to several hundred meters. Tubes constructed in this way have the advantage of helping achieve high *S/V* ratio (higher than 100 m) [48]. The *S/V* ratio decreases with increasing tube diameter - a factor that has a strong influence on microalgae growth. Furthermore, the distribution of the light is more homogeneous with what is referred to as the ''lens'' or ''focusing effect''. It dilutes the light over the circumference and focuses it, in a radial direction, towards the centre of the reactor, thereby avoiding mutual shading and increasing light intensity [48]. One of the principal drawbacks of horizontal photobioreactors is oxygen (O_2) accumulation up to inhibitory levels [64], as O_2 concentrations higher than air saturation usually impede the photosynthesis process in microalgae. Generally, a horizontal tubular photobioreactor is the most scalable and practicable culture system. However, Miron, et al. [64] claim that it is not economically suitable for large-scale production because of its requirement for cooling, as it has a high *S/V* ratio. Moreover, photoinhibition caused by O_2 accumulation and high level of light intensity cause lower rates of productivity than those observed in bubble columns and airlift bioreactors.
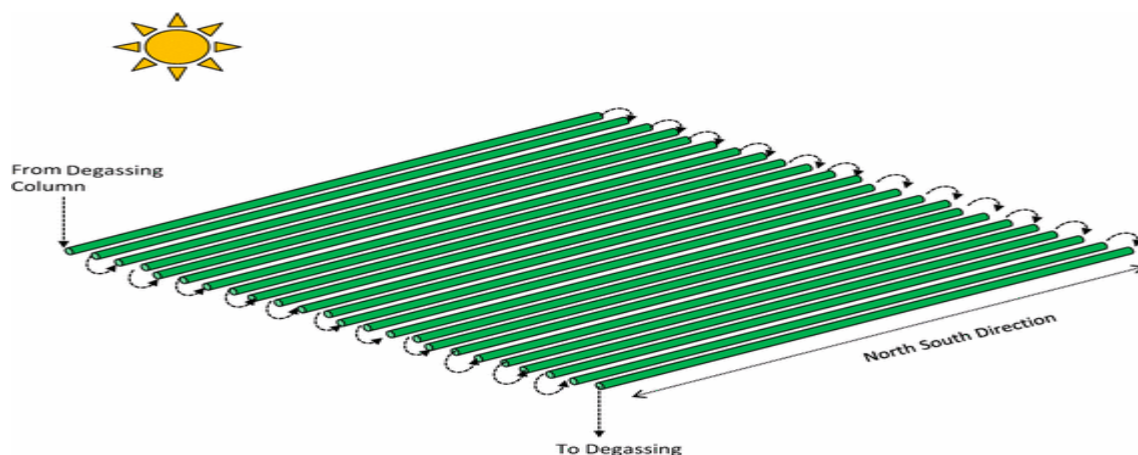
Figure 2. 7 Schematics of horizontal tubular photobioreactor [55]

2.5 Factors influencing algal growth

2.5.1 Light

The amount and availability of light are key for photosynthesis growth of microalgae [65-68]. Therefore, efficiency of light utilization and light intensity distribution are important in photobioreactor design and its performance [69]. The system of algal culture is illuminated by solar light, artificial light, or both. Light affects the algal growth under three different conditions [70]:

  i.   Light limitation - microalgae growth increases when light intensity increases.
  ii.   Light saturation - the activity of photosynthesis decreases when the absorption of photons surpasses the amount of electron turnover, and
  iii. Light inhibition - when the light intensity increases further, irreversible damage is done to the photosynthetic apparatus - a process referred to as photoinhibition.

The effective and widely applied equation for light intensity which is used for a single phase and has to be modified when used for multiphase systems is the Beer-Lambert law (2.1) [71]

$$\frac{I}{Io} = exp\left(-\beta z\right) \tag{2.1}$$

where I is the local light intensity, Io is the incident light intensity, β is the extinction coefficient, and z is the light path. Many simplifications and assumptions have been attempted to modify Beer-Lambert's equation, such as ignoring the light scattering, isotropic scattering or anisotropic scattering by gas bubbles as well as light absorption by algal cells.

There are two forms of the Beer-Lambert's equation - modification due to light scattering by the gas bubbles and light absorption by algal cells for growth:

$$\frac{I}{I_o} = exp\left(-\frac{\beta a z}{4}\right) \tag{2.2}$$

$$\frac{I}{I_o} = exp\left(-\left(\frac{\beta a z}{4} + K_a\right)z\right) \tag{2.3}$$

In Eq. (2.2), β is gas extinction coefficient and equal to 2 [72], a is the gas-liquid interfacial area per unit volume and z is the light path. The gas-liquid interfacial area is a function of gas holdup (ε_G) and bubble diameter (d_b), therefore Eq. (2.2) becomes:

$$\frac{I}{I_o} = exp\left(-\frac{3\varepsilon_G z}{d_b}\right) \tag{2.4}$$

In Eq. (2.3), the light absorption by algal cells is considered. Similar to Eq. (2.2), Eq. (2.3) is simplified as shown in Eq. (2.5):

$$\frac{I}{I_o} = exp\left(-\frac{3\varepsilon_G z}{d_b} - K_a z\right)$$

(2.5)

K_a can be estimated and its value is 1.3478 m^{-1} [73]. The difference between Eqs. (2.4 and 2.5) is the impact of algal cells on local light intensity. Zhang et al. [71], stated that in the process of light transmission, gas holdup is the effecting factor instead of algal cells concentration.

2.5.2 Temperature

Temperature is an essential factor in the process of microalgae growth and, for growth optimization, it is important to keep the temperature of the photosynthetic process under control [74]. However, in the photosynthetic process, when light or CO_2 concentration is the limiting factor, the impact of temperature is insignificant [67, 75]. Temperature impacts the overall photosynthetic activity of algal cells by subjecting them to cellular division, which, in turn, influences biomass productivity. Cell division takes place with the increase in the activities of enzymes associated with the Calvin cycle. A model has been developed to relate the rate of microalgae growth to temperature using the Arrhenius equation. According to the Arrhenius equation, when the temperature increases by 10°C, the growth doubles till the temperature reaches an optimum value, after which the growth will decrease. The reason for this decrease is the heat stress, to which the algal cells are subjected, and this results in inactivation of enzymes and the denaturation of proteins, which are involved in the photosynthetic process [76, 77].

2.5.3 pH

The pH plays an important role in the microalgae photosynthetic process as it controls the metabolism of the cell and the formation of biomass. An inadequate pH (high or low) has unfavourable influence on algal cell growth. Generally, acidic media (pH 5–7) are suitable for eukaryotic algae growth, whereas alkaline media (pH 7–9) are favourable for cyanobacteria (blue-green algae) growth [9]. On the other hand, when the pH of the culture media is decreased, sedimentation of phosphorus compounds occurs, leading to a reduction in their utilization [78, 79]. However, the proper pH for microalgae growth is dependent on aeration of the culture [42]. For example, if the algal culture is sparged with air only, there will not be a

significant variation in pH value. The influence of pH on *Chlorella vulgaris* showed that microalgae growth decreased in both acidic media and alkaline media, while maximum growth was obtained when the pH value was between 7.5 and 8.0 [80].

2.5.4 Nutrients

Nitrogen and phosphorus are essential nutrients that impact the growth rate of microalgae. Microalgae produce more lipids but grow at a low rate when deprived of partial nitrogen. Microalgae growth is directly dependent on the uptake rate of the limiting nutrients and is represented by the Monod equation as follows, Eq. (2.7) [81]:

$$\mu = \mu_{max}.\frac{S}{K_S+S} \tag{2.7}$$

where μ and μ_{max} are the growth rate and maximum growth rate, respectively, S is the concentration of limiting substrate (g L^{-1}), and K_S is the concentration of nutrients that leads to half the maximum growth rate, called the half-saturation constant (g.L^{-1}). Nitrogen is the main element for nucleic acids and portions formation [82]. Nitrate (NO_3^-) and Ammonium (NH_4^+) are the most important nitrogen components for the growth of microalgae. For example, more than 10% of produced biomass is achieved by the contribution of these components [66]. Nitrite and urea are other nitrogen compounds, but nitrite at high concentrations is considered to be very toxic [10]. In particular, ammonium is the nitrogen compound most favoured by algal cell for its growth [83].

Phosphorus is also an essential component required for the metabolism and growth of microalgae. Phosphorous should be fed as phosphate because all of the phosphorus components are bioavailable and usually available in wastewater as inorganic anions such as $H_2PO_4^-$ and HPO_4^{-2} [9]. Phosphorus can contribute to lipid formation, intermediates of carbohydrates, and proteins [66]. Algal cells tend to save the surplus amounts of phosphorus as polyphosphate granules, which can be utilized by the algal cell for its growth during conditions of phosphate starvation [10]. Therefore, a reduction in phosphate could influence the photosynthetic process and lipid production [84]

2.5.5 CO$_2$ Concentration

Carbon dioxide (CO_2) concentration is an important parameter that significantly affects the kinetics of microalgae growth. Carbon dioxide is mainly used as a carbon source for the process of microalgae cultivation. In recent years, many researchers have investigated the impact of CO_2 concentration on the growth of microalgae; however, only some of that research has been

on CO_2 uptake under conditions with relevant CO_2 concentrations [85]. Carbon dioxide is about 0.036% in the atmospheric air which is not enough for the growth of microalgae cells because of limited driving forces for mass transfer. This issue can be resolved by using either pure CO_2 or using CO_2 from flue gases, which has the additional benefits of addressing environmental problems [86]. CO_2 is injected into the culture media via spargers, causing the formation of large bubbles which decrease CO_2 utilization efficiency. Hence, the formation of small bubbles has a positive impact on CO_2 uptake [87]. Therefore, it is important to feed a rich CO_2 gas to the photobioreactor with properly designed gas distributors. With this approach, both good algal culture and high mass transfer of CO_2 can be produced.

2.6 Factors affecting algal PBR performance

Table 2.3 briefly lists the most influencing parameters (mixing, light, aeration, and nutrients) that can significantly impact the performance of the algal photobioreactor.

Table 2. 3 Parameters affecting microalgae growth

Parameter	minimum effect	maximum effect	Affected by
Light	Inadequate for photosynthesis, slow growth	Photoinhibition	Surface/volume ratio (*S/V*), Geometry, orientation, and inclination of reactor , Material and thickness of reactor walls Culture depth and density Mixing
Mixing	Insufficient mass transfer, biomass settling, anaerobic zones	Shear stress, using high energy	Reactor configuration, mixing type (e.g., mechanical, air flow, gravity flow)
Aeration	Growth inhibition	Toxicity	Types of gas distributor
Nutrients	Growth inhibition	Toxicity	Media composition CO_2 provision and O2 removal (mass transfer, sparging and degassing mechanisms, gas concentration and flow rate, headspace, gas holdup volume), Mixing

2.7.1 Mixing

Mixing has a significant influence on the performance of a photobioreactor because it is linked directly to gas-liquid mass transfer, light intensity distribution, and nutrient utilization [88]. Efficient mixing keeps the microalgae suspended in the culture media, ensuring efficient nutrient distribution, enhancing gas mass transfer, mitigating the shading in the centre of the photobioreactor, and diminishing photo-inhibition on its wall [30]. Table 2.3 shows the influence of the important factors that affect microalgae growth.

The mixing in bubble column and airlift reactors can be described by the mixing time, axial dispersion coefficient, and the circulation time [89]. Shorter mixing time was observed in bubble columns compared with airlift reactors, although airlift reactors were found to be preferable, due to considerations associated with efficiency and biomass productivity [65, 90-92]. This is due to the rising of bubbles inside the draft tube which creates a less turbid zone in the annulus region, thereby enabling improved light exposure. Moreover, the presence of a draft tube inside airlift photobioreactors leads to mixing, due to facilitated circulation of the culture through the draft tube and down through the annulus between the housing column and outside the draft tube [65]. In addition, more distinct fluid flow and relatively higher gas–liquid mass transfer rates have been observed in airlift reactors. In contrast, a bubble column is prone to generate uneven cell density along the length of the photobioreactor, which can cause algal starvation and death [91]. Ugwu et al. [39], stated that the overall gas-liquid mass transfer coefficient (k_La) is affected by mixing rate, sparger type, and temperature. Some of spargers create large bubbles, which result in undesirable mass transfer due to the reduction in contact area between gas and liquid phases. Bubbles size and bubble velocity are influenced by the liquid phase flow rate.

2.7.2 Photobioreactor configuration

Photobioreactor configuration is an important factor in the growth of microalgae. Frumento et al. [93], studied the effect of photobioreactor configuration on the cultivation of *Chlorella vulgaris* using helicoidal and horizontal tubular photo-bioreactors with an illuminance level of 5 Klux and sodium bicarbonate and air as sources of carbon. Optimum biomass productivity (84.4 mg $L^{-1}d^{-1}$) was achieved in the helicoidal photobioreactor of the fed-batch run, while the optimum lipid production was found in the horizontal photobioreactor in the batch run.

Cuaresma et al. [94], investigated the biomass productivity of *Chlorella sorokiniana* using vertical and horizontal flat panel photobioreactors. They showed that, the optimal irradiance during the day was 400 µmol m^{-2}s^{-1} in the vertical reactor and 1800 µmol m^{-2}s^{-1} in the horizontal reactor. The highest productivity was 4 g/kg of culture in the horizontal configuration, whereas it was 1.3 g in the vertical configuration. Wong and Ho [95], studied biomass and lipid production using different types of photobioreactor (bubble column, air lift, and porous air lift). They showed that the bubble column was the best photobioreactor for microalgae (*Chlorella vulgaris*) cultivation. The biomass concentration was 0.78 gL^{-1} in the bubble column and 0.09 gL^{-1} in the air lift photobioreactor. Maximum lipid content was achieved in the porous air lift and the air lift with a shorter draft tube (35 cm) was also better than that with a longer one (50cm) for cultivation. The maximum concentration of biomass can be produced under a maximum gas flowrate of 2.7 L min^{-1} whereas the lowest dry cell mass was under a minimum gas flowrate of 0.2 L min^{-1}. In addition, the production of biomass on day 10 in white LED was the highest (1.25 g L^{-1}) while blue LED, red LED and open pond were 0.80 g L^{-1}, 0.35 g L^{-1} and 0.58 g L^{-1} respectively. More details are explained in Table 2.4.

2.7.3 Gas sparger type

Gas distributor design has significant influence on flow regimes (homogenous and heterogeneous), gas hold-up, bubble size distribution and mixing in the photobioreactor [96, 97]. Therefore, for effective design and scale-up of a photobioreactor, comprehensive understanding of the impact of gas spargers on the performance of the photobioreactor is crucial [98]. Mixing plays an essential role to ensure best distribution of light intensity inside the photobioreactor, prevent cell sedimentation, support adequate CO_2 transfer and maintain a uniform pH [42, 99]. The shading problem that inhibits light absorption by algal cells is commonly connected to mixing and proper mixing by gas sparging is the effective solution to overcoming this issue [70]. Becker et al. [100], examined the flow of gas-liquid in an external loop airlift reactor. They observed that the bioreactor hydrodynamics were influenced by the type and location of gas distributor in the riser section. They used two different types of gas spargers: a tube sparger and a frit sparger. The tube sparger had a diameter of 8mm with 45 holes each of which was 0.3 mm in diameter and was positioned above the downcomer end. The frit sparger, made of sintered plastic, had a 40 mm disc diameter and 40 µm mean hole width. Two frits were fixed at the bottom of the riser, below the end of the downcomer. The

two spargers displayed different flow patterns, but both produced similar distributions in bubble size at a 3 mm mean diameter. The study showed that the tube sparger's flow structure was more uniform due to it being positioned in the riser just above the point where the circulating liquid entered. In contrast, the frits displayed a more heterogeneous flow pattern in the riser due to their positioning at the bottom of the riser. The circulating liquid coming from the downcomer drove the bubbles to the left side of the riser causing asymmetry in the flow. This asymmetry of the gas flow was sustained until approximately half the height of the riser and resulted in liquid circulation in the riser. The flow patterns in the head and the downcomer were observed to be similar to those observed in the tube sparger.

Lin et al. [101], studied the effect of the gas sparger on the local hydrodynamic behaviour of an external loop airlift reactor using a two-phase system (air-water). Two different gas spargers were used: a porous sinter sparger with a 30 μm hole diameter and a perforated plate sparger with a 1mm hole diameter and an open area ratio of 0.25%. The air was injected at a U_G ranging from 0.008 to 0.032 m s^{-1}. The gas holdup was measured and increased with increasing U_G. For the porous sintered distributor, a wall-peaking radial gas holdup profile was observed, whereas, for the perforated plate distributor, a core-peaking radial gas holdup profile was seen, due to the large bubbles formed. In the perforated plate distributor, the relatively flatter radial gas holdup profile at low U_G became more parabolic with increasing U_G. In contrast, the porous sintered plate produced a radial gas holdup profile that was much flatter. This revealed that the porous sinter sparger distributed the gas phase radially more effectively than the perforated plate sparger.

Fraser and Hill [102], investigated the impact of a spinning sparger in an external loop airlift bioreactor. It comprised a flat plate with six holes and was positioned below the downcomer connection in order to avoid the generation of a high shear rate. To support the sparger, a hollow shaft was applied, and a variable speed motor was installed to rotate the shaft. The injected air flowed through this shaft to the sparger. The study reported that the rotational speed of the sparger had a key influence on the gas holdup. The spinning motion of the sparger was found to generate smaller bubbles with higher gas holdups and interfacial areas. Lau et al. [103], investigated the influence of gas spargers (single nozzle, porous plate, and perforated plate) on the hydrodynamics of a shallow bubble column reactor in a two-phase (air-water) system.

Table 2. 4 Performance of different algal PBR configurations

Photobioreactor configuration	CO₂ concentration in gas phase	Superficial gas velocity (m s⁻¹)	Light path inside PBR (cm)	Biomass productivity (g L⁻¹d⁻¹)	Specific growth rate μ (day⁻¹)	Reference
Inclined bubble column	15%	-	4	0.3	0.1	[104]
Flat plate	2%	-	2.6	9.6	0.6	[105]
Inclined flat plate	2%	-	1.3	4	0.5	[53]
Helical tubular	-	-	3	0.9	0.4	[106]
Thin layer flat plate	-	0.013	1.4	12	5.8	[94]
Airlift	-	-	3	0.65	1.9	[62]
Tubular with static mixer	-	-	4	0.7	0.3	[107]
External loop airlift	-	0.005	3	0.1	0.1	[108]
Airlift with rotating annular	-	-	1.2	7.3	3.2	[109]
Membrane-sparged helical tubular	0.045-0.093%	-	9	0.2	0.2	[110]
Airlift	-	-	3	0.6	0.6	[111]
Thin flat plate	2%	-	-	0.93	0.414	[112]

Their findings showed that the single nozzle was not suitable for the shallow bed process. However, in the absence of solids, the porous plate and perforated plate spargers had comparable behaviour, while the presence of solid particles caused the two spargers to behave differently. The solid particles promoted bubble coalescence in the perforated plate sparger, while the same prohibited bubble coalescence in the porous plate sparger.

Bahadori and Rahimi [113], simulated the impact of gas spargers on the axial velocity of liquid phase and gas holdup by using Computational Fluid Dynamics (CFD). They found that increasing the number of orifices in the gas sparger increased the total gas holdup. Furthermore, each orifice caused an increase in the circulation and mixing of the liquid in the column. Zhang et al. [71], studied the modelling of light intensity, the kinetics of cyanobacterial growth, and fluid dynamics in a flat plate photo-bioreactor using CFD. They also studied the influence of sparger type and the flow rate of recycled gas on light intensity. They showed that, the velocity of the liquid and gas hold-up could be increased by the flow of recycled gas, although it hindered the light transfer and cyanobacterial growth. In addition, light intensity distribution and movement of the liquid was affected by sparger type. Sharaf et al. [114], investigated the influence of different types of sparger on the performance of laboratory bubble columns. They used perforated plate and spider spargers as two different types of gas distributor and the results showed that the overall gas holdup attained from the perforated plate with the uniformly spaced small diameter holes showed homogeneous, transition and heterogeneous behaviour in the gas holdup and superficial gas velocity plots. The spider sparger produced a heterogeneous regime. More details are explained in Table 2.5.

2.7 Microalgae application for CO_2 biofixation and wastewater treatment

The environmental application of microalgae that combine CO_2 fixation and wastewater treatment (Fig. 2.8) has received great attention [66, 115-117]. Microalgae can play a significant role in the removal of nutrients (nitrogen, carbon, and phosphorus) from wastewater and utilizing CO_2 from flue gases. Therefore, the microalgae cultivation technology could be a promising environmental and economical technology for algal biomass production, wastewater treatment and CO_2 biofixation [118-120].

Table 2. 5 Applied gas distributer (sparge) in bubble column reactor

Gas sparger used	Measurements technique	U_G range (m s^{-1})	System type	reference
• Sieve plate (1 hole, d_o = 25mm) • Sieve plate (1 hole, d_o = 87mm) • Sieve plate (71 holes, d_o = 3mm) • Sieve plate (315 holes, d_o = 0.8mm) • Sieve plate (623 holes, d_o = 1mm)	Gamma ray tomography	0.063-0.29	Air-water	[121]
• Single nozzle • Porous plate • Perforated plate	• Bed expansion • High-speed camera	0.0325-0.108	• Air-water • Air-water-5%wt	[103]
• Perforated plate (triangle pitch) • Perforated plate (square pitch)	• Bed expansion • High-speed camera	0.012-0.108	Air-water-50% glycerin-1.5% butanol	[122]
• Spider sparger • Perforated plate	• High speed camera • Wire mesh sensor	0.014-0.171	Air-water-0.5% butanol	[114]
• Perforated plate (open area=0.57%) • Perforated plate (open area=2.14%)	Pressure transducers	0.01-0.18	Air-water-rayon fiber	[123]
• Tree type sparger (d_o = 0.5mm)	• Two-point needle probes	0.07-0.29	Air-water	[124]

• Tree type sparger (d_o = 3mm) • Asymmetrical tree type sparger (d_o = 0.5mm)	• Differential pressure method • Single-point needle probe			
• Single orifice nozzle (d_o = 5mm) • Multiple orifice nozzle (d_o = 1mm) • Porous glass plate (d_o = 15µm)	Laser Doppler anemometer (LDA)	0.006-015	Air-water	[125]
• Perforated plate (163 holes, d_o = 0.5mm) • Perforated plate (163 holes, d_o = 1.32mm) • Cross sparger (4 holes, d_o = 2.54mm)	Optical fiber probe	0.005-0.6	Air-water	[126]
• Perforated plate (163 holes, d_o=0.4 mm) • Cross sparger (4 holes d_o= 2.6 mm) • Single nozzle (d_o=5.1 mm) • Perforated plate (163 holes d_o=0.5 mm) • Perforated plate (61 holes d_o=0.4 mm) • Perforated plate (163 holes d_o=1.25mm)	γ-ray computed tomography (CT)	0.02-0.3	Air-water	[127]
• Single orifice (d_o= 25mm) • Tree type sparger (d_o = 3mm)	Conductivity probe	0.07-0.2	Air-water	[128]
• Central nozzle sparger • Ring sparger • Plate sparger	Three-film electro diffusion measurement (EDM)	0.02-0.09	• air-water • Air-water-10vol.% K_2SO_4	[129]
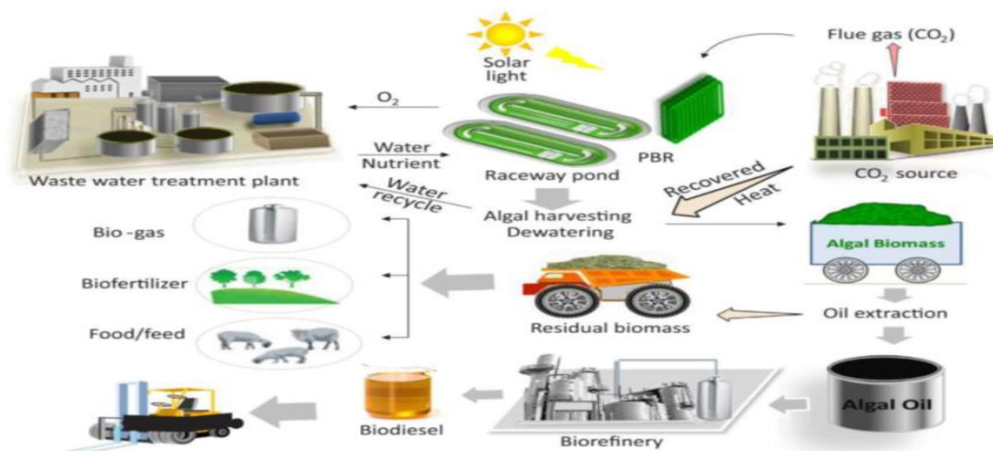
Figure 2. 8 Algal integrated system [130]

2.7.1 CO₂ fixation

Global warming, which is caused by the emitting of greenhouse gases, has attracted great attention in the scientific community and the public. CO_2 is the main greenhouse gas released by the burning of fossil fuels. The biofixation of CO_2 using microalgae is a promising process for fixing CO_2 and mitigating the greenhouse impact [131]. Algal cells are capable of fixing more than 500 tons of CO_2 and produce about 100 tons of dry biomass per hectare per year [132]. One of the most common microalgae used for CO_2 mitigation is *Chlorella vulgaris* due to its rapid growth and high capability of CO_2 fixation [25, 133, 134]. *Chlorella vulgaris* has the ability to mitigate CO_2 from air, CO_2-enriched air, and flue gases. Flue gases from combustion processes are a valuable source of CO_2 which can be introduced directly into a microalgae cultivation system, as they contain a high concentration of CO_2.

The biofixation of CO_2 in a photobioreactor generally relies on a CO_2 transfer rate from the gas phase to the liquid phase and uptake of CO_2 by algal cells. Either or both of these factors are affected by photobioreactor hydrodynamics, CO_2 concentration, light intensity, microalgae species, biomass concentration, and cultivation medium. Individual experimental studies have rarely encompassed all the relevant variables. Zhao and Su [135], stated that CO_2 biofixation and microalgae growth are highly influenced by flow and mixing rate, which are impacted by gas sparger geometry and aeration rate.

2.7.2 Wastewater treatment

Algal cells can be used efficiently to remove nutrients (nitrogen and phosphorous) from wastewater in the tertiary treatment stage. Microalgae consume nutrients in wastewater to produce more valuable environmentally friendly products such as lipids, biofuel, and carbohydrates. Researchers have suggested to use microalgae cultivation system instead of tertiary treatments due to economic considerations [136]. Wang et al. [136], investigated the ability of *Chlorella vulgaris* for nutrient removal from wastewater that is discharged from the primary treatment unit. The efficiency of TN and TP removal efficiencies were 68.5% and 90.6% respectively, while the Chemical Oxygen Demand (COD) removal efficiency was only 56.5%. Wang and Lan [137] studied the removal of TN and TP using *Neochloris oleoabundans* cultivated in a synthetic secondary municipal wastewater. Their findings showed that TN removal efficiency changed from 78% to 99% depending on the nitrogen to phosphorous ratio. The phosphorous was totally removed and independent of the N/P ratio in the medium.

Integrating the wastewater treatment with CO_2 captured from flue gas provided an economically and environmentally useful process to diminish the emission of greenhouse gases. Numerous researchers have stated that microalgae cultivated in a wastewater medium have higher productivity and efficiency when CO_2 is sparged to the culture [138-140]. Using photobioreactors for removal of nitrogen and phosphorous from wastewaters has attracted great interest because they provide a more sustainable alternative compared to the established biological wastewater treatment process, which requires high energy for mixed liquor aeration and for pumping the mixed liquor between different tanks in the treatment process.

2.9 Available growth kinetic models

The vast majority of the applied kinetic models for algal growth were based on Monod [141-144] expressed as:

$$\mu = \mu_{max} \frac{S}{K_s + S} \tag{2.8}$$

where μ_{max} is the maximum specific growth rate, S is nutrient concentration (mg L^{-1}), and K_s is the half-saturation constant (mg L^{-1}) which is the nutrient concentration when the specific growth rate is half of the maximum. The Monod and modified Monod kinetic models applied to modelling and simulating the performance of the algal photobioreactor are summarized in Table 2.6. These models consider the main algal growth factors (such as, nutrients applied and light intensity).

Table 2. 6 Previous kinetic models for microalgae growth

Model	species	Photobioreactor	Reference
Related to carbon concentration			
$\mu = \mu_{max}\dfrac{s_c}{K_{s_c}+s_c}$	*Nannochloropsis* sp. *Oculta*	Bubble column	[143]
Related to nitrogen concentration			
$\mu = \mu_{max}\dfrac{s_N}{K_{s_N}+s_N}$	*Chlorella vulgaris*	Bubble column	[141]
	Spirulina platensis	Bubble column	[145]
	Chlorella vulgaris	Bubble column	[146]
	Gracilaria gracilis	Bubble column	[147]
Related to phosphorous concentration			
$\mu = \mu_{max}\dfrac{s_p}{K_{s_p}+s_{Np}}$	*Chlorella vulgaris*	1 L flask	[141]
Related to light intensity			
$\mu = \mu_{max}\dfrac{s_I}{K_I+s_I}$	*Euglena gracilis*	Bubble column	[142]
	Chlorella pyrenoidosa	Bubble column	[148]
	Chlorella vulgaris	External loop Airlift	[149]
	Spirulina (*Arthrospira*) *sp.*	Bubble column	[150]
Related to multiple factors			
$\mu = \mu_{max}\left(\dfrac{s_N}{K_{s_N}+s_N}\right)\left(\dfrac{s_c}{K_{s_c}+s_c}\right)f_I$ $f_I = \dfrac{I_a}{I_s}exp\left(1-\dfrac{I_a}{K_I}\right)$	-	Algal pond	[151]
$\mu = \mu_{max}\left(\dfrac{s_N}{K_{s_N}+s_N}\right)\left(\dfrac{s_I}{K_I+s_I}\right)$	*Chlorella vulgaris*	Bubble column	[152]
$R = R_{max}\left(\dfrac{s_N}{K_{s_N}+s_N}\right)\left(\dfrac{s_p}{K_p+s_p}\right)$	*Scenedesmus* sp.	250 mL flasks	[144]
$\mu = \mu_{max}\left(\dfrac{s_C}{K_{s_c}+s_C}\right)\left(\dfrac{s_p}{K_p+s_p}\right)$	*Chlamydomonas acidophila*	Bubble column	[153]
$\mu = \mu_{max}\left(\dfrac{s_N}{K_{s_{cN}}+s_{CN}}\right)\left(\dfrac{K_X}{K_X+X}\right)$	*Dunaliella tertiolecta*	0.5 L falsk	[154]

Chapter Three
Experimental and Analytical Methods

3.1 Introduction

This chapter illustrates in detail the experimental works conducted in this thesis to achieve the objectives mentioned in chapter one.

A detailed experimental set-up for both photobioreactors (bubble column and draft tube airlift) will be explained including the three different spargers (perforated plate, cross, and ring) applied and investigated in this work. Also, this chapter details the analytical methods applied such as optical fibre probe for hydrodynamic measurements. Microalgae cultivation conditions and the medium (standard medium MLA and primary wastewater) used are also explained. Techniques used to measure and analyse the light intensity and distribution, lipid contents, CO_2 concentration, COD, total phosphorus and nitrogen are also introduced.

3.2 Photobioreactors (PBRs) setup

In this study two different pneumatically agitated photobioreactor configurations were designed:

3.2.1 Bubble column PBR

A cylindrical bubble column made of clear acrylic material with a diameter (*D*) of 10 cm, and height (*H*) of 100 cm created a working volume of 5200 cm^3. A sparger was allocated at the base of the photobioreactor in order to inject the air/CO_2 into the medium. The culture was bubbled continuously with filtered air and a sampling port was provided to withdraw the samples (Fig. 3.1).
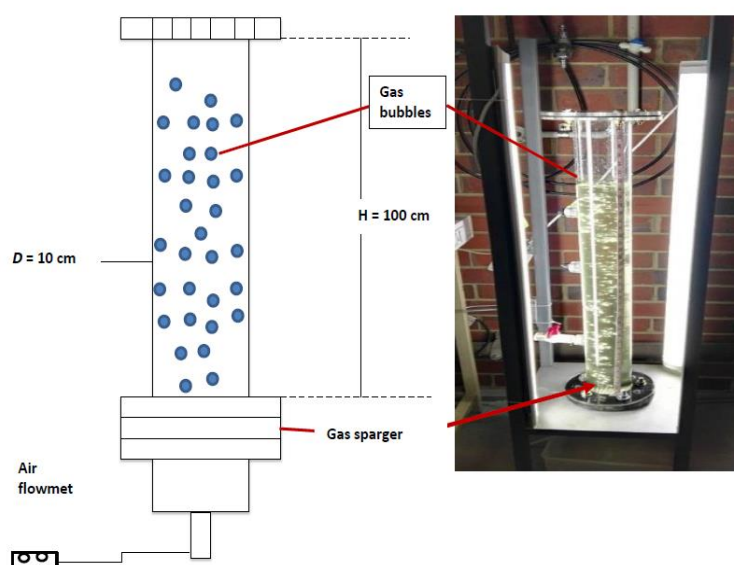
Figure 3. 1 Bubble column PBR experimental set up including the spargers.

3.2.2 Draft tube air lift PBR

A cylindrical draft tube airlift column made of a transparent acrylic material was created with 6 L working volume, 10 cm O.D, 100 cm height, 0.3 cm thickness, a ratio of the downcomer to the riser cross-sectional area (A_d/A_r) of 1.77, and a working volume of 5200 cm^3. A sparger was allocated at the base of the photobioreactor in order to inject the air/CO_2 into medium. The draft tube was made of transparent acrylic material with 6 cm O.D, 60 cm in height, 0.3 cm thickness, and was placed 5 cm above the sparger, as shown in Fig. 3.2.
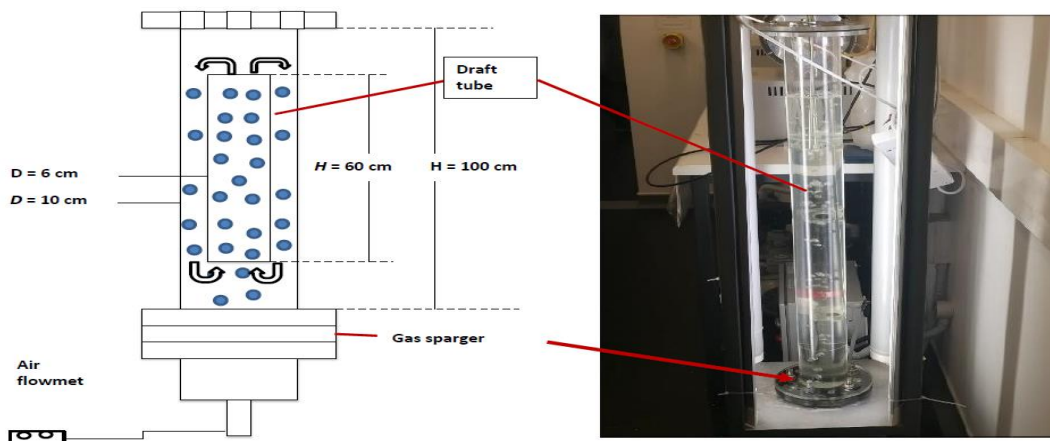
Figure 3. 2 Schematic diagram of draft tube airlift reactor

3.2.3 Gas spargers investigated

Figure 3.5 shows the three types of gas sparger applied and investigated in this study for both bubble column and airlift photobioreactors (perforated plate sparger, cross sparger, and ring sparger) (Figs. 3.3 and 3.4). These spargers are made of acrylic, 1 cm in thickness. The orifice diameter in all these spargers was 1 mm. The number of orifices in the perforated plate sparger, cross sparger, and ring sparger was 134, 25, and 33, respectively.

(a) Perforated plate   (b) cross sparger   (c) ring sparger
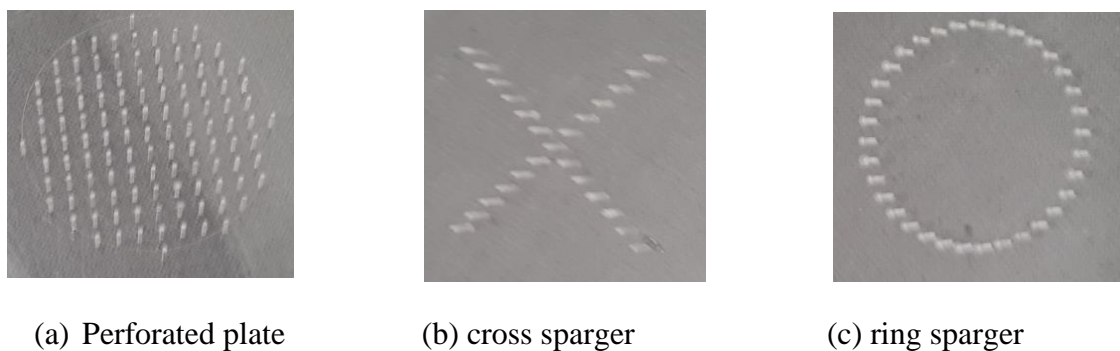
Figure 3. 3 Schematic diagram of: (a) perforated plate sparger, (b) cross sparger, and (c) ring sparger

3.3 Optical fibre probe

Optical fibre probes are used to distinguish between gas phase and liquid phase through measuring the reflected laser beam at the tip of the probe. The refractive index of the gas is lower than that for the liquid, therefore, the reflected laser intensity is higher when it is exposed to gas. The local bubbles dynamics (such as gas hold up, chord length, bubble velocity) were measured and analysed according to the obtained signals from the optical fibre probe. Local gas holdups, bubble arrival frequency, bubble velocity, and bubble chord length were measured simultaneously through knowing sensing tip length (L_S). The signal was measured by an optoelectronic module (Fig. 3.5) that emitted the laser to the tip of the probe and turned the reflected optical signal into a digital signal.

Local gas holdups (ε_G) were calculated as the ratio of the cumulated bubble residence times (t_B) on the probe tip over the total measuring time (t_T).

$$\varepsilon_G = \frac{\sum_i t_{Bi}}{t_T} \tag{3.1}$$

Bubble rise velocities (v_B) were estimated from the probe sensing length (L_S) and signal rise time (t_R) using Eq. 3.2, which is the time observed between selected lower and upper thresholds based on the gas and liquid voltage difference. Lower and upper threshold of 10% and 80% were used for these experiments based on recommendations from the manufacturer.

$$v_B = \frac{L_S}{t_R} \tag{3.2}$$

Given the rise in velocity and residence time, the chord length (C_B) can be determined using the following relation:

$$C_B = t_B \, v_B \tag{3.3}$$

The SO6 software provided by A2 Photonic Sensors analysed the digital signal obtained by the optoelectronic module. Arrival times, rise times, and residence times were recorded for each bubble. Signals that do not reach the upper threshold were distinguished from fully detected bubbles. This may occur if the bubble is small relative to the probe sensing length or if the bubble is pierced off-centre. Data acquisition was dependent on the number of bubbles measured or a set time limit.

The optical fibre probe consisted of the following components (Fig. 3.4):

S1: Sensing tip of the probe.

S2: Supporting tube for the optic fibre and the sensing tip. This tube can be straight or bent (L-shape).

S3: Probes can be equipped with a sealing gland to allow for a watertight assembly.

S4: Fibre optic cable transporting the optical signal from the sensing tip (S1) to the optoelectronic module.

S5: Optical connector, to connect the fibre optic cable to the optoelectronic module.
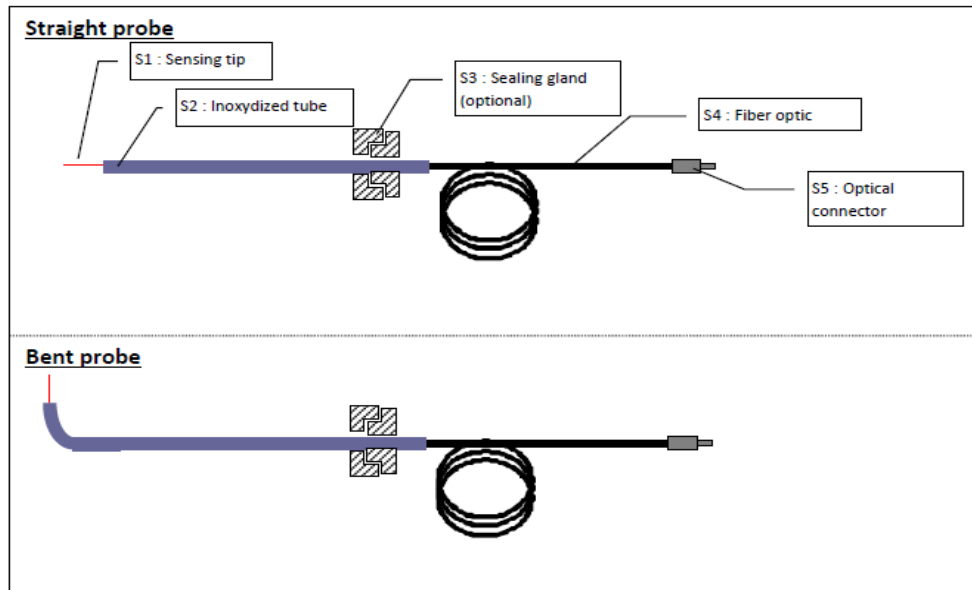
Figure 3. 4 Optical fibre probe
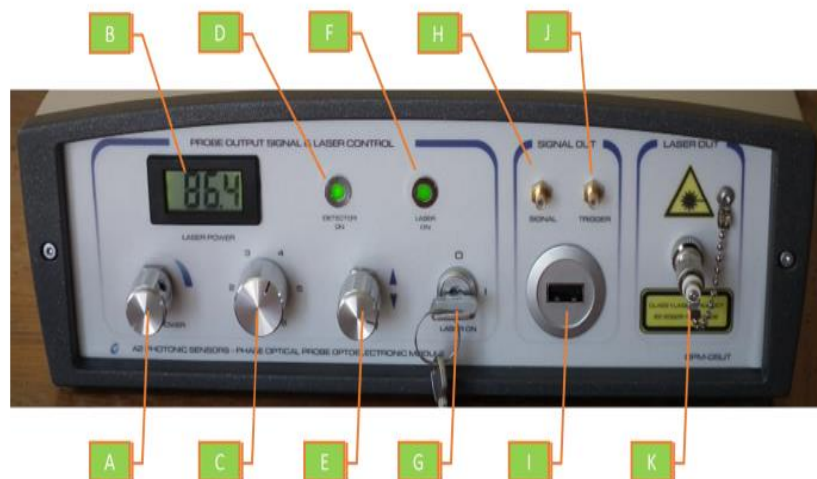
Figure 3. 5 Optoelectronic module, front panel (A. Laser intensity potentiometer; B. Laser control display; C. Laser gain selection switch; D. General power LED; E Laser offset potentiometer; F. Laser operation LED; G. Laser switch key; H. Raw (analogue) output; I. Digitized output; J. External trigger connector; K. Fibber optic connector for the probe).

3.4 Microalgae strain and cultivation media

Chlorella vulgaris (strain: CCAP 211/11B, CS-42) was provided by the Australian National Algae Culture Collection/CSIRO Microalgae Research and cultivated at Curtin University (Chemical Engineering labs). The standard medium (MLA, *Marine labs American society of microbiology-derived medium*) was used for the cultivation. All the high-grade chemicals that were used to prepare MLA were purchased from Sigma-Aldrich Pty Ltd, Australia and Chem-supply, South Australia. A variety of fully sterilized glassware items (beakers, Erlenmeyer flasks, flasks, cylinders, spatulas, funnels, filter holders and burets) were used to prepare the cultivation media. All the macro and micronutrients necessary for microalgae growth, and the preparation of stock solutions were obtained (see Table 3.1). They were then stored in the refrigerator at 4 °C. The medium was sterilized using a floor autoclave (Floor Autoclave, LABEC, Australia) at 120°C temperature for 15 minutes. To prepare the MLA Medium x40 concentrated nutrients (250mL volume) To 130 mL of distilled water, add 10 mL of $MgSO_4.7H_2O$, 20 mL of $NaNO_3$, 50 mL of K_2HPO_4, 10 mL of H_3BO_3, 10 mL of H_2SeO_3, 10 mL of Vitamin stock, and 10 mL of Micronutrient stock. Then, filter sterilize by placing a 0.22 μm filter into a sterile 250 mL Schott bottle. To prepare 1 L of fully autoclaved MLA medium, 973 mL of distilled water was added to 25 mL sterile MLAx40 and 1 mL of each sterilized $NaHCO_3$ and $CaCl_2.2H_2O$. Immediately, the pH value was adjusted to between 7.5 and 8 with HCl (often no adjustment was required). Using a fully sterilized laminar fume-hood (HWS Series, CLYDE-APAC, Australia) equipped with UV light, the surface was regularly wiped clean with 70% ethanol, the stock solutions and cultivation media poured directly into fully sterilized Schott bottles (1 or 2 L) and finally, stored in a refrigerator (5 °C) for further use.

3.4.1 Characterization and preparation of wastewater

Primary wastewater (P_{WW}) was collected from Beenyup municipal wastewater treatment plant, Western Australia. After that the *PWW* was filtered with 0.2 µm microfilters and autoclaved for 15 min at 120°C, the main characteristic of the *PWW* are summarized in Table.3.2

Table 3. 1 Components of the MLA standard medium used for cultivation.

Macro nutrients	Stock solution (g/L of distilled water)	Quantity used (ml)
$MgSO_4.7H_2O$	49.40	10.00
$NaNO_3$	85.00	20.00
K_2HPO_4	6.96	50.00
H_3BO_3	2.47	10.00
H_2SeO_3	1.29	10.00
$NaHCO_3$	16.90	1.00
$CaCl_2.2H_2O$	29.40	1.00
Micronutrients	Stock solution (g/800 ml of distilled water)	Quantity used (ml)
Na_2EDTA	4.36	10.00
$FeCl_3.6H_2O$	1.58	10.00
$NaHCO_3$	0.60	10.00
$MnCl_2.4H_2O$	0.36	10.00
$CuSO_4.5H_2O$	1.00	10.00
$ZnSO_4.7H_2O$	2.20	10.00
$CoCl_2.6H_2O$	1.00	10.00
$Na_2MoO_4.2H_2O$	0.60	10.00
Biotin	10 mg/100 ml dH_2O	0.05
Vitamin B12	10 mg/100 ml dH_2O	0.05
Thiamine HCl	10 mg/100 ml dH_2O	0.05

Table 3. 2 Nutrients content of the used PWW.

Nutrients	Concentration (mgL^{-1})
Total Nitrogen (TN)	30.60±1.21
Total phosphorous (TP)	6.60±0.24
Chemical oxygen demand (COD)	109.60±4.76

3.4.2 Pre-cultivation and preparation of stock culture

Chlorella vulgaris was inoculated in 250 mL Erlenmeyer flask containing 150 mL of autoclaved MLA medium at 10% concentration. The microalgae cells were cultivated in an incubator shaker (Bench Top Orbital Shaker, LABEC, Australia) at 150 rpm and 20°C under continuous illumination of white fluorescent light at 50 μmol m^{-2} s^{-1} for 2 weeks inside an incubator refrigerator (Temperature Cycling Chamber, LABEC, Australia) (Fig. 3.6). The Erlenmeyer flasks were shaken by hand to prevent sedimentation and adhering of microalgae cells inside the glass.

Sub-culturing, inoculation, sampling and medium transfer were carried out in Laminar Flow Workstation (HWS Series, CLYDE-APAC, Australia) equipped with UV-light sterilization and surfaces were cleaned with 70% ethanol. Algal media and flasks were all sterilized at 120° C for 15 minutes.

Figure 3. 6 Refrigerator incubator and shaker

3.5 Light intensity measurements

The photobioreactor was continuously illuminated by four white florescent lamps (each x 36 W). The external incident light on the photobioreactor's wall was measured using a quantum sensor (LI-192SA, LI-Core Inc.) (Fig. 3.7b). It was made of corrosion resistant metal with an acrylic diffuser (3.18 cm diameter × 4.62 cm height) and had a flat, high-stability, silicon photovoltaic detector. To measure the local light intensity inside the culture of the photobioreactor, a spherical micro quantum sensor (US-SQS, WALZ) was used (Fig 3.7a. It had a 3.7 mm diameter sphere made from highly scattering plastic. The number of florescent lamps was adjusted to get various light intensities between 150-400 μmol m^{-2} s^{-1} emitted to the photobioreactor.

Figure 3. 7 (a) Light meter connected with spherical sensor, (b) quantum sensor

3.6 Overall volumetric gas-liquid mass transfer coefficient

The mass transfer rate in the photobioreactor includes the exchange transfer of CO_2 and O_2 with the liquid cultivation medium. The mass transfer between gas-liquid interfaces can be explained on the basis of the film theory. The overall mass transfer coefficient $K_L a_L$ is given by [155]:

$$\frac{1}{K_L a_L} = \frac{1}{H k_G a_L} + \frac{1}{k_L a_L}$$

(3.4)

where $k_G a_L$, $k_L a_L$ are volumetric mass transfer coefficients of gas and liquid phases respectively. Assuming Henry's constant (H) is very large, then; $\frac{k_L}{H k_G a_L} \ll 1$;

Hence, the mass transfer can be considered to be dominated by the transfer resistance in the liquid phase. By disregarding the first term in Eq. (3.4), it is further simplified to Eq. (3.5):

$$\frac{1}{K_L a_L} \cong \frac{1}{k_L a_L} \tag{3.5}$$

where k_L is the liquid phase mass transfer coefficient, while a_L represents the interfacial area per unit volume. In addition, the boundary-layer theory in mass transfer was taken into consideration in predicting and correlating data for the hydrodynamic effects, such as the diffusion kinetics of gas absorption rate in mass transfer. The microalgae cell density was directly proportional to the O_2 and CO_2 utilization rates, and thus, with lower cell density culture, the biological utilization within liquid film and gas–liquid interface was negligible. Therefore, for an aerated bubble column photobioreactor system, the K_L was proportional to the square root of the diffusivity, D, which obeyed the penetration theory under identical hydrodynamic conditions. Throughout the measurable value of dissolved oxygen (DO) transferred to the culture medium, the transfer of CO_2 can be correlated by Eq. (3.6)[156]:

$$K_L a_L (CO_2) = \sqrt{\frac{D_{CO_2}}{D_{O_2}}} \, K_L a_L (O_2) \tag{3.6}$$

Where D_{O_2} and D_{CO_2} are the O_2 and CO_2 diffusivities at 25 ºC were $2 \times 10^{-9} m^2 s^{-1}$ and $2.41 \times 10^{-9} m^2 s^{-1}$, respectively.

Combining Eqs. (3.5) and (3.6) will result in eq. (3.7):

$$k_L a_L (CO_2) = \sqrt{\frac{D_{O_2}}{D_{CO_2}}} \, k_L a_L (O_2) \tag{3.7}$$

The dynamic gassing out method which measures the dissolved O_2 (DO) concentration as a function of time through a step change in O_2 inlet approach was used for determining the volumetric mass transfer coefficient of O_2 ($k_L a_L(O_2)$) in the photobioreactor. Firstly, the DO in the culture medium was stripped off by sparging nitrogen gas into the photobioreactor cultivation system. Then, the concentration of DO was monitored and recorded simultaneously, based on the aeration rates of individual bubble column photobioreactor cultivation system at steady state. The correlation of $k_L a_L(O_2)$ with DO concentration is indicated in Eq. (3.8) [157]:

$$ln\left(\frac{C^* - C_o}{C^* - C}\right) = k_L a(O_2).(t - t_o) \tag{3.8}$$

Where C^*, C_o, and C represent the DO concentration at saturation condition, initial DO concentration at initial time, t_o, and DO concentration at any time, t, respectively, for aeration rate from 1 to 10 L min^{-1}.

3.7 Mixing time (T_m)

The mixing time was measured for the two-phase system (air-water system). The acid tracer method [89, 158, 159] was used to measure the mixing in the bubble column and airlift reactors. Mixing time (T_m) was calculated as time required to attain 95% of complete homogeneous concentration after trace addition. After the reactor had been filled with tap water, the pH was dropped from 7 to 5 by adding hydrochloric acid (35% w/v). The reactor was then bubbled with air for 20 min to remove any carbonates as carbon dioxide. The pH was then raised to 4.5 by adding 12 M sodium hydroxide. Next, the acid tracer (40 ml of 35% HCL) was added instantaneously at the centre of the surface of dispersion. The change in pH with time was measured using two pH electrodes.

3.8 Instruments and analytical techniques

3.8.1 Cell counting

Microalgae cells were counted by placing a 10 μL sample in a Marienfeld Thoma counting chamber, which was placed under a light microscope at x40 magnification (ACHRO 40X/0.65, Saxon, New Zealand). The number of cells was enumerated in nine large squares of Thoma chamber, each measuring 16 x 0.0025 mm^2 with total area of 0.04 mm^2. The average number of cells was counted per small square. Then the cell number (D) was calculated using the following equation:

$$D = a \times [1/ (0.1 \times 0.2 \times 0.2 \times 1000)] \times 2500 \tag{3.9}$$

where D is the cells number in 1 ml, and a is the cells counted (Fig. 3.8). The ideal number of cells was between 30 and 70; however, for dense cultures, algal cells need to be diluted enough to ensure the cells distribute uniformly and can be counted accurately.
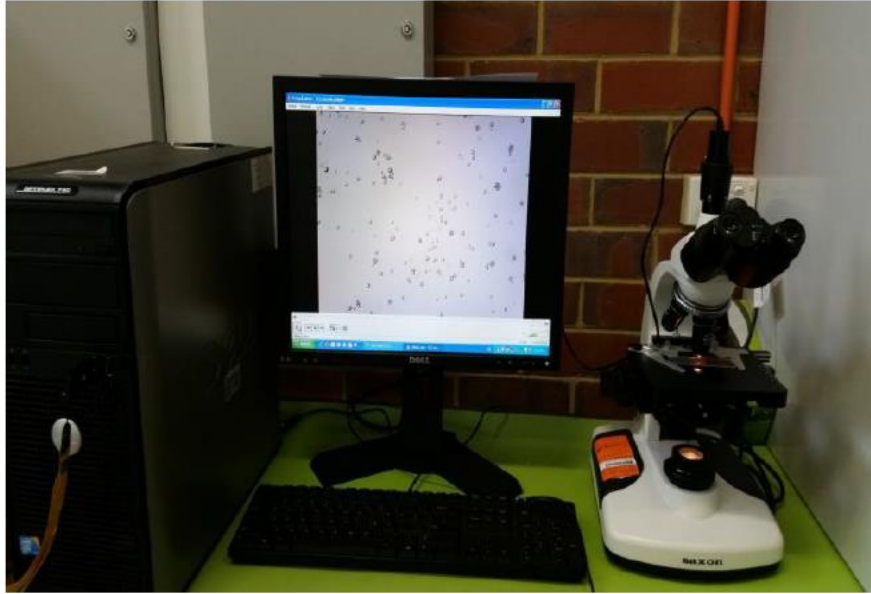
Figure 3. 8 Light microscope

3.8.2 Optical density and dry weight of biomass

Dry weight biomass of *Chlorella vulgaris* was determined through measuring the optical density (OD) using UV-Vis spectrophotometer (Jasco *V-670*) (Fig. 3.9). To determine a suitable wavelength that can detect *Chlorella vulgaris*, UV-vis absorbance was scanned over the spectrum range of 400 to 800 nm. At 692 nm, the maximum peak absorbance was observed and the optical density of *Chlorella vulgaris* was evaluated at this wavelength. Triplicate measurements were conducted for OD.

Algal biomass samples (10 mL) were filtered using a pre-weight glass filter (ADVANTEC type GC-50, 47 mm diameter, 0.45 μm). The algal dry weight samples were measured by drying the filter paper in the oven at 80°C for 24 hours. The initial and final weight of the filter paper was determined by lab analytical balance (AND HR-200). Biomass concentration was calculated from a pre-determined calibration equation of the OD at 692 and dry weight cell as in Eq. (3.10):

$$X \ (g \ L^{-1}) = 0.5544 \ OD_{692} + 0.3554 \qquad (R^2 = 0.99) \qquad (3.10)$$

The specific growth rate (μ) was then calculated from the initial and final biomass concentrations and the corresponding cultivation time:

$$specific\ growth\ rate\ (\mu) = \frac{\ln(X_t - X_o)}{\Delta t} \qquad (3.11)$$

where X_o and X_t are the initial and final biomass concentrations (g L^{-1}), respectively, and t is the cultivation time in days.

Biomass productivity, P_X, was calculated using the following equation:

$$Biomass\ productivity\ P\ (gL^{-1}day^{-1}) = \frac{X_t - X_o}{\Delta t} \qquad (3.12)$$
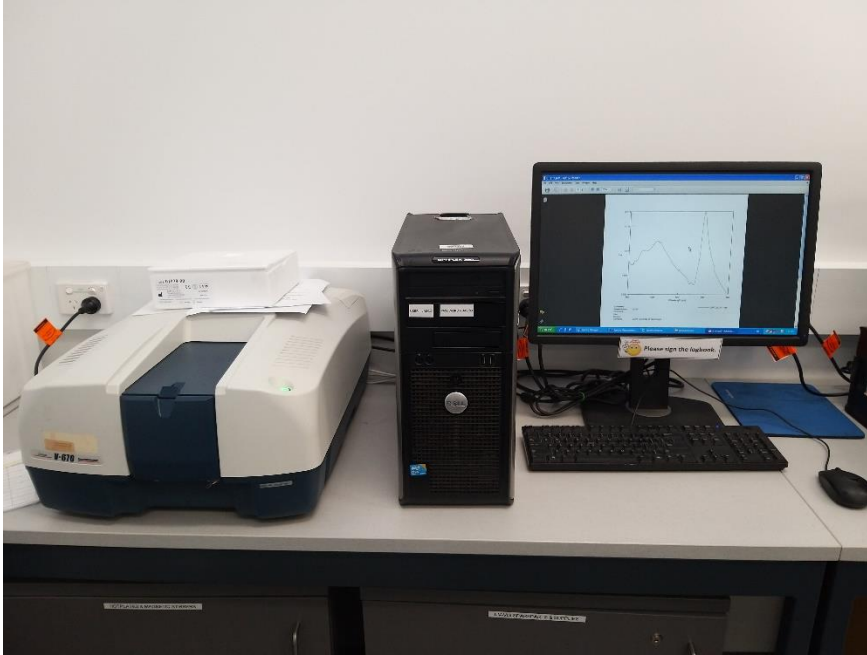
Figure 3. 9 UV-vis spectrophotometer

3.8.3 Lipid extraction

Lipid content was measured using a modified Bligh and Dyer method [160]. 0.05 g of biomass freeze dried sample was used. A mixture of 2 ml chloroform and 2 ml methanol solvent (1:1) in a test tube, then a 2 ml of 0.88% NaCl was added and shaken to enhance the lipid extraction. The mixture centrifuged at 5000 rpm for 3 minutes. Two phases were observed: top layer (methanol/water) and bottom layer (chloroform). The chloroform-methanol layer that contained the extracted lipids was separated and placed in a vacuum rotary evaporator (R-201, Rose Scientific Ltd, Canada) at 5 psi pressure and temperature of 70°C to remove the solvent. Lipid content (%) was calculated using the Eq. (3.13):

$$Lipid\ content\ (\%) = \frac{weight\ of\ extracted\ lipid}{weight\ of\ biomass} \times 100 \qquad (3.13)$$

3.8.4 CO_2 biofixation and removal efficiency

The total carbon content of dried biomass (%C) was measured by the elemental analyser (PerkinElmer, 2400 Series II CHNS/O), (Fig.3.10). Microalgae cells were harvested by centrifugation at 5000 rpm for 15 min (C-28A, BOECO, and Germany) and the supernatant decanted. The cell pellets were washed with distilled water and then freeze-dried at -50 °C for 15 h (Alpha 2-4 LDplus Laboratory Freeze Dryer, Christ, and Germany). The CO_2 biofixation rate (g CO_2 L^{-1} d^{-1}) was calculated according to Eq. (3.14):

$$CO_2 \, biofixation \, rate = \%C \times Biomass \, productivity \times \frac{MW_{CO_2}}{MW_c} \tag{3.14}$$

where MW_{CO_2} and MW_c are the molecular weight of CO_2 and carbon respectively. In order to calculate the CO_2 removal efficiency, the CO_2 concentration was controlled and measured in the inlet and outlet flow of the photobioreactor. The CO_2 concentration at the inlet flow of air/CO_2 was set on 2% (v/v). The result of the outlet CO_2 concentration from the bioreactor was an average of 20 times measurement during the day by the CO_2 meter (Viasensor, G110). The CO_2 removal efficiency (%) was calculated by using Eq. (3.15).

$$CO_2 \, removal \, efficiency \, (\%) = \left(1 - \frac{CO_2 \, outlet}{CO_2 \, inlet}\right) X \, 100 \tag{3.15}$$

Figure 3. 10 Element analyser

3.8.5 Total nitrogen (TN) and total phosphorous (TP) analysis

Total Nitrogen (TN) and Total Phosphorus (TP) concentrations in wastewater samples were measured calorimetrically using HACH test kits (DR/890 Colorimeter, HACH, USA) (Fig. 3.11). A 0.45 μm-filter was used to separate the algal cells. For TN determination method, an

alkaline persulfate digestion was used to convert all nitrogen forms to nitrate. Then, 1 pillow of sodium metabisulfite was added after the digestion in order to eliminate halogen oxide interference. Nitrate reacts with chromotropic acid (1 vail) under strongly acidic conditions to form a yellow complex with an absorbance peak near 420 nm.

For TP analysis, phosphates present in organic and inorganic forms (meta-, pyro- or ortho) must be converted to reactive orthophosphate before analysis. Pre-treatment of sample with acid and heat provides the conditions for hydrolysis of the inorganic forms. Organic phosphates are converted to orthophosphate by heating with acid and persulfate. These examinations were adopted from a standard persulfate digestion method ((HACH DR/890 colorimeter procedure manual, 2013, method 10072).

3.8.6 Analysis of chemical oxygen demand (COD)

COD was analysed using DR/890 HACH spectrophotometer (Method, 8000). COD measured by mg of O_2 consumed per litre of sample. In this procedure, samples were heated for 2 hours with strong oxidizing agent, potassium dichromate. Oxidizable organic compounds reacted, reducing the dichromate ion ($Cr_2O_7^{-2}$) to green chromic ion (Cr^{3+}). Then, the amount of Cr^{3+} produced was determined. The COD reagent also contained silver and mercury ions. Silver is a catalyst, and mercury is used to complex the chloride interference.

Figure 3. 11 HACH Spectrophotometer

3.8.7 Experimental Design and regression analysis

Box Behnken Design (BBD) experimental design employs a matrix of tests based on a number of parameters. The impact of each parameter is evaluated by selecting three or more values (or

"levels") of these parameters and then conducting tests which encompass every combination of each parameter value. The results of the experiments in terms of the impacting (or "response") parameters can then be evaluated through a statistical model. Two such multi-level, three-parameter BBD matrices were created to examine the synergistic relationships between these sets of three parameters within specific limits. A total of 15 experimental runs, randomly sequenced in duplicate to reduce the effect of the temporal-related errors were conducted to determine the 10 coefficients of the second order polynomial generated from the statistical model. *JMP* statistical discovery software (SAS v11.2.1) was used to complete the regression analysis and generate the graphical relationships. The variability of the factors was expressed as coefficient of determination (R^2) values. The model equation was then used to identify the interaction between the variables within the specified experimental boundary conditions. To identify the maximum conditions of the selected responses, the desirability function in Derringer's desired function (DDF) methodology was maximized.

BBD was employed to the algal growth, expressed as μ in d^{-1}, biomass productivity *PX* in g (dry weight) biomass $L^{-1} d^{-1}$, CO_2 capture (*RC*), as a function of feed C_{CO_2}, *I*, and *T*, and, (b) nutrient removal, as a function of feedwater composition with reference to *TN* and *TP*.

The quadratic model used to predict the optimum response is expressed as follows:

$$Y = \beta_o + \sum_{i-1}^{k} \beta_{ii}\, y_i^2 + \sum_{i-1}^{k}\sum_{j-1}^{k} \beta X_i + \varepsilon \tag{3.16}$$

where *Y* is the response variable; *i* and *j* are the index numbers for the patterns; β_o is the constant coefficient; β_i, β_{ii} and β_{ij} are the regression coefficients for linear, quadratic, and interaction influence, respectively. The coded value (x_i) of the independent parameters (*X*) is defined by the following equation:

$$x_i = \frac{X_i - X_o}{\Delta X_i} \tag{3.17}$$

where X_i is the actual value of the independent factors, X_o is the actual value of the factor at the centre point, and ΔX_i is the step change value.

Chapter Four
Influence of Gas Sparger Type on the Hydrodynamics of Bubble Column in Bubbly Flow

4.1 Introduction

A bubble column is a multiphase reactor that is widely used in biochemical, chemical, petrochemical, and environmental engineering [161]. The industrial importance of bubble columns as gas-liquid contactors is mainly due to several reasons, such as their easy construction, low operating cost, high energy efficiency, high mass and heat transfer. Bubble columns can provide a high interfacial area for mass and heat exchange, good mixing, and high thermal stability due to the presence of a gas phase dispersed in a liquid phase. In addition to the qualities of mass transfer, it is important to inject and distribute the gas effectively with minimal pressure drop, thereby saving energy. The gas dispersion into the column is an important aspect that determines the performance of bubble columns [162]. Despite their widespread usage, scaling up bubble column reactors remains an ongoing challenge [161]. The scaling up and design of bubble columns have attracted considerable interest recently because of their complex hydrodynamics and their effect on transport characteristics. Despite the simple construction of bubble columns, proper and successful design and scaling up demand a better understanding of the hydrodynamics of multiphase fluid and its influences [59].

Hydrodynamics in bubble columns have been studied extensively in recent years due to their wide range of applications. Important hydrodynamic parameters include flow regime, gas holdup, gas-liquid interfacial area and bubble size distribution [163]. The hydrodynamics of bubble columns are highly affected by operating conditions, reactor geometry, and gas sparger design. Two flow regimes are noticed in bubble columns: homogenous, which occurs at low superficial gas velocity (U_G<5 cm s^{-1}), small bubble size, identical bubbles and a radically uniform gas holdup profile; and heterogeneous, which occurs at high superficial gas velocity, where small bubbles coalesce and form large bubbles [162]. Therefore, homogenous flow is more desirable in biochemical processes due to its capacity to provide a maximum contact area and minimum shear rate that can influence the microorganisms inside the bubble column.

Gas holdup (ε_G) is defined as the ratio of gas phase volume to the total volume of the system. It is one of the most important parameters that affect the performance of the bubble column due to the combining of the phase fraction and residence time of the gas phase which is important for mass transfer between the gas and liquid phases [164]. It has been reported that gas holdup is affected by superficial gas velocity, liquid properties, and gas sparger design [59]. Gas holdup is related linearly to superficial gas velocity. Increasing gas velocity leads to an increase in gas holdup, which is desirable due to an increase in the gas-liquid interfacial area

and hence, an increase in mass transfer rate. Many researches have stated that the effect of column dimensions ($D > 10$ cm and $H > 100$cm) is insignificant.

Specific gas-liquid interfacial area (*a*) is characterized by the available mass transfer area between the gas and liquid phases, an important goal of the process. Enhancement of the gas-liquid interfacial area is achieved by creating small bubbles or increasing the number of bubbles [59]. Similar to gas holdup, it depends on the superficial gas velocity, liquid properties, and gas sparger design. For a given gas holdup, a maximum interfacial area is gained if the gas bubbles created are small [59]. In addition, the interfacial area is linearly related to superficial gas velocity in a homogenous flow regime, and it decreases on transition and within a heterogeneous flow regime due to the forming of large bubbles.

In addition to gas holdup and gas-liquid interfacial area, another important hydrodynamic parameter of the bubble column is the bubble size. The bubbles created at the gas sparger change size gradually along the bubble column due to coalescence and break-up phenomena [165]. Smaller bubble size is favourable for producing a maximum gas-liquid interfacial area that increases the mass transfer rate in the bubble column. Gas sparger and superficial gas velocity also influence the bubble size distribution inside the bubble column.

Several sparger types may be used to disperse the gas into the column. These are perforated plates, cross spargers, and ring spargers. Many researchers have found that the sparger design for a specific geometry of bubble columns, as well as for a particular reaction, is crucial for overall bubble column performance [166]. In addition, designing a sparging device that covers all hydrodynamic flow regimes is crucial to prevent maldistribution at low superficial gas velocities [103]. The type of sparger and the sparger orifice determine the initial bubble size in the lower section of the bubble column. The bubble size, in turn, determines the bubble rise velocity and with it, the average gas holdup, as well as its radial profile. Furthermore, it is well-known that the liquid velocity profile follows the gas holdup profile [124] and is decisive for the mixing behaviour. Therefore, the design of the gas sparger determines overall bubble column hydrodynamics and, thus, bubble column performance [167].

The main objective of this study was to investigate the hydrodynamic influence on the bubble column and its performance using three different types of gas spargers: perforated plate sparger, cross sparger, and ring sparger. Gas holdup, gas-liquid interfacial area, and bubble size were measured using optical probes and the results obtained were compared for the three different types of gas sparger. The findings of this study will be applied in a real system in a bubble column photo-bioreactor to see how the presence of microalgae affects the parameters that are being measured.

4.2 Materials and Methods

A cylindrical bubble column of clear acrylic material with working volume of 5200 cm^3 (as described in Chapter 3) was used to investigate the influence of three different gas spargers (Table 4.1) on the hydrodynamic behaviour. Experiments were performed at superficial gas velocities (U_G) of 0.48, 0.96, 1.44, 2.4, and 4.8 cm s^{-1}. Air/tap water was used as the gas and liquid phases. All experiments were conducted at room temperature.

Table 4. 1 Characteristics of gas spargers applied

Sparger type	Sparger geometry	Open area ratio (%)	Orifice Diameter, d_o (mm)
Perforated Plate		3.14	1
Cross Sparger		0.972	1
Ring Sparger		0.573	1

The bubbles properties (local gas holdups, bubble arrival frequency, bubble rise velocity, and bubble chord length) were measured and analysed using the optical fibre probe (for full details, see Chapter 3). Gas holdup, bubble arrival frequency, gas-liquid interfacial area, and bubble chord length were measured using an optical fibre probe at various *H/D* ratios of 2, 3, and 5. Measurements were done in triplicate at radial positions of *r/R*= 0 mm, ± 0.575, and ± 0.787 with the probe pointing down. For all results, data were generally collected for a period of 60 s with a minimum of 1000 bubbles.

4.3 Results and discussion

4.3.1 Gas Holdup (ε_G)

Gas holdup is the most important parameter used for the design and scaling up of bubble column reactors. The optical fibre probe was placed in three different axial positions (H/D = 2, 3, and 5 cm) from the base of the reactor. During preliminary experiments in the centre of each axial position of the reactor, no significant statistical axial variation of gas holdup was observed, and hence, the gas holdup data reported at each axial location were the average of three measurements carried out at the radial centre. Gas holdup data reported for the bubble column were studied against the superficial gas velocity (U_G).

Fig. 4.1 shows the variation of gas holdup and superficial gas velocity for the three types of gas sparger (perforated plate sparger, cross sparger, and ring sparger) at different heights (H/D ratios). The results revealed that the gas holdup increased linearly with superficial gas velocity. This trend was consistent with previous studies [168, 169]. The reason is the creation of bubbles, small and uniform in shape, that do not coalesce and break up in this flow regime. Smaller bubbles rise inside the column with low rising velocity which leads to an increase in the residence time of the bubbles, resulting in an increase in gas holdup [170]. The highest gas holdup at different *H/D* ratios was achieved when the perforated plate sparger was applied regardless the *H/D* ratios (Fig. 4.1) which is attributed to the higher bubble arrival frequency (later shown in Fig. 4.2) and the small bubble size that led to increase gas holdup [171].
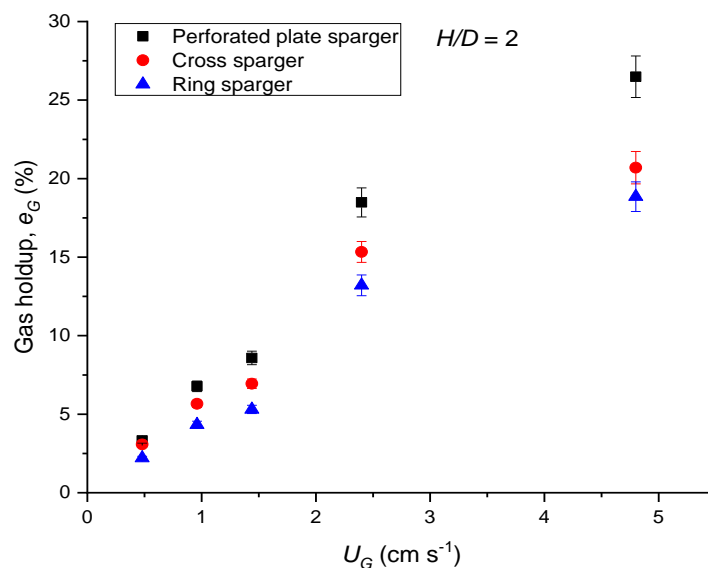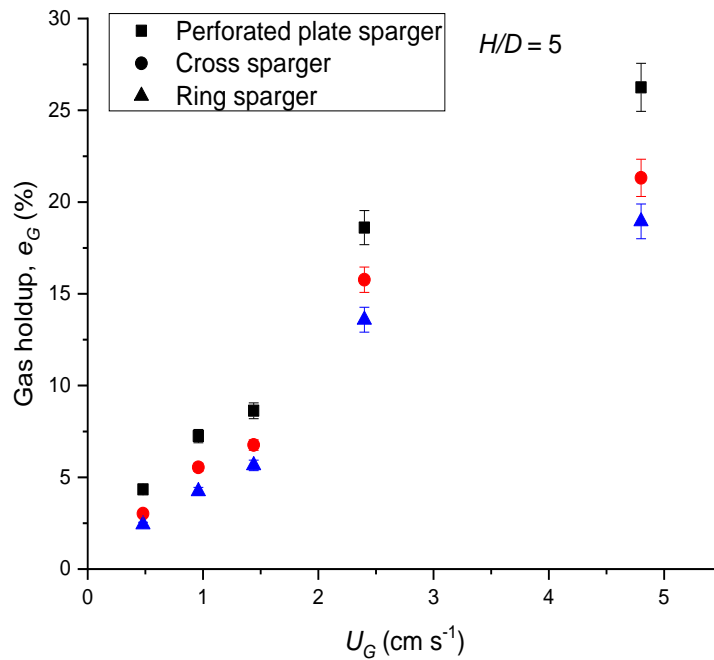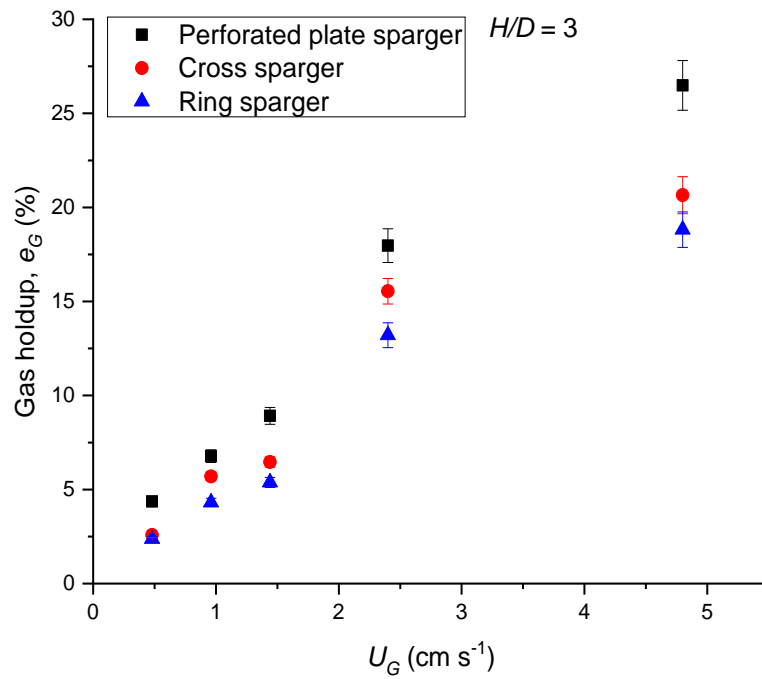
Figure 4. 1 Variation of gas holdup with superficial gas velocity using different spargers and at different *H/D* ratios (2, 3, and 5)

As shown in Fig. 4.1, at low superficial gas velocity (0.48 cm s^{-1}), the three sparger types showed comparable values of gas holdup. Therefore, there is no significant influence of sparger type on gas holdup. Similar findings were reported by Lau et al. [103], who concluded that there is no considerable difference in gas holdup at low superficial velocities for different types of sparger. At higher superficial gas velocities ($U_G > 0.48$ cm s^{-1}), the rate of gas holdup becomes higher, due to the production of more uniform and smaller bubbles.

4.3.2 Gas Holdup Correlation Development

The relationship of gas holdup to gas superficial velocity is governed by Eq. (4.4) [172]:

$$\varepsilon_G = \alpha\, U_G^n \tag{4.4}$$

where α and n are constants. In the bubbly flow (homogenous flow), n is in the range of 0.7 to 1.2 while in churn turbulent flow (heterogeneous flow), it is in the range of 0.4 to 0.7. The values for α and n for the three spargers are listed in the Table 4.2.

Table 4. 2 Gas holdup correlations for the three spargers

Sparger type	Correlation	R^2
Perforated Plate	$\varepsilon_G = 0.0875 U_G^{0.8114}$	0.9773
Cross	$\varepsilon_G = 2.8083 U_G^{1.0002}$	0.9974
Ring	$\varepsilon_G = 2.1367\, U_G^{1.0233}$	0.9965

In the literature, many correlations for gas holdup predictions can be found. Some of these correlations are listed in Table 4.3.

Figure 4.2 illustrates the comparison of the experimental data with these correlations (in Table 4.3). It appears that there is good agreement between the experimental data and the gas holdup correlations (in Table 4.2), while a big discrepancy was noticed when applying the correlations in Table 4.3. The reason may be because of the type of sparger used.

Table 4. 3 Various gas hold ups correlations for bubble column and 2 phase system (Gas/liquid system).

Author	Correlation
Kumar, et al. [173]	$\varepsilon_G = 0.728\,U - 0.485\,U^2 + 0.0975\,U^3$
	$U = U_G \left[\dfrac{\rho_l^2}{\sigma\,(\rho_l - \rho_g)g} \right]^{0.25}$
Hikita and Kikukawa [174]	$\varepsilon_G = 0.505\,U_G^{0.47} \left(\dfrac{0.072}{\sigma}\right)^{\frac{2}{3}} \left(\dfrac{0.001}{\mu_l}\right)^{0.05}$
Reilly, et al. [175]	$\epsilon_G = 296\,U_G^{0.44}\,\rho_l^{-0.98}\,\sigma_l^{-0.16}\,\rho_g^{0.19} + 0.009$
Hikita, et al. [176]	$\epsilon_G = 0.672\,U_G^{0.574}\,\rho_l^{0.069}\,\rho_g^{0.062}\,\sigma^{-0.185}\,\eta_l^{-0.053}\,\eta_g^{0.107}\,g^{-0.131}$
Hughmark [177]	$\epsilon_G = \dfrac{1}{\left[2 + \left(\dfrac{0.35}{U_G}\right) \left(\dfrac{\rho_l\,\sigma}{72}\right)^{\frac{1}{3}}\right]^{0.5}}$
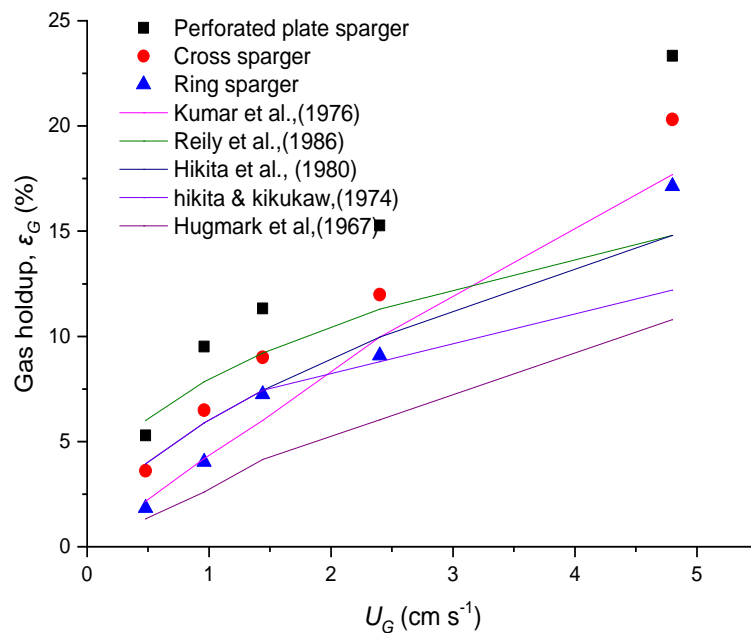
Figure 4. 2 Comparison between experimental data and correlations

Mersmann [178], stated that the Weber number is important for designing the gas sparger to show the effect of sparger type (number of holes and size of orifice diameter) and for enhancing the axial mixing in the liquid phase. A Weber number is a dimensionless number and can be calculated by:

$$W_e = \frac{\rho_g \, U_{Go}^2 \, D_c^4}{N_o^2 \, d_o \, \sigma} \tag{4.5}$$

where ρ_g is gas density (kg m^{-3}), U_{Go} is gas velocity through orifice (m s^{-1}), D_c is column diameter (m), N_o is number of orifices, d_o is orifice diameter, and σ is liquid surface tension. Fig. 4.3 shows the relationship between the Weber number for the three spargers and overall gas holdup. The relationship is linear for all spargers and the Weber number is the same as the relationship between gas holdup and superficial gas velocity. The values for W_e for the three spargers are listed in the Table 4.4.
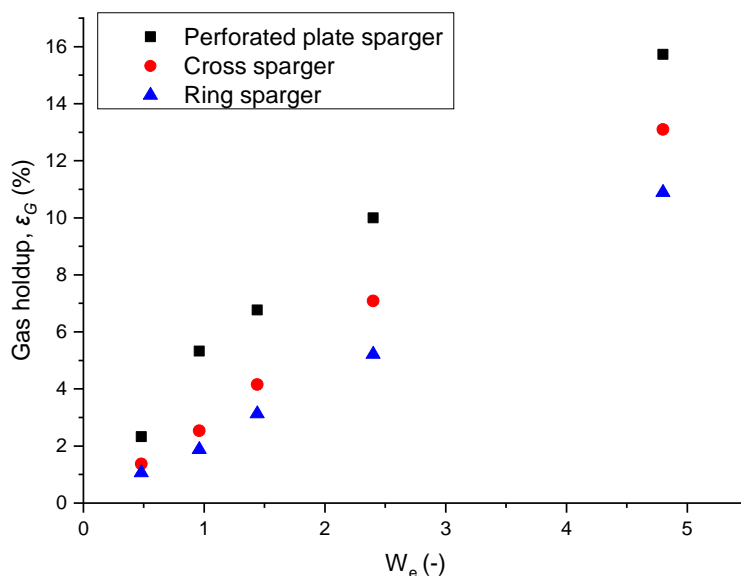
Figure 4. 3 Effect of sparger type on overall gas holdup

Table 4. 4 Correlations to predict the overall gas holdup for the three sparger types

Sparger type	Correlation	R^2
Perforated Plate	$\varepsilon_G = 4.7974 W_e^{0.4053}$	0.9775
Cross	$\varepsilon_G = 2.8112 W_e^{0.5}$	0.9974
Ring	$\varepsilon_G = 2.1387 \, W_e^{0.5116}$	0.9965

Figure 4.4 illustrates the local gas holdup profile for the three sparger types at different *H/D* ratios. The error bars of triplicate measurements are also displayed. Increasing superficial gas velocity led to an increase in gas holdup with a minimum value at the centre of the bubble column and minimum value near the wall. The gas holdup profile was flat at low superficial velocity and became parabolic with increasing U_G, with a similar trend was achieved by other studies [124, 179]. In addition, Razzak et al. [14] stated that at the wall, the shear rate or velocity gradient was high which led to a pressure difference allowing the bubbles to move to the column centre.
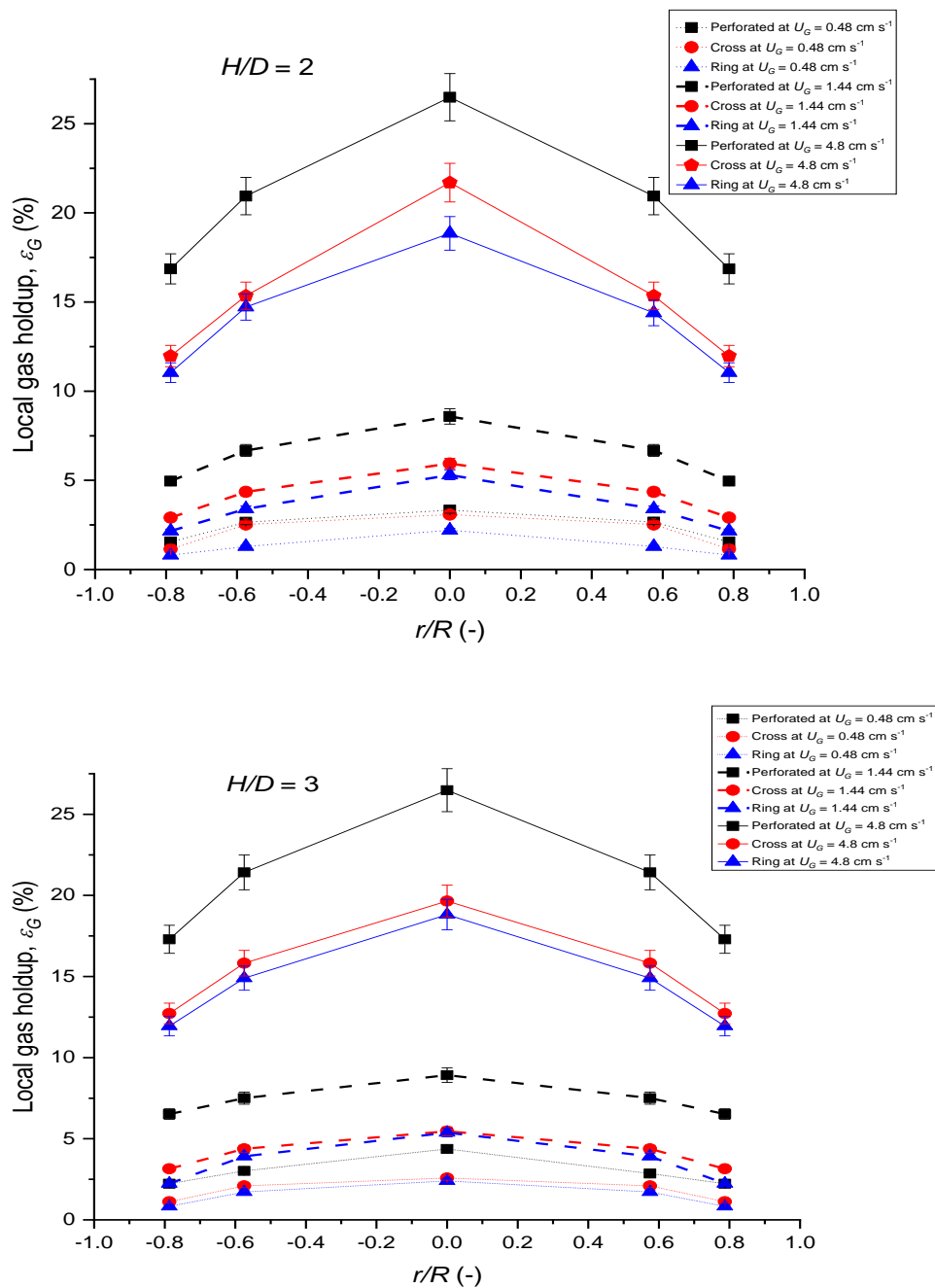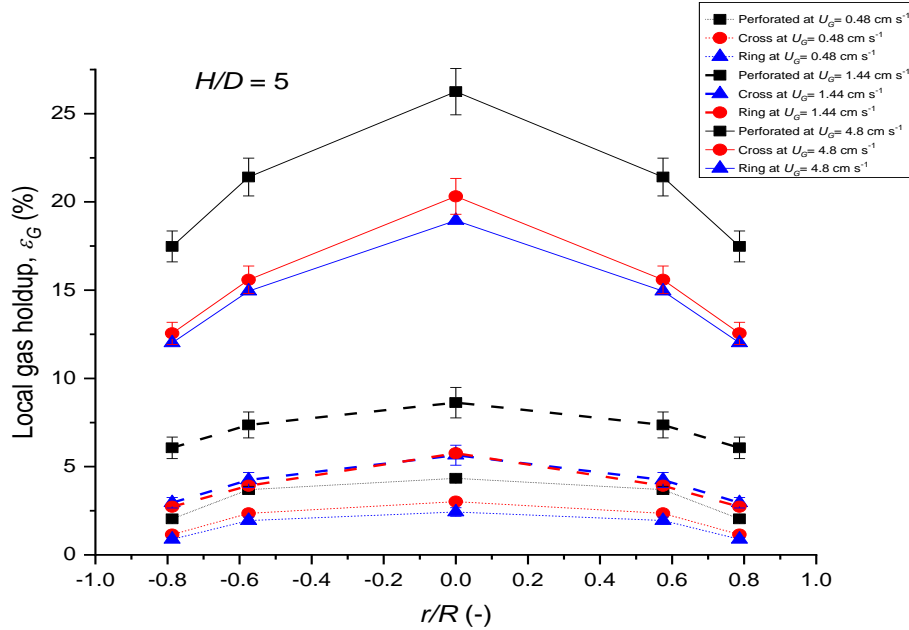
Figure 4. 4 Sparger effect on local gas holdup profile at various H/D ratios (2, 3, and 5)

The possible reason for this trend is that the number of bubbles increased with increasing superficial gas velocity leading to an increase in gas holdup. Xue et al. [180], investigated the measurement of bubble column hydrodynamics using a four-point optical probe. They reported that at $U_G \leq 2$ cm s^{-1}, the gas holdup and interfacial area profiles were flat and became parabolic with an increase in superficial gas velocity. According to Jin et al. [179], the large bubbles concentrated in the centre of the bubble column while the smaller bubbles were denser near the wall. As a result, the gas holdup profile was much more non-uniform with increasing superficial gas velocity.

Results demonstrated in Fig.4.4 show that among the spargers investigated, the perforated plate provided the highest local gas hold up profile across the column in all the *H/D* ratios. The perforated plate sparger was characterised by the highest numbers of activated orifices that generated large amount of small bubbles rising upward at low superficial velocity (U_G) without bubble-bubble coalescence, and this characteristic was even more prominent at high U_G.

4.3.3 Bubble Arrival Frequency (f)

Bubble arrival frequency refers to the number of bubbles that hit the central tip of the fibre optical probe per total time of sampling [181]. There have been few studies in the literature investigating the bubble arrival frequency in bubble column reactors [181-183]. However, none of these investigated the influence of gas sparger on bubble arrival frequency. Figure 4.5

illustrates the variation of bubble arrival frequency at different H/D ratios (2, 3, and 5) with superficial gas velocity ranging from 0.48 cm s^{-1} to 4.8 cm s^{-1}. From the data in Fig. 4.5, it is apparent that the bubble arrival frequency follows a similar trend to that of gas holdup. Increased superficial gas velocity led to an increase in bubble arrival frequency, supporting the findings of previous studies [184, 185]. In addition, as shown in Fig 4.5, there is little variation in bubble arrival frequency with axial position in all three sparger types. The results of this study revealed that a higher value of bubble arrival frequency was obtained with the perforated plate sparger due to the high gas holdup achieved. Choi and Lee [186], stated that gas holdup, bubble size, and bubble rise velocity influence the bubble arrival frequency. Like gas holdup, there was no significant effect of sparger type on bubble arrival frequency at low superficial gas velocity ($U_G < 0.48$ cm s^{-1}).
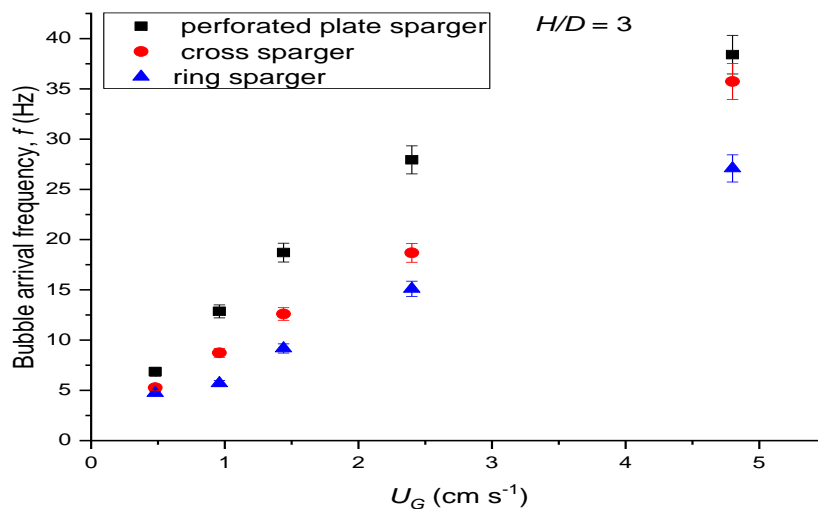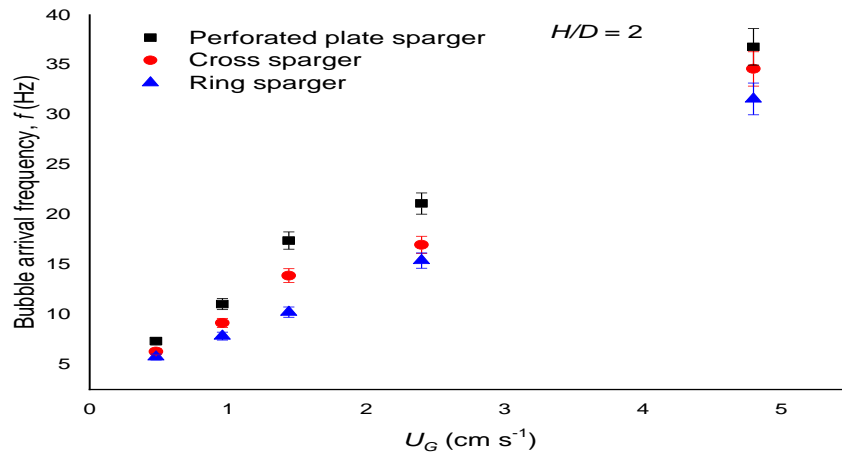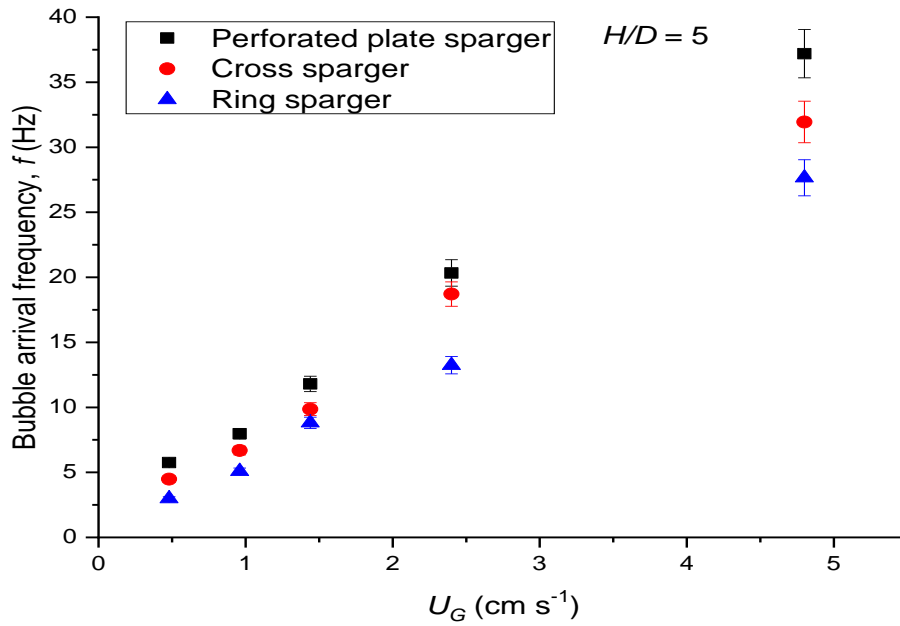
Figure 4. 5 Comparison of bubble arrival frequency for various spargers with different U_G at different H/D ratio (2, 3, and 5)

4.3.4 Gas-Liquid Interfacial Area (a)

Gas-liquid interfacial area is defined as the ratio of bubble surface area to liquid unit volume [187]. Gas-liquid interfacial area is an important parameter that influences the performance of bubble column reactors. It depends on gas holdup and bubble size, which in turn depend on the gas flow rate and liquid phase properties. The gas-liquid interfacial area can be calculated from Eq. (4.6):

$$a = \frac{\varepsilon_G}{d_b} \tag{4.6}$$

where a is the gas-liquid interfacial area (m^2/m^3), ε_G is the gas holdup, and d_b is the bubble diameter (m).

Figure 4.6 shows the variation of gas-liquid interfacial area (a) with superficial gas velocity at different heights, *H/D* (2, 3, and 5). For all types of spargers, the gas-liquid interfacial area increased with an increase in superficial gas velocity. Similar behaviour was observed by Hernandez-Alvarado et al. [188], who measured the gas holdup, bubble size, and interfacial area in bubble columns. The reason is that at a higher gas flow rate, a larger amount of bubbles are entrained which leads to an increase in gas holdup and bubble population, and thus, an

increase in gas-liquid interfacial area. The higher interfacial area in all axial locations obtained with perforated plate sparger was due to higher gas holdup and bubble frequency compared with the other types of sparger used. Gas-liquid interfacial area increased with increasing superficial gas velocity which was due to the dependency on the gas holdup and bubble size. The interfacial area at the centre of the bubble column is the maximum value due to the bubbles' tendency to move towards the centre instead of the wall region [14]. The high interfacial area was found at *H/D* ratio of 5. The main explanation is that larger bubbles are created due to bubble coalescence and move to a higher region that leads to a concentration of the large bubbles. In addition, Kagumba and Al-Dahhan [184], reported that the increase in the gas-liquid interfacial area was higher with superficial gas velocity in the range ≤ 10 cm s^{-1}.
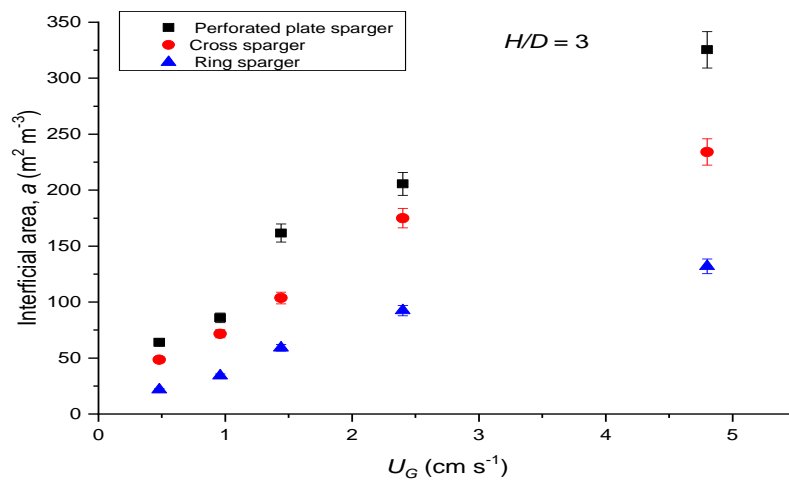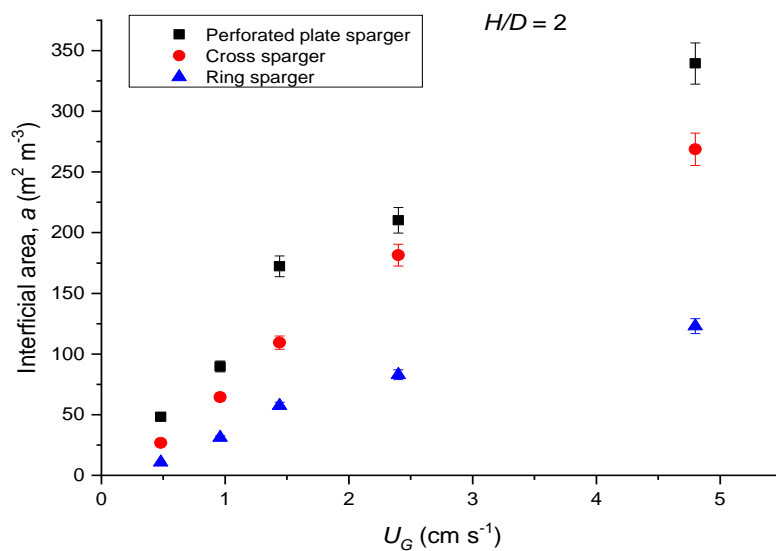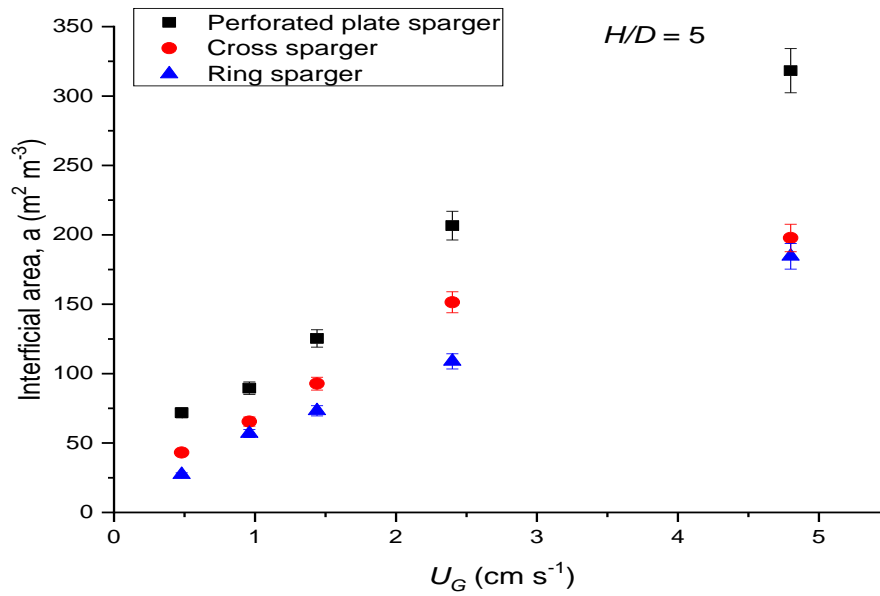
Figure 4. 6 Variation of gas-liquid interfacial area with U_G for various spargers and at different H/D ratio (2, 3, and 5).

Figure 4.7 illustrates the radial profile ($r/R = 0$, $r/R = \pm 0.575$, and $r/R = \pm 0.787$) of the gas-liquid interfacial area at various axial positions ($H/D =2$, $H/D = 3$, and $H/D = 5$) with different superficial gas velocity (0.48, 1.44, and 4.8 cm s⁻¹). It is noteworthy that the radial profile trend of the interfacial area was similar to the gas holdup profile [184]. As shown in Fig. 4.7, the interfacial area profile is flat at low superficial gas velocity ($U_G < 0.48$ cm s⁻¹) and becomes parabolic with increasing superficial gas velocity due to the bubbles' tendency to move towards the centre region of the bubble column, not to the reactor wall. Razzak et al. [14], reported that the shear rate or velocity gradient is high at the wall leading to a pressure difference allowing the bubble to move to the centre. Increasing superficial gas velocity causes an increase in gas-liquid interfacial area as a result of a significant increase in bubble population, consequently increasing the interfacial area[184]. From the data in Fig. 4.7, it is apparent that the higher value of the interfacial area obtained with perforated plate sparger is due to the higher value of gas holdup and bubble frequency achieved with the perforated plate sparger. Wu [189], reported that gas holdup and interfacial area increased with an increase in bubble frequency.
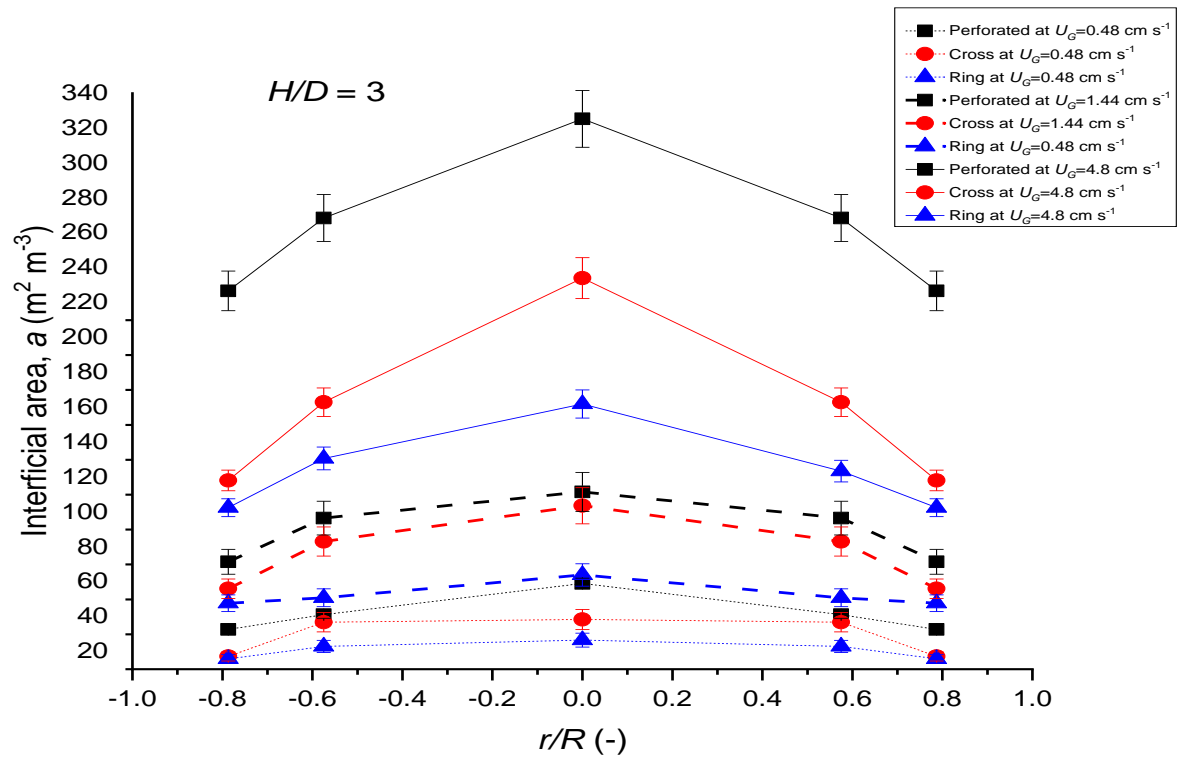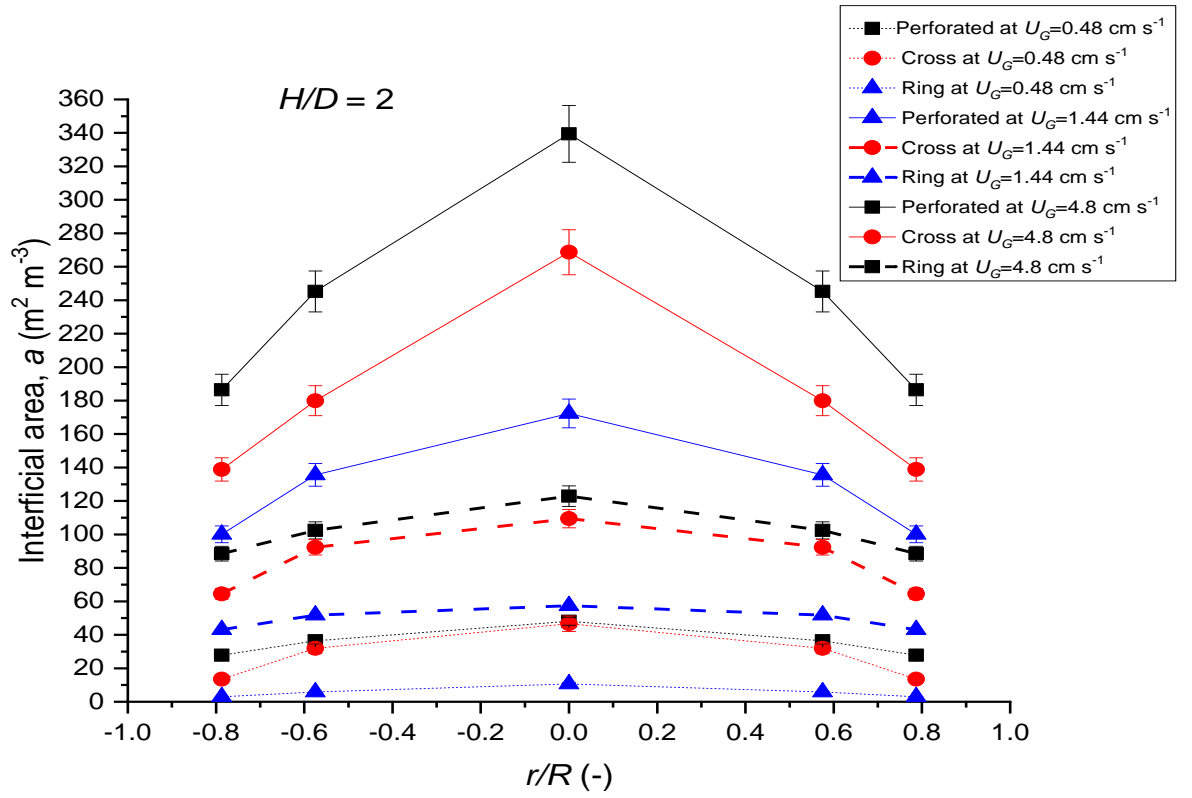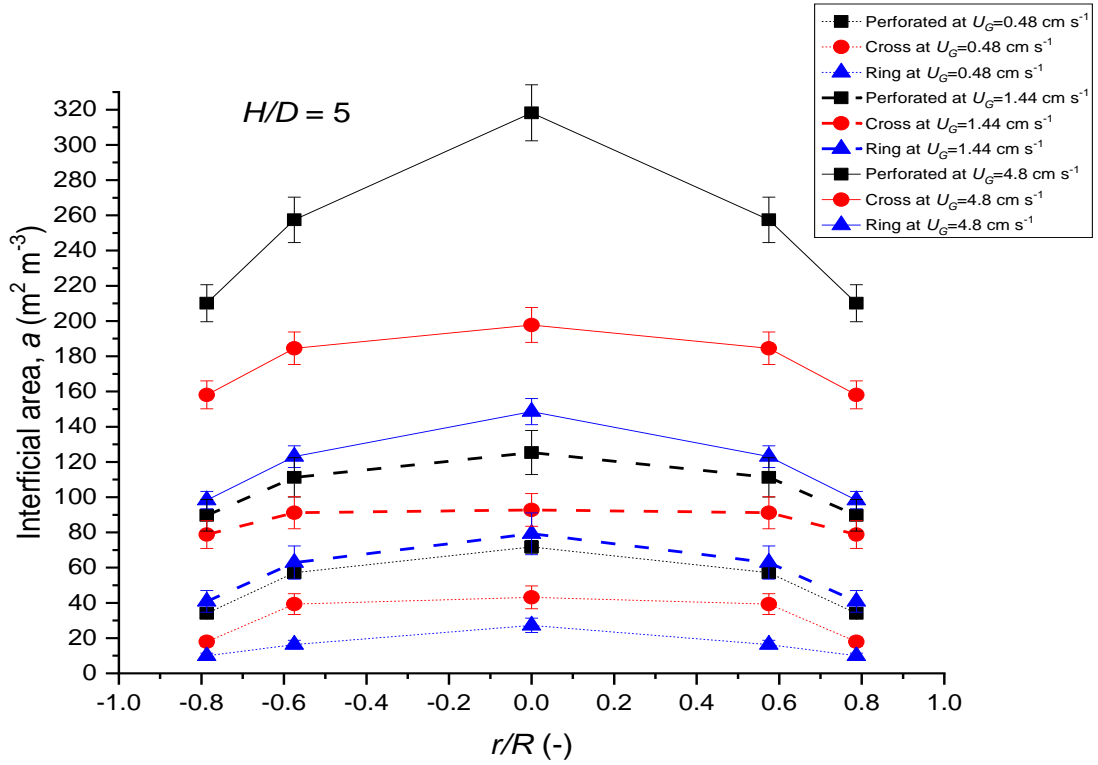
Figure 4. 7 Sparger effect on gas-liquid interfacial area profile at various H/D ratio (2, 3, and 5) and U_G (0.48-4.8 cm s^{-1}).

4.3.5 Bubble Chord Length (l_c)

In order to better investigate the influence of gas spargers on the hydrodynamics of bubble columns with respect to gas holdup and gas interfacial area, the bubble chord length must be determined. Lau et al. [103], stated that bubble size identified by chord length is an essential parameter to determine the performance of bubble column reactors. Luewisutthichat et al. [190], reported that log-normal distribution is a good way of representing bubble size distribution. Log-normal distribution is expressed as shown in Eq. (4.7) [184]:

$$PDF(l_c) = \frac{1}{\sigma l_c \sqrt{2\pi}} \, exp\left[-\frac{(ln l_c - \mu)^2}{2\sigma^2}\right] \tag{4.7}$$

where l_c is the chord length measured by the optical probe, μ and σ are parameters in log-normal distribution related to the variance υ and mean m. μ and σ are calculated from:

$$\mu = log \frac{m^2}{\sqrt{\upsilon + m^2}} \tag{4.8}$$

$$\sigma = \sqrt{log\left(\frac{m^2 + \upsilon}{m^2}\right)} \qquad (4.9)$$

Figure 4.8 presents the effect of gas spargers on bubble size distribution at the centre of the bubble column with different *H/D* ratios 2, 3, and 5 at a superficial gas velocity of U_G (0.48 and 4.8 cm s^{-1}). The hydrostatic liquid height was below 1 m, therefore, the effect of liquid height on the bubble size was negligible. Lau et al. [103], stated that the pressure of the liquid height less than 100 cm is about 0.1 atm and has almost no influence on the bubble size. At low superficial gas velocity ($U_G = 0.48$ cm s^{-1}), the bubble size distribution is narrow which indicates the generation of small and uniform bubbles with low or zero coalescence rate for perforated plate sparger and cross sparger (Fig. 4.8). On the other hand, the bubble size distribution for ring sparger was wider because of the enhanced bubble coalescence. As the superficial gas velocity increased, the bubble size distribution became wider for all spargers. Ojha and Al-Dahhan [185], observed a similar trend, as did Kagumba and Al-Dahhan [184]. From Figs. 4.8 at *H/D* ratios of 2,3, and 5 at $U_G = 0.48$ cm s^{-1}, sharp chord length distribution was obtained for the perforated plate sparger and cross sparger at *H/D* ratios. However, the distribution was wider for the ring sparger at the same superficial gas velocity. The distribution for cross sparger at *H/D* = 5 at $U_G = 0.48$ cm s^{-1} became wider as compared to the same sparger at *H/D* =2 and 3 for the same superficial gas velocity. The reason for this behaviour is related to the high interaction between the bubbles, producing large bubbles.
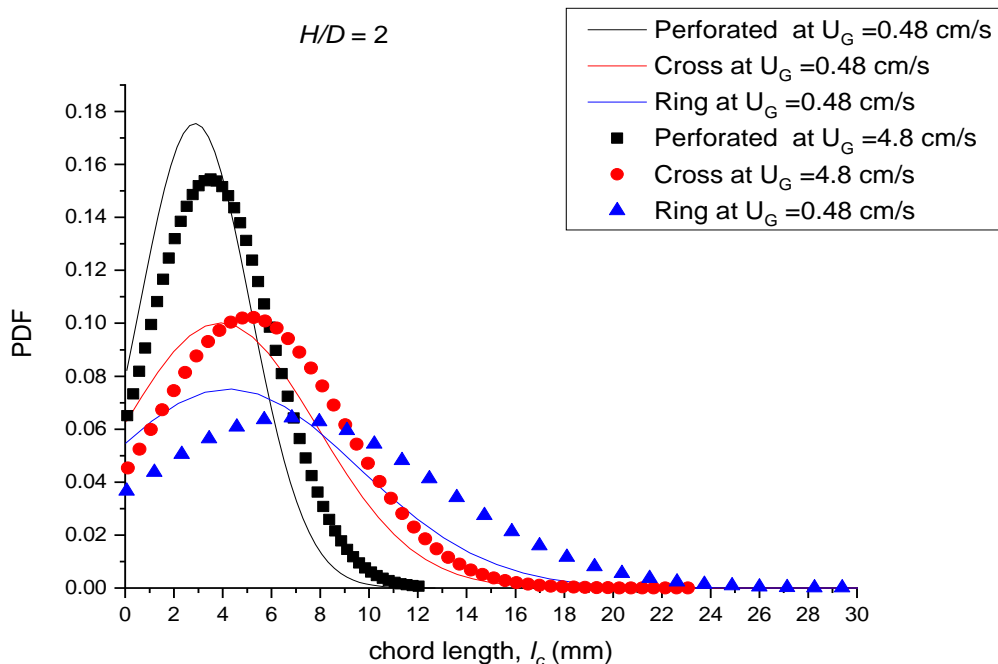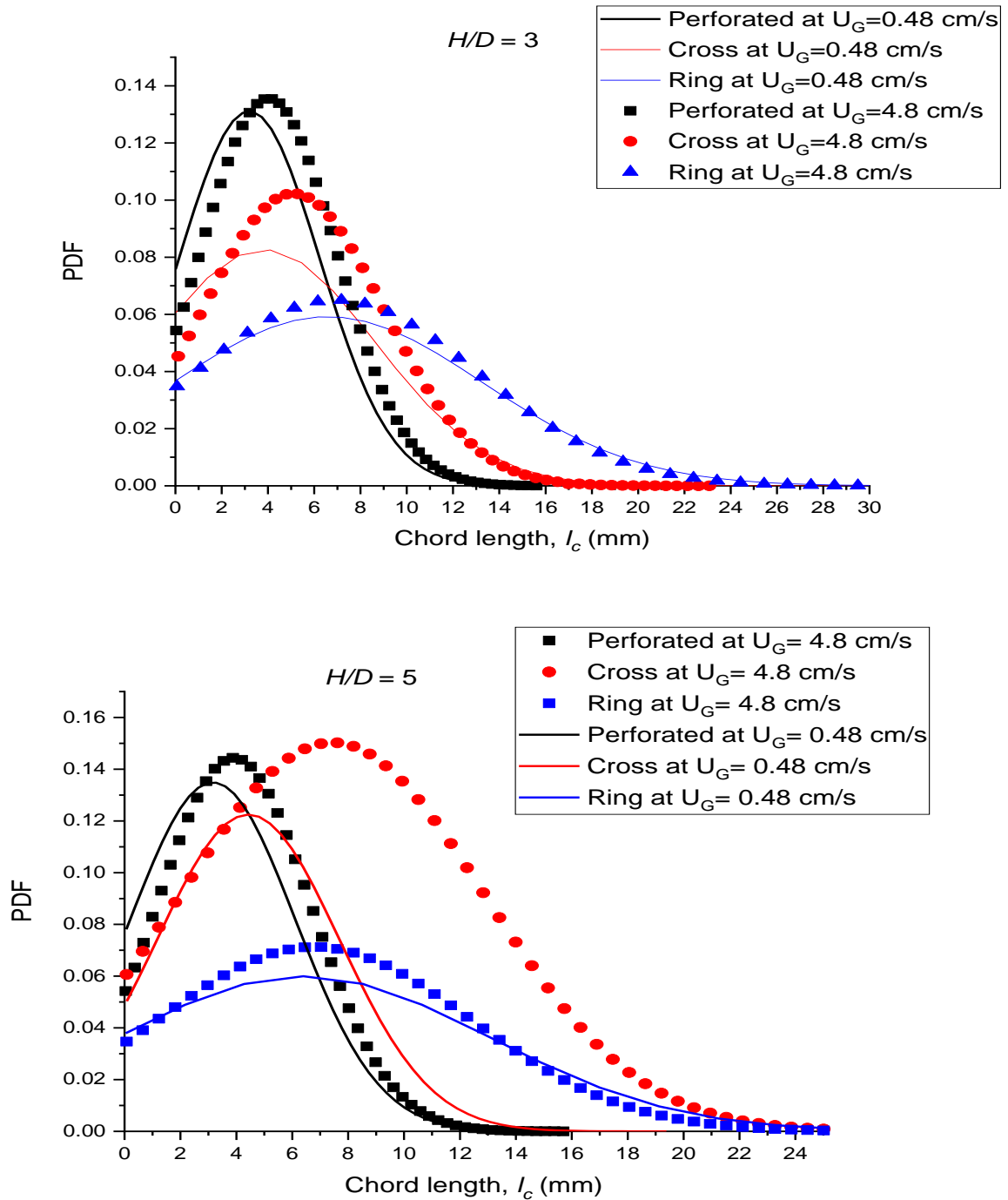
Figure 4. 8 Comparison of sparger influence on chord length distribution at various H/D ratios (2, 3, and 5) and U_G (0.48 and 4.8 cm s^{-1}).

Generally, bubble coalescence happens when two bubbles collide and the little amount of trapped liquid between the two bubbles drains until it becomes a thin layer that leads to rupture then coalescence of the bubbles. It is thought that the drainage of the liquid film is the controlling step and the instantaneous step is the rupturing [164]. In a homogenous flow regime, increasing superficial gas velocity leads to an increase in bubble chord length due to

bubble break-up being lower than bubble coalescence [161]. The bubble chord length is larger at the centre region of the column than the wall region because of lift force action [191]. Thus, the larger bubble moves to the centre region rather than the wall region. These findings are consistent with that of Manjrekar et al. [192], where, in an air-water system, the bubbles of larger chord length that were formed by coalescence tended to move to the centre of the bubble column instead of the column wall.

4.4 Summary

The influence of gas sparger geometry (perforated plate sparger, cross sparger, and ring sparger) on the bubble column hydrodynamics was investigated. Local gas holdup (ε_G), gas-liquid interfacial area (a), bubble arrival frequency (f), and bubble chord length (l_c) distribution were measured by using a fibre optical probe at superficial gas velocities (U_G) of 0.48, 0.96, 1.44, 2.4, and 4.8 cm s^{-1}. It was concluded that gas holdup, interfacial area, and chord length had a linear relationship with superficial gas velocity. It was observed that the perforated plate sparger was the best geometry to obtain the highest gas holdup at 15.73% compared to 13.1% and 10.89% for cross sparger and ring sparger, respectively. Furthermore, the highest results for interfacial area and chord length distribution for the range of superficial gas velocity were obtained with the perforated plate sparger. For example, at U_G = 0.48 cm s^{-1}, chord length distribution was sharper for the perforated plate sparger and cross sparger at all H/D ratios, while wide distribution of chord length was observed for the ring sparger at the same U_G. These results improve our understanding of the best sparger type to influence bubble column hydrodynamics in useful ways. Considerably more work is needed to be done to determine how the perforated plate sparger can enhance the performance of a photobioreactor in terms of biomass productivity, CO_2 biofixation rate, specific growth rate, and lipid formation.

Chapter five
Influence of gas sparger geometry on Carbon Dioxide (CO2) biofixation by chlorella vulgaris and light intensity distribution inside photo-bioreactor

5.1 Introduction

The growth in human population and industrial development have led to an increase in fossil fuel utilization, and consequent energy consumption. It is estimated that fossil fuel combustion produces yearly more than 75% of the energy around the world [193]. Emission of carbon dioxide (CO_2) as a result of combustion of fossil fuels is one of the major issues of global warming. Consequently, CO_2 emission and its increase in concentration in the atmosphere cause the average temperatures of the earth to rise. Therefore, many attempts have been made to decrease the CO_2 emissions to the atmosphere such as the Kyoto Protocol in 1997, and Paris COP 21 in 2015 advocate international restrictions on CO_2 release [194].

Open systems (e.g. raceway ponds) and closed systems (photobioreactors) are the commonly used systems for microalgae cultivation. Higher CO_2 biofixation efficiencies, better operating conditions control, and minimum contamination could be achieved effectively in the closed system. Bubble column, airlift (internal and external loop), and flat plate photobioreactors are different types of closed systems widely used for microalgae cultivation. Bubble columns have good mixing performance and high rate of mass and heat transfer compared to other types [195].

The essential factors that influence the performance of photobioreactors are hydrodynamics, degree of mixing, aeration, light intensity, and biomass concentration [196]. The geometry and holes of the gas sparger determine the bubble size distribution, bubble velocity, and gas holdup, which are crucial for mixing in the liquid phase. Therefore, sparger design is one of the important parameters that determines the photobioreactor performance in terms of CO_2 fixation and biomass productivity. CO_2 biofixation studies have focused on the influence of CO_2 concentration in the inlet gas, species of microalgae, temperature, and the light intensity [197, 198]. However, the literature to date has barely looked at the influence of the sparger on the performance of the algal photobioreactor.

The degree of mixing is a key parameter that affects light distribution and light availability in the cultivation system. In closed photobioreactor systems, parameters such as length of the light path, light intensity, biomass concentration, and degree of turbulence, influence the light and dark cycles to which the cells are exposed. In high-density microalgae cultivation, the light availability in the reactor system decreases with distance from the irradiated surface due to light absorption and mutual self-shading of algal cells. Better hydrodynamics facilitate a

higher degree of mixing, allowing algal cells to be exposed to light intermittently, and to result in effective utilization of light.

Gas sparger design (and consequently aeration rate) is one of the key parameters to improve growth of microalgae. Chandra et al. [196], studied the effect of gas flow rate and its influence on the gas holdup, mixing time, circulation time, and growth of *Scenedesmus obtusus* in an airlift photo bioreactor. They concluded that biomass concentration and productivity increased with an increase in gas flow rate from 1 L min^{-1} to 4 L min^{-1} and the maximum productivity achieved 3 L min^{-1} gas flow rate. Khoo et al. [155], investigated the impact of superficial gas velocity on the biomass production of *Chlorella vulgaris* and overall volumetric mass transfer coefficient in a pilot-scale bubble column. The results of their study were an optimum biomass concentration and volumetric mass transfer coefficient attained at 0.185 m s^{-1} superficial gas velocity.

Aeration is essential to the culture to increase the mass transfer, avoid deficiency of CO_2, control the toxic level of dissolved oxygen and the inhibitory level of CO_2, reduce nutrient gradient in the culture, avoid cell sedimentation, dead zones, clumping of cells, fouling in the reactor, and create an optimized light/dark cycle to enhance the photosynthesis. However, excessive aeration may produce cell damage, affecting the culture performance as some microalgae are susceptible to mechanical shear forces. Furthermore, a high aeration rate leads to high running costs, and is not recommended for mass cultivation. To achieve high productivity, the fluid dynamic and the mass transfer must satisfy the culture requirements in addition to providing an adequate light regime for the efficient use of light. Therefore, it is necessary to determine the limiting factors for the growth in the cost-effective operations. The results from a previous study on CO_2 biofixation using microalgae are summarized in Table 5.1. Researchers have used different reactors/ microalgae species, and sparger configurations to investigate the growth and CO_2 biofixation. Despite the findings from these studies, a clear and systematic study on the effect of sparger design on photobioreactor performance is in need for better design and scale up of the cultivation system.

Therefore, the aim of the study underpinning this chapter was to investigate the influence of gas sparger design on CO_2 biofixation. The growth of *Chlorella vulgaris* microalgae in a bubble column photobioreactor was studied. The performance of three different gas sparger designs namely, perforated plate sparger, cross sparger, and ring sparger was compared at constant light intensity and CO_2 concentration. Bubble column hydrodynamics were also evaluated under different input of superficial gas velocities.

Table 5. 1 Summery of previous studies

Reactor configuration	species	Sparger	Inlet CO_2 (%)	Light intensity (μmol m^{-2}s^{-1})	Growth rate (g L^{-1} d^{-1})	CO_2 biofixation rate (gCO$_2$ L^{-1} d^{-1})	Ref.
Bubble column	*Chlorella sp.*	Perforated plate	2	300	1.21	0.261	[25]
BioFlo fermenter	*Botryococcus braunii*		5	50	-	0.497	[199]
Tubular PBR	*Haematococcus pluvialis*	-	0.036	-	0.076	0.143	[200]
Airlift	*Aphanothece m. Nageli*	Tube diffuser	15	150	-	14.5	[201]
Bubble column	*Anabaena sp.*	4 μm pore size sparger	0.036	900	1.4	1.45	[202]
Photobioreactor (flask)	*Chlorogleopsis sp.*	Tube diffuser	5	250	0.044	0.2045	[203]
Bubble column	*Chlorella sp.*	Tube diffuser	0.03	350	0.7511	1.38	[204]
Membrane photobioreactor	*Chlorella vulgaris*	-	1	157.6	-	6.24	[85]
Bubble column	*Dunaliella tertiolecta*	Tube diffuser	0.04-12	350	0.71	0.51	[205]

5.2 Materials and methods

Experiments were conducted at five different gas superficial velocities 0.48, 0.96, 1.44, 2.4, and 4.8 cm s^{-1} at constant atmospheric pressure. The photobioreactor (Bubble column of 100 cm in height and 10 cm in diameter) was filled with 5.2 L standard medium culture. Enriched

air, including 2% (v/v) CO_2 was sparged continuously in the algae culture at two gas superficial velocities of 0.48 and 1.44 cm/s for CO_2 fixation, separately. The bioreactor was exposed to uniform light intensity of 200 µmol m^{-2} s^{-1} using two LED lights (Mercator 1200mm 36W LED Faber Batten Light) for 10 days. During the culture periods, samples were taken at 24 h intervals from the photobioreactor in order to measure CO_2 biofixation rate and biomass concentration. Light intensity on the surface and inside the photobioreactor was measured using a spherical micro quantum sensor (US-SQS, WALZ). The green algae, *Chlorella vulgaris,* (strain: CCAP 211/11B, CS-42) were supplied by the Australian National Algae Culture Collection/CSIRO Microalgae Research. For more details, refer to Chapter 3.

5.3 Results and discussion

5.3.1 Influence of gas sparger geometry on gas holdup (ε_G)

Figure 5.1 shows the gas holdup for the three different spargers (perforated plate sparger, cross sparger, and ring sparger) at a gas flow rate of 1 L min^{-1} and fixed light intensity of 200 µmol m^{-2} s^{-1}. The overall gas holdup decreases with increasing time of cultivation or biomass concentration. Increasing solid biomass concentration leads to an increase in bubble size, which consequently creates faster and larger bubbles resulting in a decrease in the overall gas holdup. Tirunehe and Norddahl [164], reported that overall gas holdup decreased with increasing Carboxylic methyl cellulose (CMC) concentration which was used to simulate the solid phase. They found that increasing CMC concentration led to the formation of large bubbles with higher rise velocity due to bubble coalescence, subsequently decreasing the gas holdup. De Swart et al. [206], investigated the influence of porous silica particles (38 µm in diameter) on the overall gas holdup in an air/paraffin system. They found overall gas holdup decreased with increasing solid particle concentration due to destruction of the population of small bubbles. For all the investigated spargers, the trend of gas holdup reduction with cultivation time can be classified into three distinguished regions: (i) slow reduction in gas hold up during the first 3 days; (ii) sharp reduction during days 4 to 7; (iii) very slow or levelled off reduction during the last 3 days. In this region, the dense microalgae culture significantly reduced the gas hold up, which could be attributed to the bubble-bubble coalescence occurring at high biomass (solid) concentration. Over the 10 days of the cultivation period, the gas hold up dropped 1.6 % to 0.61 %); (1.12 % to 0.458 %), (0.75 % to 0.306 %) for perforated plate,

cross, and ring sparger, respectively. Mena et al. [207], investigated the impact of solid (1% to 30%) concentration on bubble column hydrodynamics.
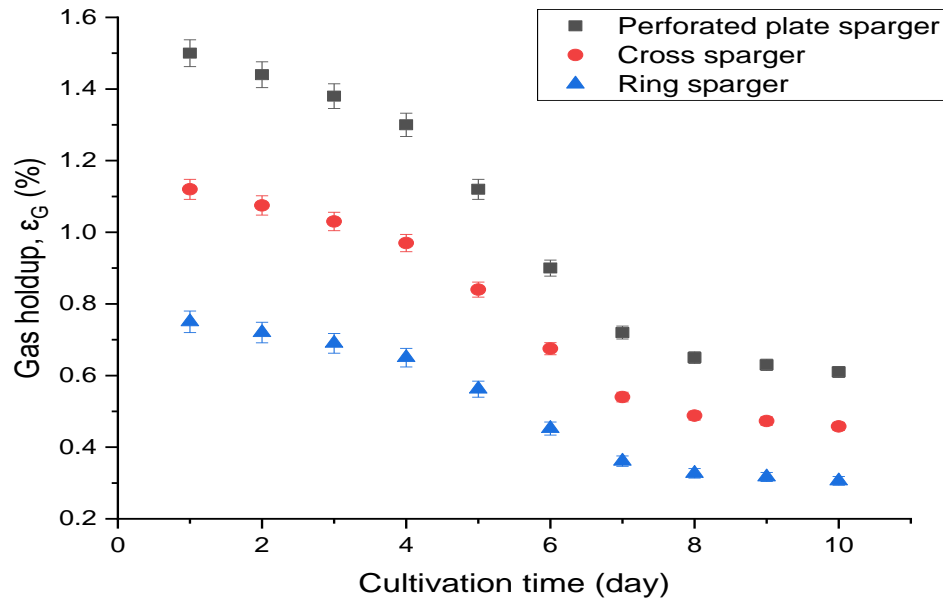
Figure 5. 1 Overall gas holdup for different types of sparger at flow rate of 1 L min^{-1}

They concluded a sharp reduction in overall gas holdup with increasing solid concentration. Gandhi et al. [208], investigated the influence of glass beads (35 µm size) as the solid phase in water on the overall gas holdup. They reported that the reduction rate of the overall gas holdup decreased as the solid concentration increased.

5.3.2 Influence of sparger geometry on volumetric mass transfer coefficient (k_La)

The mass transfer rate has a significant influence on the performance of a photobioreactor. Therefore, the mass transfer coefficient was estimated using three types of sparger. Figure 5.2 shows the influence of gas sparger at different aeration rates (1-10 L min^{-1}) on the volumetric mass transfer coefficient (k_La). As the superficial velocity increased, the mixing improved which led to an enhanced volumetric mass transfer coefficient, where k_La *was* observed to increase linearly for all three spargers. The highest k_La of 0.0114 s^{-1} was observed for perforated plate sparger compared to 0.0062 s^{-1} and 0.00396 s^{-1} for cross sparger, and ring sparger respectively. The obtained results in this study are in a good agreement with the previous reported results [209-211].

The percentage of the open area (activated sparger pores) in the applied spargers was 8%, 2.7%, and 1.2 % for perforated plate sparger, cross sparger, and ring sparger, respectively. The highest activated sparger pores/orifices created a large number of small bubbles, with high superficial surface area (a) raising at low velocity without interaction, which led to high k_La values. This is evidence for the higher performance of the perforated plate spargers. Orifice activity is an important parameter for producing a uniform gas holdup distribution and bubbles that lead to more stability in the flow (homogeneous), and higher gas-liquid mass transfer rate [163]. Chakraborty et al. [162], reported that a higher number of activated sparger pores led to the formation of a higher number of small bubbles in sizes with low rising velocity, without interaction observed among the bubbles which led to an increase in overall gas holdup and volumetric mass transfer coefficient.
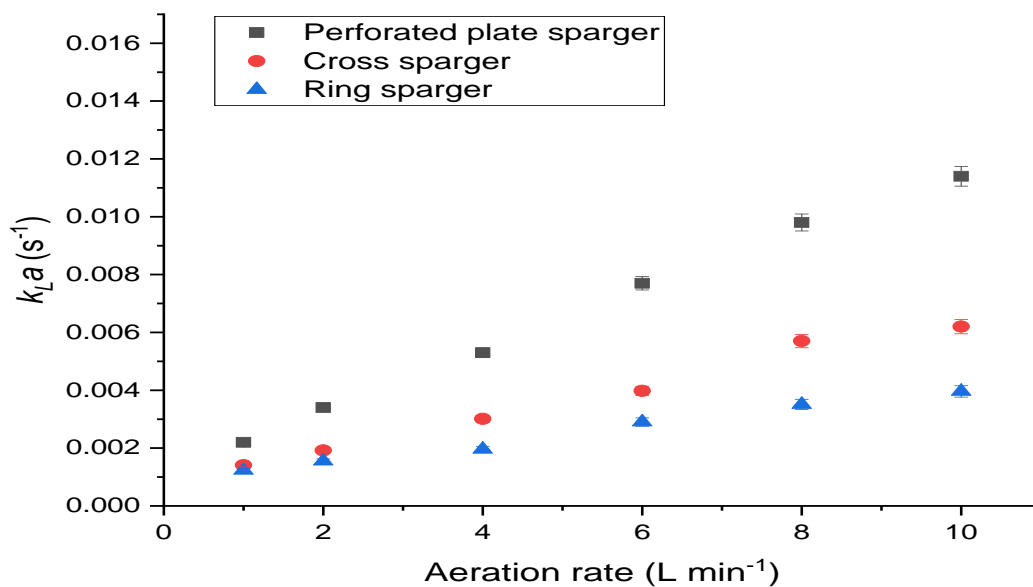
Figure 5. 2 Variation of mass transfer coefficient (k_La) with aeration rate for different types of sparger

5.3.3 Influence of sparger geometry on mixing time (T_m)

Mixing time is a very important factor affecting the performance of photobioreactor especially in batch processes. For instance, adequate mixing prevents a high local concentration of additives which leads to cell damage. Figure 5.3 shows mixing time (sec) versus aeration rate (L min^{-1}). In all three spargers used, the behaviour was a decline in mixing time with increased gas flow rate. This trend is comparable with previous studies [212, 213]. However shorter

mixing time was observed with the perforated plate sparger. At low air flow rate 1 to 6 L min^{-1} there was a sharp decrease in mixing time for the three spargers. Then, as can be shown in Figure 5.3, there was a slight decrease in mixing time after increasing the air flow rate. Low flow rate (few bubbles) had a significant effect on mixing time compared with high flow rate due to more bubbles, higher coalescence rate, and already considerable turbulence in the reactor.
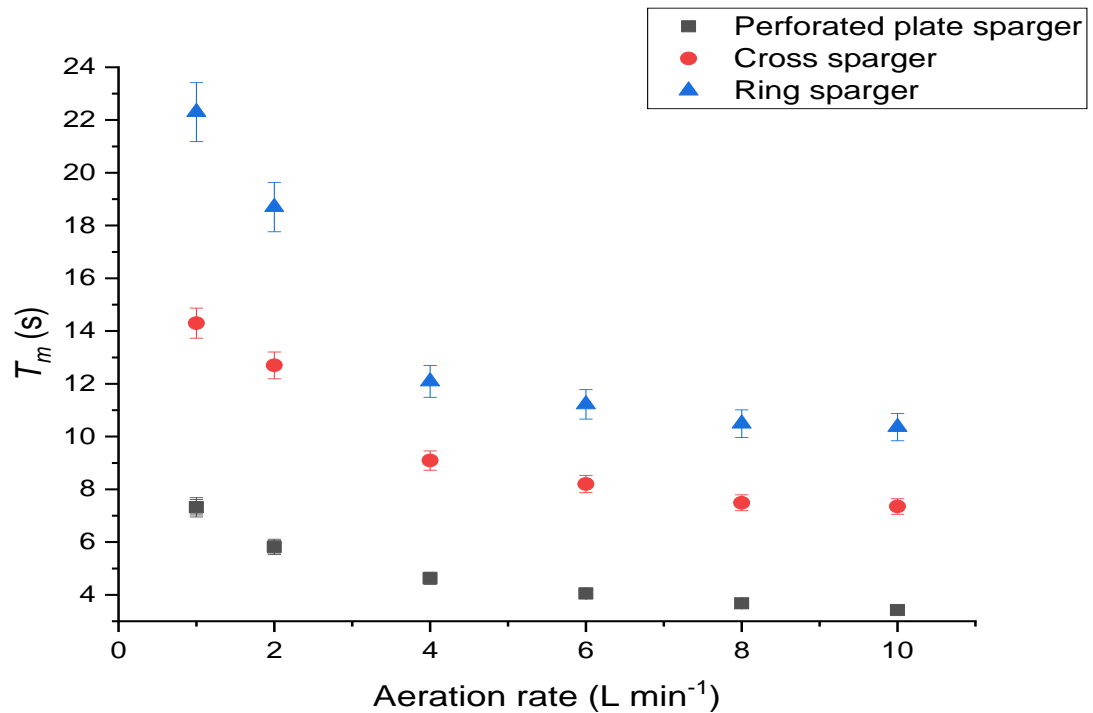
Figure 5. 3 Mixing Time for different sparger

5.3.4 Influence of sparger geometry on microalgae growth

Figure 5.4 illustrates *Chlorella vulgaris* growth at fixed light intensity of 200 µmol m^{-2} s^{-1} for the three spargers during 10 days of cultivation time. The culture showed an exponential growth phase after 3 days of lag growth phase for up to 5-6 days. The growth rate decreased after 8 days but did not stop due to an increase in biomass concentration and decreased available light intensity as a result of cell shading effects. The lag phase of the growth rate was near zero and was dependent only on the culture medium, and the adaptation capacity of the microalgae. The high growth rate observed in the exponential phase led to an exponential increase in biomass concentration. In the last 3 days, the essential compounds in the culture medium (phosphorous, nitrogen, and carbon dioxide) were exhausted, and self-shading was observed as light intensity

decreased due to high biomass concentration. The maximum biomass concentration and specific growth rate (μ) of 4.06 g L^{-1} and 0.2 d^{-1} were achieved by using the perforated plate sparger, while the respective values for the cross and ring spargers were 3.7 g L^{-1}; 0.127 d^{-1} and 2.48 g L^{-1}; 0.0561 d^{-1}, respectively. This may be due to the higher degree of mixing, and lower mixing time for the perforated plate sparger. The mixing of the liquid in the photo-bioreactor had an indirect effect on exposure of microalgae to light and dark phases. In addition, the air bubbles rising through the bubble column photobioreactor were the only driving force for culture mixing in the reactor. In the two-phase system (air-water), the perforated plate sparger showed higher gas hold-up, gas-liquid interfacial area, and small bubble size distribution compared to the other spargers (Chapter 4). Thus, the hydrodynamics (gas holdup, gas-liquid interfacial are, and bubble size) had a significant positive effect on overall growth rate and biomass productivity of microalgae in the photobioreactor [214].
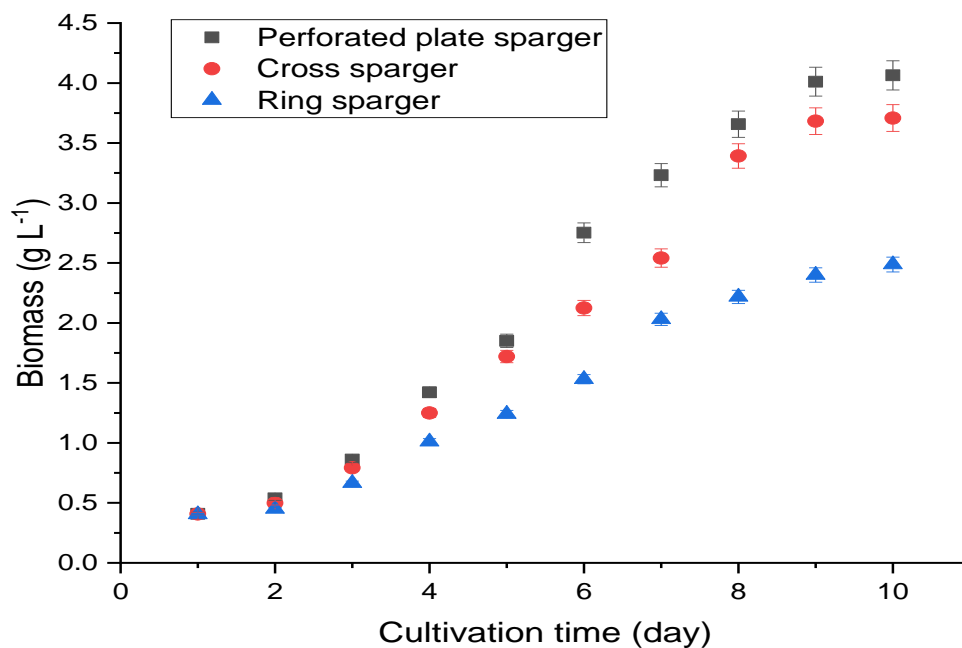
Figure 5. 4 biomass concentration (g/L) for using different sparger

5.3.5 Influence of sparger geometry on the bubble column PBR performance

Figure 5.5 shows the influence of three different spargers on biomass productivity and CO_2 biofixation. The sparger type had a significant effect on the CO_2 biofixation and biomass

productivity. The perforated plate sparger enhanced the biomass productivity and CO_2 biofixation by 76.2% and 57.1%, respectively, when used instead of the ring sparger. CO_2 biofixation rate for the perforated plate sparger was 0.51 g $L^{-1}d^{-1}$ due to a higher mass transfer rate obtained and better mixing efficiency, compared to 0.314 g $L^{-1}d^{-1}$ and 0.264 g $L^{-1}d^{-1}$ for the cross sparger and ring sparger respectively. The essential step to enhance the CO_2 biofixation was to obtain extensive gas liquid interfacial area. In addition, other important factors which influence the CO_2 biofixation are light intensity, and mixing time [8]. As mentioned previously, the best mixing time and highest volumetric mass transfer coefficient was obtained using the perforated plate sparger. Therefore, a higher productivity and CO_2 fixation rate was observed when using the perforated plate sparger.
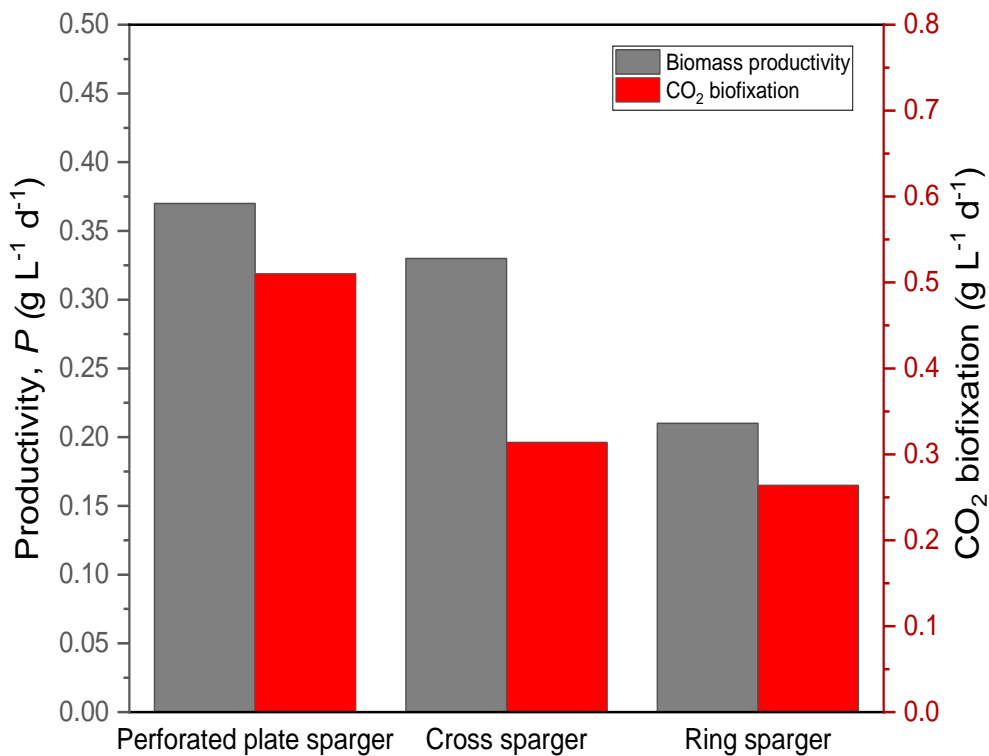
Figure 5. 5 Influence of sparger type on CO_2 biofixation & biomass productivity

Figure 5.6 shows the influence on the specific growth rate and lipid content. Sparger type has a significant effect on the specific growth rate, where it was 0.2 d^{-1} for the perforated plate sparger and 0.127 d^{-1} and 0.0561 d^{-1} for the cross sparger and ring sparger, respectively. The

lipid content did not change significantly with sparger type, as the lipids mainly depend on the microalgae species and the stress conditions of nutrients (nitrogen content). The lipid content produced for the three applied spargers was comparable.
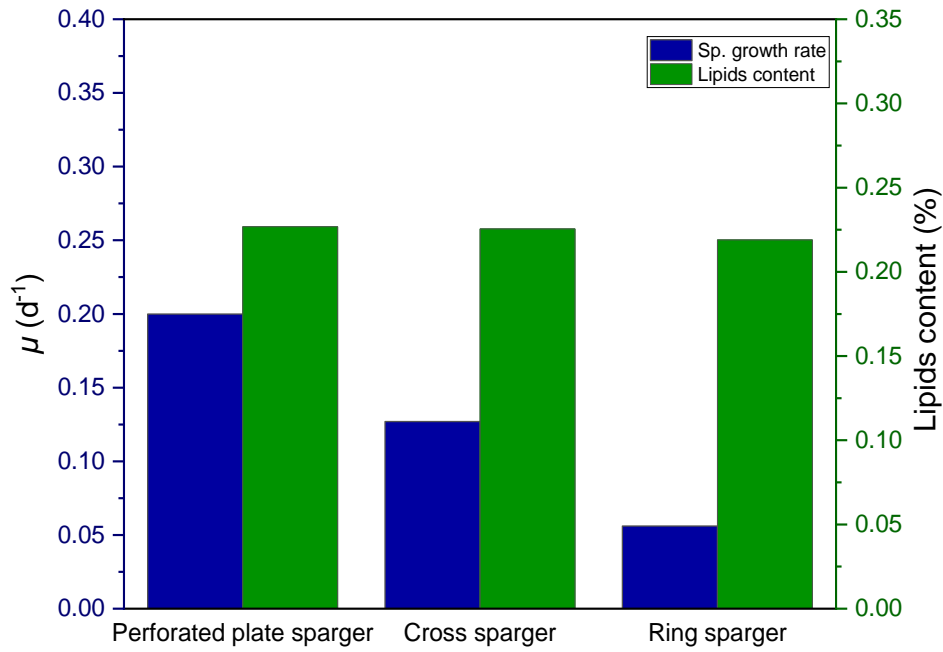
Figure 5. 6 Lipids content, specific growth rate, and CO_2 Biofixation rate for different spargers

5.3.5 Influence of sparger geometry on CO_2 Removal efficiency

Figure 5.7 demonstrates the daily CO_2 removal efficiency observed during the 10 days of cultivation using three different spargers at 1 L min^{-1} air flowrate enriched with 2% of CO_2. The results showed a linear increase in CO_2 removal efficiency over cultivation time for all spargers applied. The highest CO_2 removal of 70.1% was achieved when the perforated plate sparger was used, compared to 57.2% and 50.1% for cross sparger and ring sparger, respectively. As mentioned in the previous sections, the perorated plate sparger provided the highest mass transfer coefficient, which is the limiting factor for CO_2 transfer from the gas to liquid phase then is subsequently consumed by the microalgae species. Also, increasing the biomass concentration led to a reduction in the outlet CO_2 concentration due to increasing gas retention time and CO_2 consumption. Table 5.2 shows the comparison with previous studies.

Table 5. 2 shows a comparison with other previous studies, the table demonstrated that the obtained %CO_2 removal in this study is comparable with others.

Microalgae species	Inlet CO_2 conc. (%)	Sparger type	CO_2 removal (%)	Ref.
Chlorella sp.	2	-	46	[215]
Scenedesmus obliquus	20	-	40.2	[216]
Chlorococcum sp.	10	Membrane	65	[193]
Mixed culture (*Chlorella* sp., *Scenedesmus obliquus, and Ankistrodesmus* sp.)	10	-	63.1	[217]
Chlorella sp.	0.36	Fine diffuser	80	[218]
Chlorella vulgaris	2	Perforated plate	70.1	This study
		Cross	57.2	
		Ring	50.1	
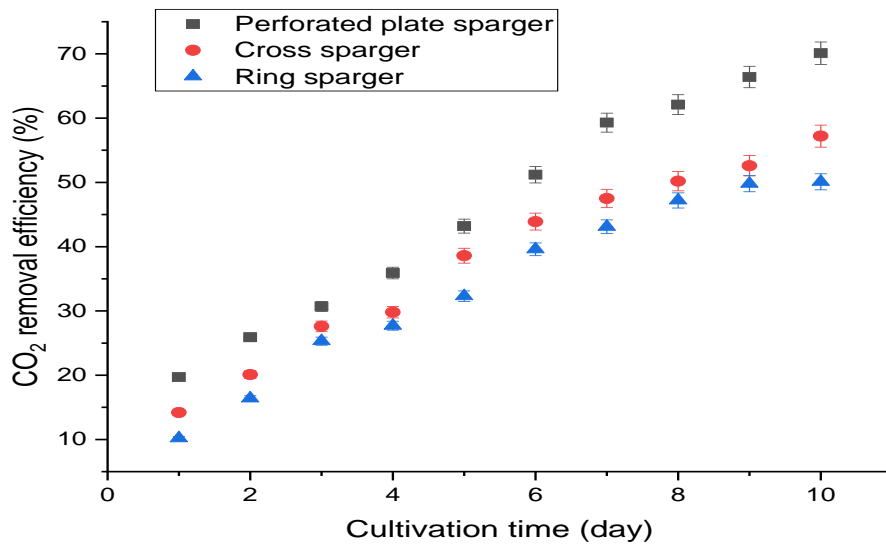
Figure 5. 7 CO_2 removal efficiency for different spargers

5.3.6 Influence of sparger geometry on light intensity distribution

As the light penetrates culture inside a photobioreactor, its intensity decreases due to absorption and scattering by the microalgae cells. This makes it difficult to obtain a homogeneous light intensity distribution inside the photobioreactor [219]. Light intensity was measured inside the photobioreactor at different distances from the photobioreactor wall at a fixed incident light intensity of 200 µmol m^{-2} s^{-1} and two different flow rates 1 L min^{-1} (Fig. 5.8) and 5 L min^{-1} (Fig. 5.9). Figure 5.8 illustrates the light intensity distribution inside the bubble column photobioreactor for the three spargers at an air flow rate of 1 L min^{-1}. Light measurements were taken daily for 10 days at different depths along the column diameter. The light intensity dropped exponentially when the light passed through the biomass culture due to scattering and shading effects of cells. Thus, an increase in biomass concentration led to a decrease in the light intensity distribution inside the photobioreactor. As shown in Fig. 5.8, the light intensity decreased rapidly in the first five days of cultivation for all spargers used, mainly due to the high rate of cultivation. After that, the effect of sparger on the light intensity distribution was less significant due to the high biomass concentration especially at the dense centre (at r/R=0).

For example, the light intensity decreased rapidly in the first 5 days of cultivation for all spargers used in the experiments due to the high rate of cultivation. After that, the effect of sparger on the light intensity distribution was less significant due to the high biomass concentration especially at r/R=0 and day 10 of cultivation, where there was no difference for all spargers used. However, when the gas flow rate increased to 5 L min^{-1} (Fig. 5.9), the perforated plate sparger resulted in better distribution inside the bubble column even in the dense culture (day 10), due to a higher mixing rate, which prevented the microalgae settling and moving from the centre to the wall of the column to capture more light.
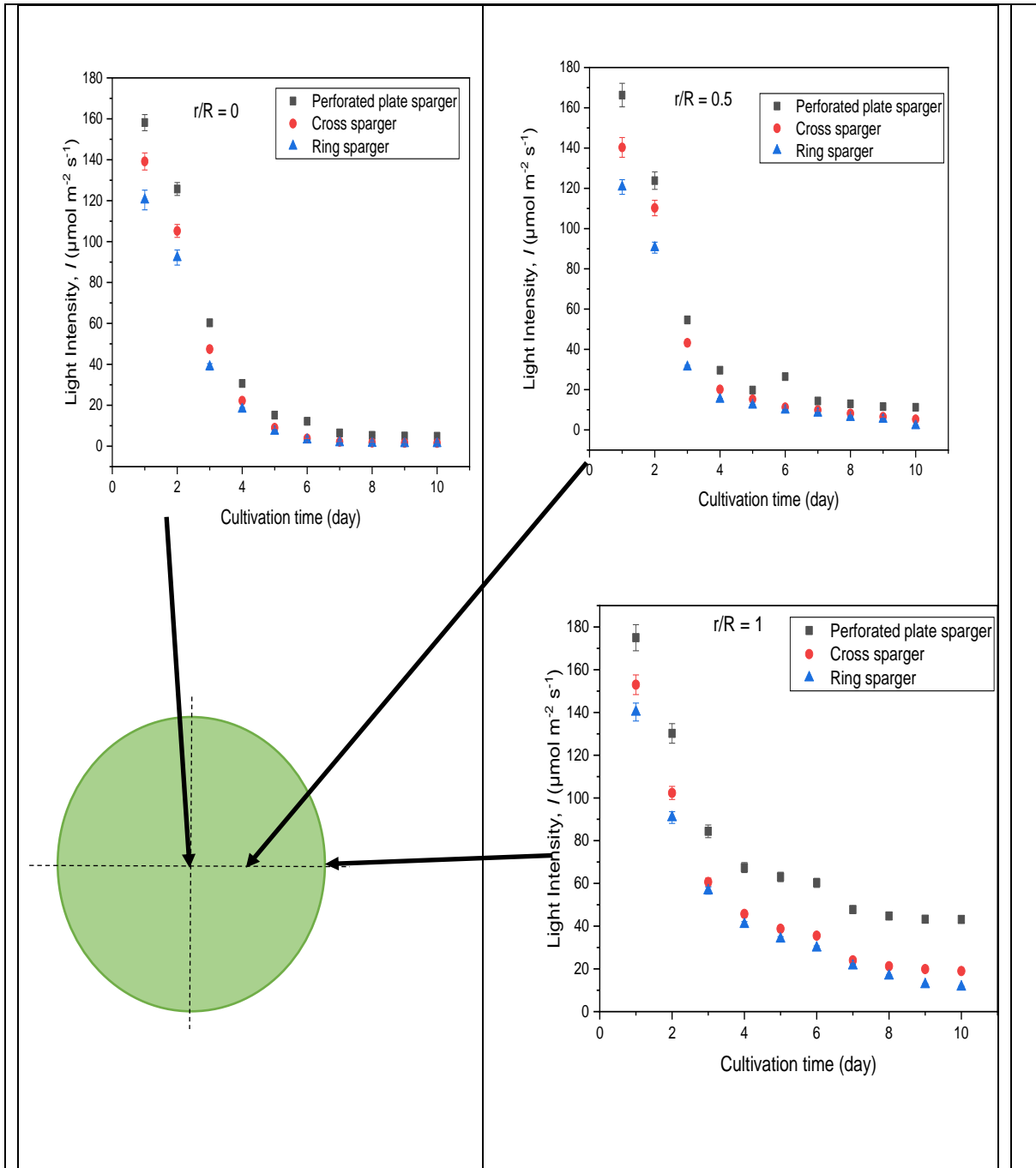
Figure 5. 8 Light intensity distribution inside the culture at different radial positions at gas flow rate of 1L min $^{-1}$
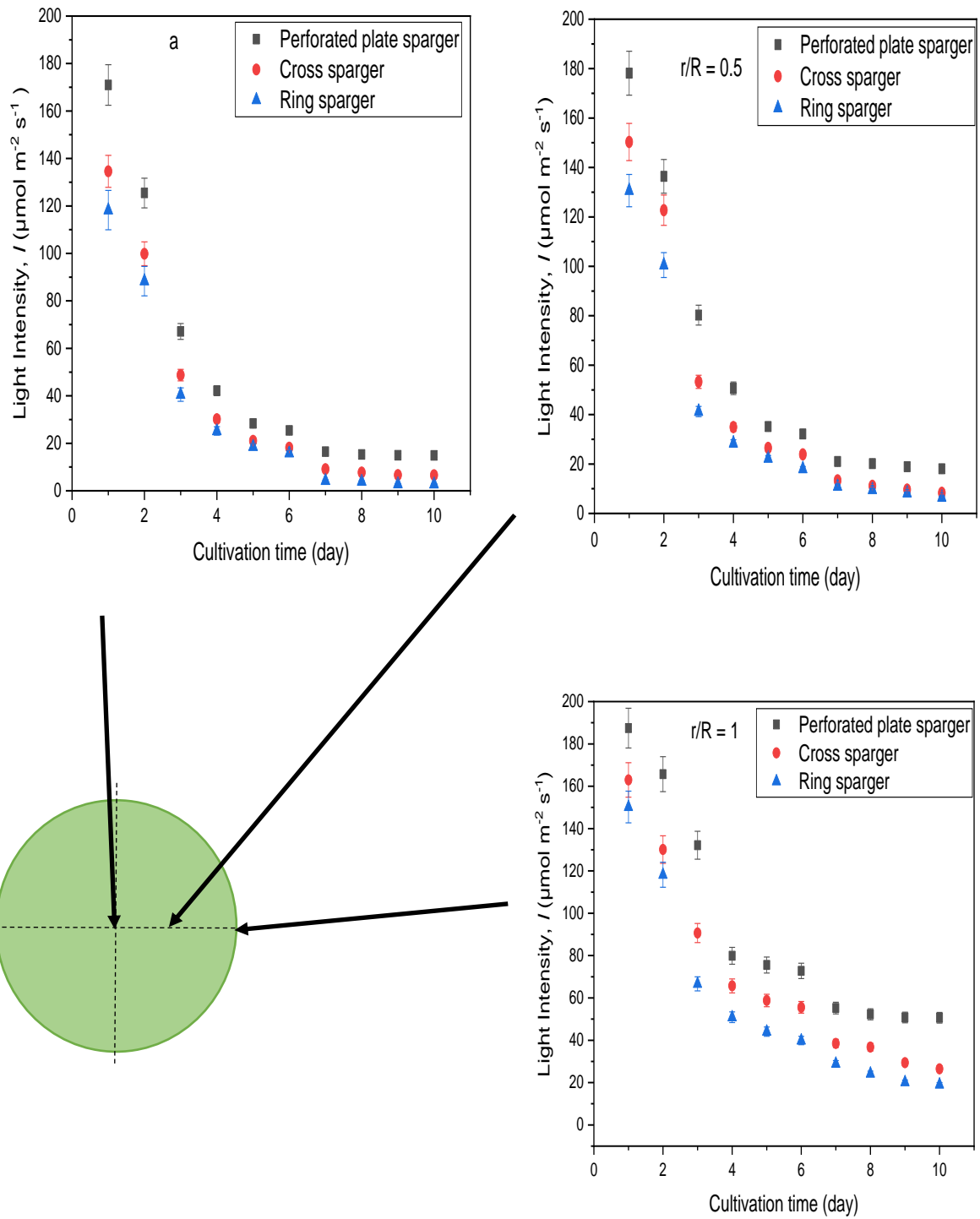
Figure 5. 9 Light intensity distribution inside the culture at different radial positions at gas flow rate of 5 L min⁻

5.4 Summery

CO_2 biofixation by *Chlorella vulgaris* cultivation and light intensity distribution inside a bubble column photobioreactor were investigated using three different spargers (perforated plate sparger, cross sparger, and ring sparger) for 10 days cultivation time. CO_2 biofixation rate for the perforated plate sparger was 0.51 g L^{-1} d^{-1} due to a higher mass transfer rate obtained and better mixing efficiency, while the rates were 0.314 and 0.264 g L^{-1} d^{-1} for the cross sparger and ring sparger, respectively. The biomass productivity, CO_2 fixation rate, and nutrient removal efficiency were increased when using perforated plate sparger. The highest removal efficiency on Day 10 was 70.1% using the perforated plate compared with 57.2%, and 50.1 for the cross sparger and ring sparger, respectively. In addition, the best light intensity distribution inside the photobioreactor was obtained when using the perforated plate sparger as a result of it achieving the lowest mixing time.

Chapter six

Influence of gas sparger on Chlorella vulgaris performance for nutrients removal from wastewater in a draft tube airlift photobioreactor and kinetic modelling and simulation

6.1Introduction

Airlift photobioreactors are a special type of multiphase pneumatic contactor that is widely used in chemical and biotechnological processes, wastewater treatment, and various fermentation systems. Airlift photobioreactors are characterized by simple construction, effective heat transfer, good mixing, lack of moving parts, relatively low energy consumption, and minimal space requirement [220, 221]. Airlift photobioreactors can be classified into internal-loop airlift and external-loop airlift bioreactors.

When designing airlift photobioreactors, it is necessary to understand their hydrodynamic behaviour, such as gas holdups, liquid circulation and mixing [7]. Gas holdup is one of the most important hydrodynamic parameters that affects the liquid recirculation, flow regime, mixing, and the gas-liquid mass transfer rate in the bioreactors. Gas sparger type also has an influence on the gas holdup. This influence is complex and generally a function of the fluid properties. The gas sparger design has a major effect on the initial bubble size and, hence, on the hydrodynamics of the airlift photobioreactor. Cao et al. [222], performed experiments in a three-phase external loop airlift reactor (ELAR) with four sparger types. They reported that the sparger design had a noticeable effect on the gas holdup at low gas velocities ($< 0.025 \, \mathrm{m \, s^{-1}}$) but only a slight effect at high gas velocities ($> 0.030 \, \mathrm{m \, s^{-1}}$). Similar observations were reported by Šijački et al. [223], who demonstrated that, at lower gas velocities, gas holdup values were the highest in a two-phase internal loop airlift reactor (ILAR), obtained using a sinter plate sparger, compared with a perforated-plate sparger or single-orifice sparger. At higher gas velocities, when plug flow occurred in the riser, the differences between the spargers were negligible. Snape et al. [224], also observed that the gas holdup was dependent on the geometry of the gas sparger, as gas spargers have an equal open area ratio with different orifice diameters. On the other hand, Merchuk [225], reported the opposite conclusion. He used four different gas spargers in an ELAR and did not find a major influence on gas holdup. The gas spargers were straight copper tubes with orifice diameters of 0.003, 0.005, and 0.01 m and a perforated plate. Miyahara et al. [226], conducted experiments in an ELAR with two different gas spargers, a single-hole plate and a perforated plate with different hole diameters. They did not notice any remarkable effects of the plate geometry. However, in the range of relatively low gas velocities, the gas holdup was quite small for single-hole plates with a large hole diameter.

Wastewater treatment using microalgae has been investigated for over 4 decades as an environmentally sound alternative for removing nutrients and heavy metals from wastewater sources [227]. Table 6.1 lists previous studies of microalgae capability for wastewater treatment. The advantages of using algae for wastewater treatment include low operational cost, creation of a food source for fish or farm animals, avoidance of the sludge handling problem, and direct discharge of oxygenated effluent water into the water bodies [228, 229]. Furthermore, nutrients are not only removed from the wastewater, but can also be captured and returned to the terrestrial environment as agricultural fertilizer. Another advantage is photosynthetic CO_2 fixation, which contributes to mitigating greenhouse gases [230, 231]. Microalgae are able to serve a dual role of bioremediation of wastewater as well as generating biomass for biofuel production [232]. Usually, algae, which are isolated from a wastewater treatment plant site or real water body, can adapt better to the practical conditions and show higher efficiency of inorganic nutrient removal [232].

Modelling of microalgae growth provides a better understanding for the growth mechanisms, biomass production, consumption rate of nutrients, and optimization of operating conditions. In addition, it provides useful information for design and scale-up of efficient algal photobioreactors. Many kinetic models have been developed and proposed for modelling the performance of algal photobioreactors, including Monod and Droop models [233]. Efficient microalgae growth depends essentially on: (i) light intensity distribution inside the photobioreactor [234], (ii) gas-liquid mass transfer rate enhancement [235], (iii) nutrient availability [236], and (iv) efficient fixation of CO_2 [236].

Nitrogen and phosphorous are essential elements for microalgae growth and metabolism of cells. Chavan et al. [236], reported that nitrogen deficiency enhanced biosynthesis and lipid accumulation, while it led to a decrease in protein content. Razzak et al. [9], stated that the condition of phosphorous starvation in the culture media led to lipid accumulation. In general, nitrogen, phosphorous, and carbon are limiting factors to growth rate and oversupply may lead to a decrease in algal growth [237]. Moreover, carbon is one of the most important nutrients for microalgae growth which could be found in the culture in several forms: carbonate, carbon dioxide, and bicarbonate and microalgae largely utilize CO_2 compared to the other forms [238].

In spite of several previous investigations that related to algal photobioreactor applications for wastewater treatment (Table 6.1), none of these studies have investigated the influence of the hydrodynamics and the type of gas sparger applied. Therefore, the purpose of the study

underpinning this chapter was to investigate the impact of different types of gas spargers (perforated plate sparger, cross sparger, and ring sparger) in the airlift algal photobioreactor on nutrient removal from primary wastewater. Furthermore, in this chapter, a kinetic model that considers the nutrients (C, N, P) and light intensity is proposed.

6.2 Materials and methods

6.2.1 Experimental setup

Experiments were conducted in an acrylic tubular airlift photobioreactor, with a 6L working volume (for more details about wastewater characterizations and photobioreactor, see Chapter 3). Experiments were conducted with five different gas superficial velocities (0.0024, 0.0048, 0.0096, 0.0144, and 0.0192 m s^{-1}) at constant atmospheric pressure and room temperature. The photobioreactor was filled with 6 L of sterilized and filtered primary wastewater (*Pww*) as a sole culture medium. Air with 2% (v/v) CO_2 was sparged continuously into the algae culture through different gas spargers (perforated plate sparger, cross sparger, and ring sparger). The concentrations of TN and TP were determined calorimetrically using HACH test kits. A HACH spectrophotometer was used to measure COD. The measurement procedures are detailed in Chapter 3.

6.2.2 Model limitations and assumptions

The steps involved in the model development procedure are shown in Figure 6.1. The mass balance equations, gas, liquid, and biological phases were derived based on the following assumptions:

- The photobioreactor is fully mixed.
- The specific growth rate of algae is affected by nitrogen, phosphorous, carbon, and light intensity.
- The photobioreactor worked in a batch mode.
- The ideal gas law is applicable to the air bubbles.
- Bubble size is assumed to be constant due to the short length of the reactor (100 cm).
- pH and temperature are constant in the culture.
- Algal cells are assumed to be able to fix all forms of dissolved inorganic carbon (CO_2, HCO_3 and CO_3).

- To avoid the complexity of the model parameters, the specific growth rate of algal cells is assumed to not be limited by carbon concentration or nutrients.
- Gas phase is uniformly distributed in the culture media due to constant gas flow rate used.
- Henry's law constant is taken at 25∘C and atmospheric pressure.

```
┌─────────────────────────────────────┐
│   Set initial conditions of model input │
│        (TN, TP, %CO₂, and I)         │
└─────────────────────────────────────┘
                 │
                 ▼
┌─────────────────────────────────────┐
│     Calculate model parameters       │
│     KN, KP, kLa, KI, µmax., KC       │
└─────────────────────────────────────┘
                 │
                 ▼
┌─────────────────────────────────────┐
│  Set time step change, simulation time, │
│             growth rate              │
└─────────────────────────────────────┘
                 │
                 ▼
┌─────────────────────────────────────┐
│        Start model simulation        │◄─────────┐
└─────────────────────────────────────┘          │
                 │                                │
                 ▼                                │
┌─────────────────────────────────────┐          │
│     Calculate model parameters       │          │  t=t+dt
│     KN, KP, kLa, KI, µmax., KC       │          │
└─────────────────────────────────────┘          │
                 │                                │
                 ▼                                │
┌─────────────────────────────────────┐          │
│   Calculate light intensity distribution │       │
│              profile                 │          │
└─────────────────────────────────────┘          │
                 │                                │
                 ▼                                │
┌─────────────────────────────────────┐          │
│  Calculate Biomass concentration, TN and │──────┘
│             TP uptakes               │
└─────────────────────────────────────┘
                 │
                 ▼
┌─────────────────────────────────────┐
│          Simulation output           │
└─────────────────────────────────────┘
```
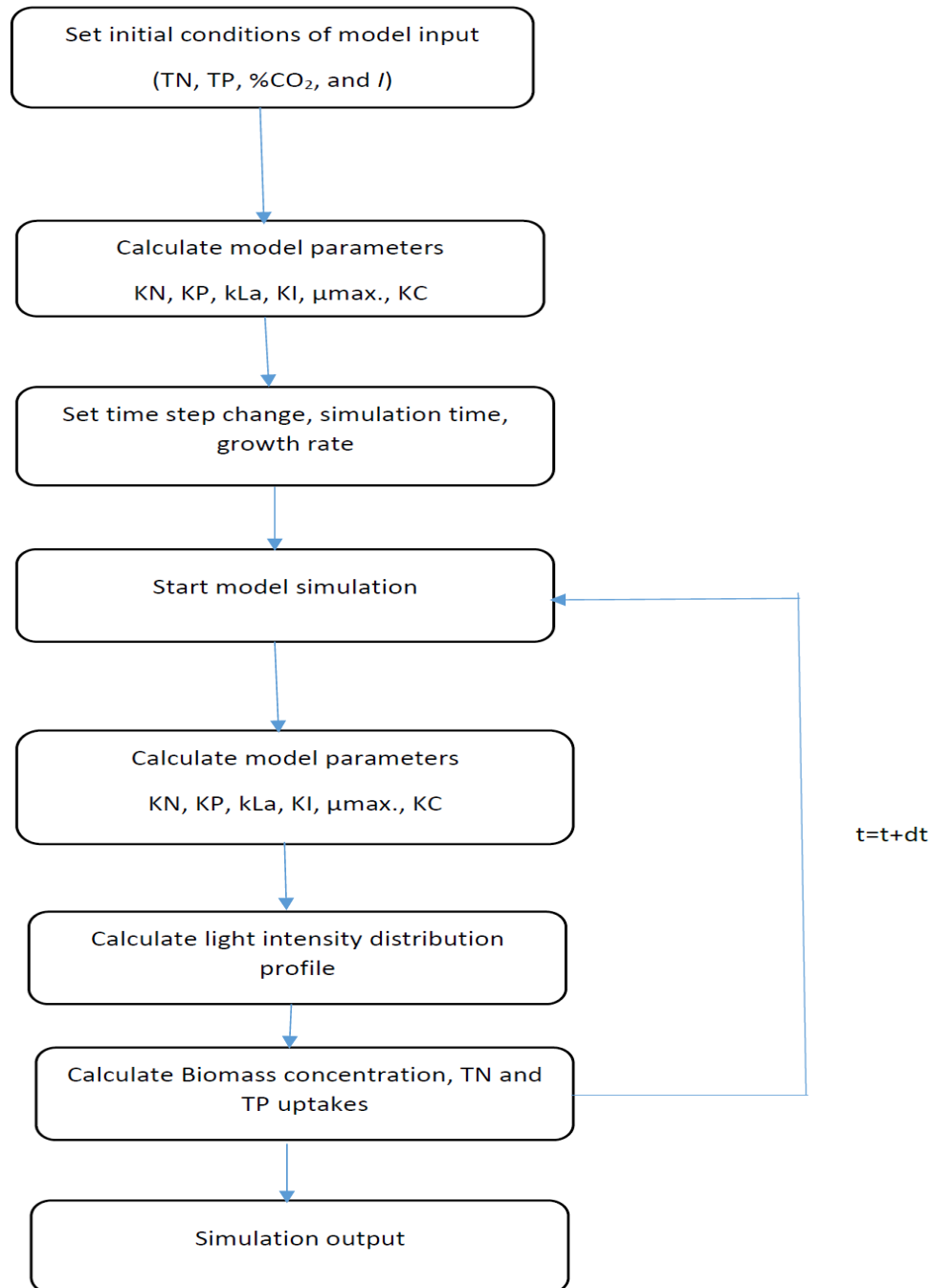
Figure 6. 1 Flowchart describes the operation of the Matlab model

6.2.3 Model development

Carbon is provided by air injection into the photobioreactor, where the dissolved CO_2 in the air is transferred to the culture. Therefore, the input rate of CO_2 into the culture will be:

$$R_c = K_L a (C_s - C) V (1 - \varepsilon_G) \tag{6.1}$$

where Rc is the input rate of CO_2 from the air in bubbles into the culture, K_L is the overall mass transfer coefficient, a is the surface area available for mass transfer per volume of the system, Cs is the liquid-phase concentration of CO_2 in equilibrium with air in the bubble, C is the concentration of inorganic carbon, V is the reactor volume, and ε_G is the gas holdup.

Cs is related to the gas-phase concentration of CO_2 at the air-water interface (Ys) by:

$$C_s = \frac{Y_s}{H} \tag{6.2}$$

where H is the Henry's law constant and is equal to 1.1 for CO_2 at 25°C. Ys is calculated using ideal gas law:

$$Y_s = \frac{V_{CO_2}}{V_{air}} \frac{P_{air}}{RT} \tag{6.3}$$

where P is the pressure, H is Henry's law constant which is the ideal gas constant and is equal to 0.0821 L atm mol^{-1} K^{-1}, T is the temperature.

The uptake rate of carbon (dC/dt) by the algal culture can be expressed as a function of biomass concentration (X), the yield coefficient (total carbon consumed per algal biomass produced $Y_{C,tot}$) and μX, the algal specific growth rate:

$$\frac{dC}{dt} = - \frac{\mu_x X}{Y_{C,tot}} \tag{6.4}$$

Therefore, the total dissolved carbon in the algal culture can be calculated from:

$$\frac{dC_{tot.}}{dt} = K_L a (C_s - C) - \frac{\mu_x X}{Y_{c,tot.}} \tag{6.5}$$

The first term on the right-hand side of Eq. (6.5) takes into account mass transfer phenomena from the gas to liquid phase and the second term is the CO_2 consumption and concomitant liquid phase of the microalgae production process.

The mass balance for total dissolved nutrients (N and P) not involved in the gas-liquid mass transfer phenomena can be expressed as follows:

$$\frac{dC_{N,P}}{dt} = - \frac{\mu_X X}{Y_{N,P}} \tag{6.6}$$

The final growth rate of algal biomass, dX/dt, can be written as:

$$\frac{dX}{dt} = r \mu_X X \tag{6.7}$$

The final growth rate of algal biomass, dX/dt, can be written as:

$$\mu_X = \mu_{max} \left[\frac{S_i}{K_i - S_i}\right] \tag{6.8}$$

where S_i is the nutrient (N or P) concentration, K_i the nutrient half saturation constant and, μ_{max} the maximum specific growth rate.

The following integrated Monod model considering the effect of multiple factors (N, P, C and light intensity) on the specific growth rate of the algae was proposed by extending Equation (6.8):

$$\mu_X = \mu_{max} \left[\frac{S_N}{K_N - S_N} \times \frac{S_P}{K_P - S_P} \times \frac{S_C}{K_C - S_C} \times \frac{I}{K_I - I}\right] \tag{6.9}$$

where S_N, S_P, S_C are the respective N, P and total carbon concentrations in the culture and K_N, K_P, K_C, K_I are the corresponding half saturation constants for nitrogen, phosphorus, total carbon and light respectively. The light intensity I within the culture in cylindrical bubble PBR can be expressed by [71]:

$$I = I_o \cdot \exp\left(-\frac{3\varepsilon_G z}{d_b}\right) \tag{6.10}$$

Where I_o the incident light intensity, z is the light path, ε_G is the gas holdup, and d_b is the bubble diameter.

6.2.4 Sensitivity analysis

Sensitivity analysis identify the impact of fluctuation in model input parameters to output key of the model. The sensitivity analysis was calculated to show how that biomass concentration X (g L^{-1}) could affected by any change in a certain parameter. Sensitivity coefficient $\emptyset i$ which represent the sensitivity analysis can be calculated by [239]:

$$\emptyset i = \frac{\Delta X}{X} / \frac{\Delta P}{P} \tag{6.11}$$

Where X is the model output, which is the biomass concentration, P is input parameter, ΔX change in model output, and ΔP variation in input parameter. The input model parameters were varied by ±20% to determine the sensitivity of biomass concentration to the model parameters [240].

Table 6. 1 Previous studies of nutrient removal using microalgae

Microalgae species	PBR type	WW	Sparger Type	TN Initial conc. (mg/L^{-1})	TN Removal efficiency (%)	TP Initial conc. (mg/L^{-1})	TP Removal efficiency (%)	COD Initial conc. (mg/L^{-1})	COD Removal efficiency (%)	Ref.
Chlorella vulgaris	Airlift	Municipal	-	46.67±0.27	93.4	19.5±0.24	94.1	293±3.3	76.3	[241]
Chlorella vulgaris	Bubble column	Municipal	-	55.33	84.3	6.23	33.23	270.35	80.23	[228]
Chlorella vulgaris	Erlenmeyer flask	Industrial	-	9650±1582	45.5-59.9	343±43	85.8-94.6	134800±2287	50-60.9	[242]
Chlorella vulgaris	Triangular flask	Synthetic		-	32-50	-	55-75	-	68-85	[243]
Chlorella vulgaris	Membrane	Treated sewage effluent	Fine bubble diffuser	18.8	63.6	1.01	78.5	-	-	[244]
Chlorella vulgaris		Brewery		48.6-76.3	82.05	33.7-53.9	54.32	2987-5864	71.44	[245]
Chlorella zofingiensis	Tubular bubble column	Piggery (50%)	-	148.0 ± 4.0	82.70	156.0 ± 8.0	98.17	3500 ± 63	79.84	[246]
Chlorella zofingiensis	Tubular PBR	Dairy	Glass-filter	118.0 ± 2.8	51.7	149.0 ± 2.8	97.5	1195 ± 7.0	-	[247]
Chlorella sp.	Erlenmeyer flasks	Manure	-	118 ± 7.8	77.16	76.7 ± 5.0	90.04	-	-	[248]

6.3 Results and discussions

6.3.1 Influence of sparger type in riser (ε_{Gr}) and downcomer gas holdup (ε_{Gd})

Figure 6.2a shows the variation of riser gas holdup with superficial gas velocities U_G 0.0024-0.0192 m s^{-1}. The riser gas holdup was studied in the centre of a draft tube at a distance of 50 cm from the photobioreactor base. Riser gas holdup increased linearly with increased superficial gas velocity for all spargers used (perforated plate sparger, cross sparger, and ring sparger). A similar trend was observed in a number of other studies [249-251]. Higher values for riser gas holdup were achieved with the perforated plate sparger compared with the cross sparger and ring sparger. The reason for this is that gas holdup increases with an increasing number of sparger orifices. Bahadori and Rahimi [113], also found an increase in the gas holdup as a result of increasing the number of orifices in the gas distributor. Furthermore, there was no significant difference in riser gas holdup for all the spargers used. As superficial gas velocity was increased, the difference between the three sparger types became greater.

Figure 6.2b illustrates the variation of local gas holdup in the downcomer section with superficial gas velocities. A similar trend for ε_{Gd} was also observed for all the investigated spargers and over the whole range of U_G (0.0024 - 0.0192 m s^{-1}). Increasing U_G led to increasing liquid circulation velocity, which in turn increased the number of gas bubbles entering the downcomer section of the bioreactors, consequently increasing the gas hold up in the downcomer section [252]. For both riser and downcomer sections, the perforated plate sparger provided the highest gas holdups in comparison with the cross and ring spargers. This is mainly attributed to the high number of bubbles generated by the perforated plate sparger compared with the cross sparger and ring sparger.

For a real algal culture system (Fig. 6.3), the overall gas hold up inside the algal airlift photobioreactor was measured during the first day of cultivation time using three different gas spargers (perforated plate sparger, cross sparger, and ring sparger). The perforated plate sparger provided the highest gas hold up even using a real algal culture (3 phases). The reason for this was the creation of bubbles, small in size and uniform in shape, and no coalescence and break up of bubbles in this flow regime. Smaller bubbles rose inside the column with low rising velocity, which led to an increase in the residence time of the bubbles.
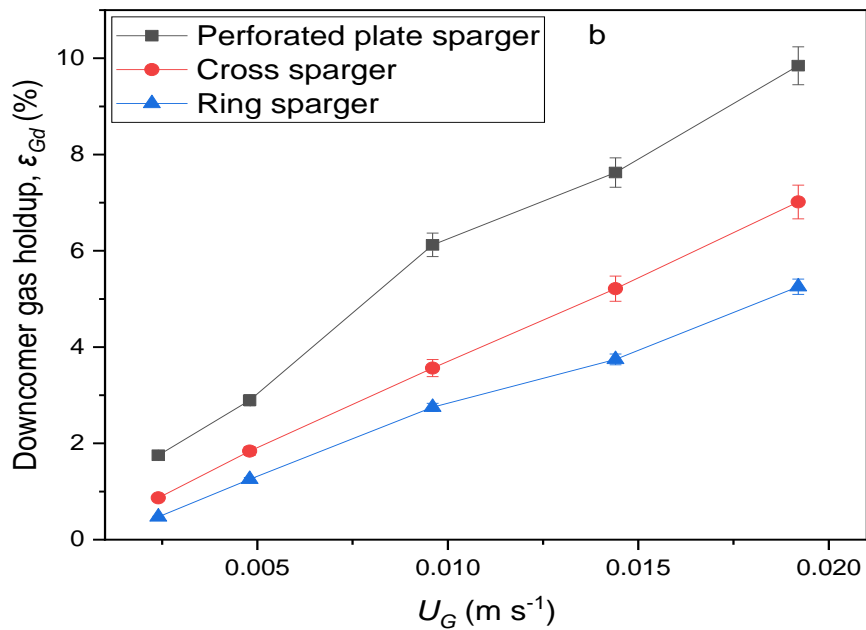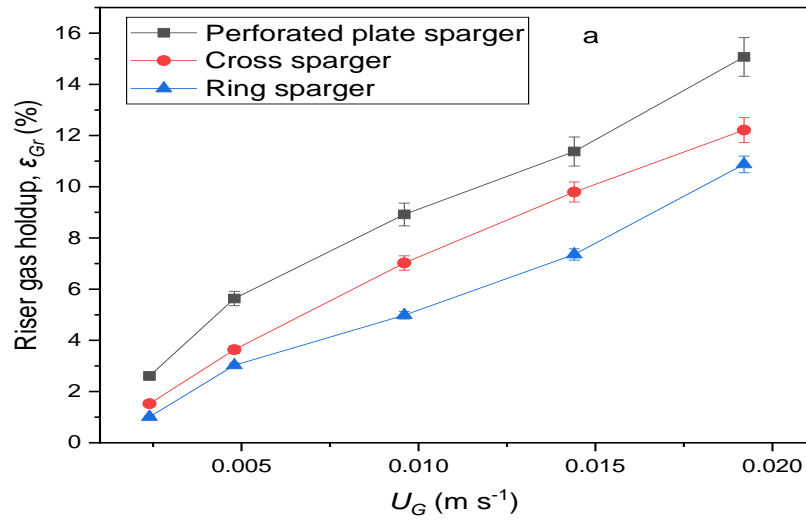
Figure 6. 2 Variation of gas holdup in the (a) riser and (b) downcomer at different superficial gas velocities.

This behaviour is probably because of the presence of the microorganisms constituting the consortium, which helped to reduce the size of the bubbles and prevent their coalescence, diminishing its rising velocity [253].
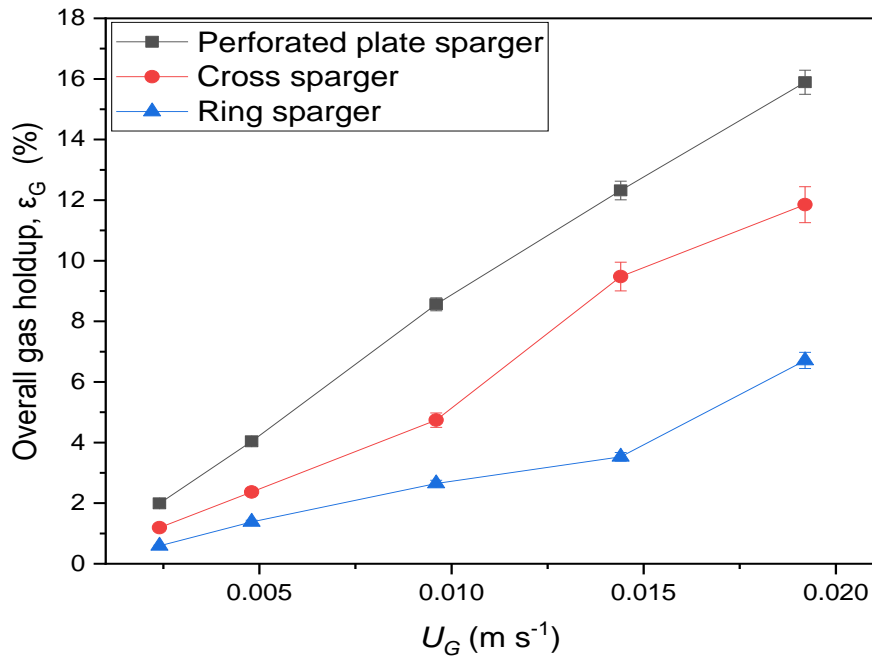
Figure 6. 3 Variation in overall gas holdup in a triphasic system for different types of sparger

6.3.2 Influence of sparger type in riser and downcomer bubble frequency

Figure 6.4a exhibits the change in mean bubble arrival frequency in the riser with increasing superficial gas velocity from 0.0024 m s^{-1} to 0.0192 m s^{-1}. Bubble arrival frequency is the ratio detected by the optical probe bubbles to the sampling time, which is an important parameter that gives an indication of the mixing and gas-liquid interaction in the photobioreactor [252]. An increase in superficial velocity leads to an increase in bubble numbers and a consequent increase in bubble arrival frequency. Similar behaviour was observed by Vial et al. [125], who analysed the hydrodynamics of external loop airlift reactors. Figure 6.4a shows that bubble arrival frequency with the perforated plate is higher than with the cross sparger and ring sparger. These findings are in line with those of Camarasa et al. [254], who investigated the effects of liquid properties and gas spargers on bubble column hydrodynamics. They concluded that bubble frequency was higher with a porous plate sparger than with a single orifice sparger. As can be seen, the bubble arrival frequency values with a perforated plate sparger are triple those achieved by a ring sparger.

Figure 6.4b shows that increasing superficial gas velocity, a higher volume of gas enters the photobioreactor, which leads to a linear increase in downcomer bubble frequency [249].

According to these experimental results and those obtained by several other authors, riser and downcomer gas holdups increase linearly with volumetric air flow rates. From visual observation at $U_G = 0.0024$ m s^{-1}, no bubbles entered the downcomer section with circulating liquid for all three spargers used. Therefore, bubble arrival frequency was almost zero at that superficial velocity. The result is in line with an earlier study by Rengel et al. [250], who found that at low superficial gas velocity, the circulating liquid velocity was not enough to entrain a large number of bubbles when circulating through the downcomer.
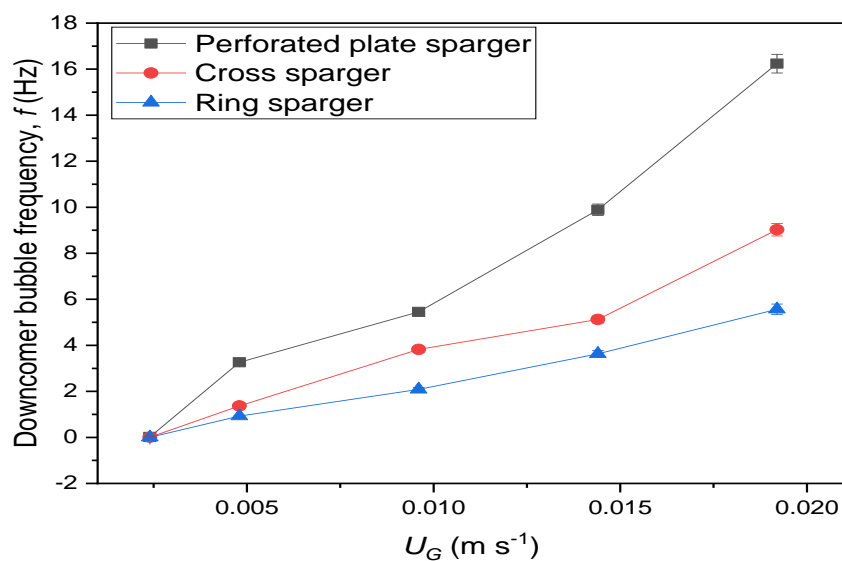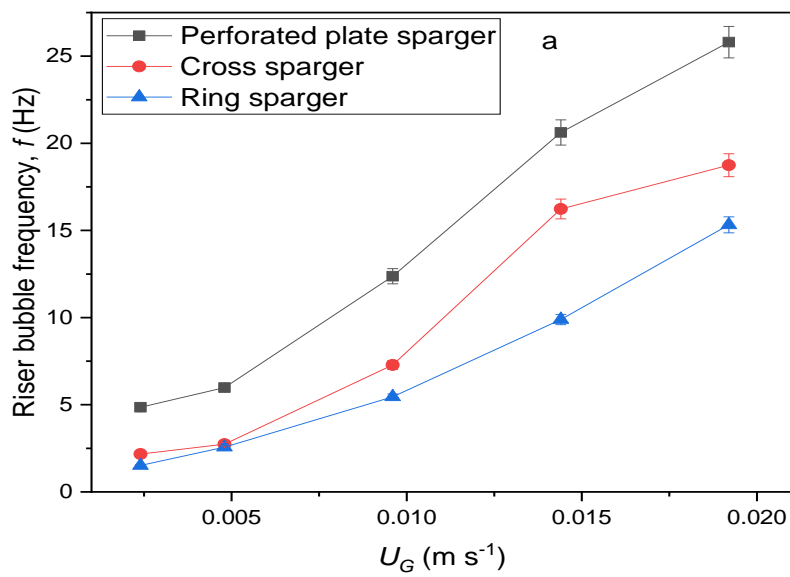
Figure 6. 4 Influence of gas spargers on the bubble frequency in the (a) riser and (b) downcomer at different superficial gas velocities

6.3.3 Influence of sparger type on the overall volumetric mass transfer coefficient K_{La}

The volumetric mass transfer coefficient ($K_{L}a$) is an essential parameter that can affect the photobioreactor productivity [235]. Figure 6.5 shows the effect of superficial gas velocity (U_G) using different gas spargers on the overall gas-liquid mass transfer coefficient ($K_{L}a$). The results show that KLa increased linearly with superficial gas velocity. This trend was in line with the findings of Guo and Huang [235], who investigated the effect of superficial gas velocity on $K_{L}a$ in a rectangular airlift loop photobioreactor. Pirouzi et al. [255], studied the influence of airlift photobioreactor hydrodynamics on microalgae growth. They found that superficial gas velocity had a significant effect on the volumetric mass transfer coefficient, which was in harmony with the current study. It can be seen that the value of $K_{L}a$ increased 3.33 times (from 0.0021 s^{-1} to 0.0091 s^{-1}) with increasing U_G (from 0.0024 m s^{-1} to 0.0192 m s^{-1}) for the perforated plate sparger compared with a slight increase (from 0.000951 s^{-1} to 0.00435 s^{-1} and from 0.00085 s^{-1} to 0.00402 s^{-1}) in both the cross sparger and ring sparger, respectively. The reason for this is that the perforated plate sparger produced a higher number of smaller bubbles compared with the other types of sparger used. Therefore, the perforated plate sparger produced a higher value of gas holdup and $K_{L}a$. Similar findings were reported by Miyahara et al, [226], who reported that the perforated plate sparger created a larger number of smaller bubbles, which led to obtaining a higher overall gas holdup and $K_{L}a$.
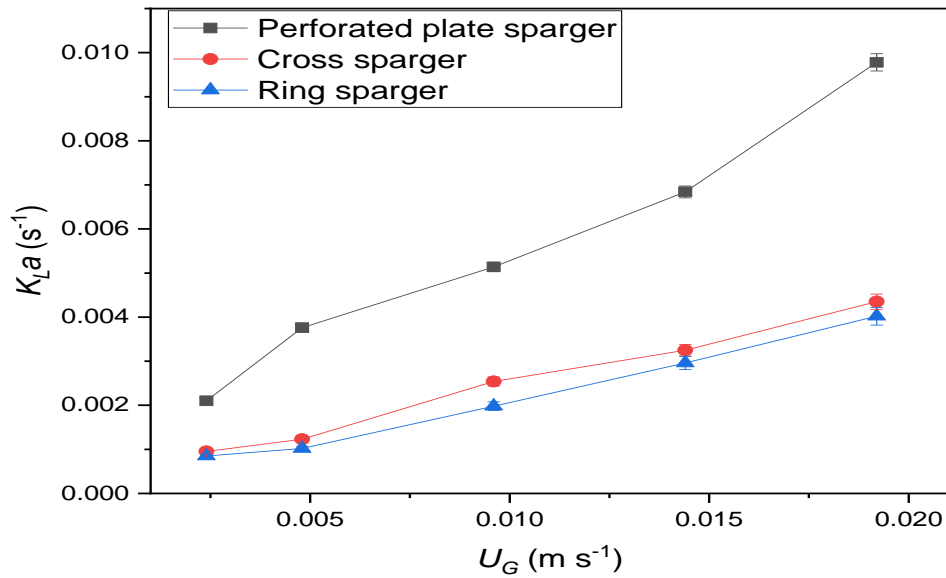
Figure 6. 5 Effect of superficial gas velocity on volumetric mass transfer coefficient for different types of sparger.

6.3.4 Influence of sparger type on mixing time (T_m)

Figure 6.6 presents the effect of superficial gas velocity (U_G) on mixing time (T_m) for the different types of sparger used (perforated plate sparger, cross sparger, and ring sparger). In all three spargers, the mixing time was enhanced with increasing aeration rate. From the data in Fig. 6.6, it is apparent that the slopes of the three curves decreased with increased U_G. However, T_m was the shortest for the perforated plate sparger compared with the other types. At higher gas superficial gas velocities, the effect of sparger and gas velocity diminished. Thus, under some conditions, mixing time became independent of sparger type or gas flow rate. Similar results were obtained by Merchuk et al. [256], who studied the mixing time in a concentric airlift reactor with different types of gas distributor.
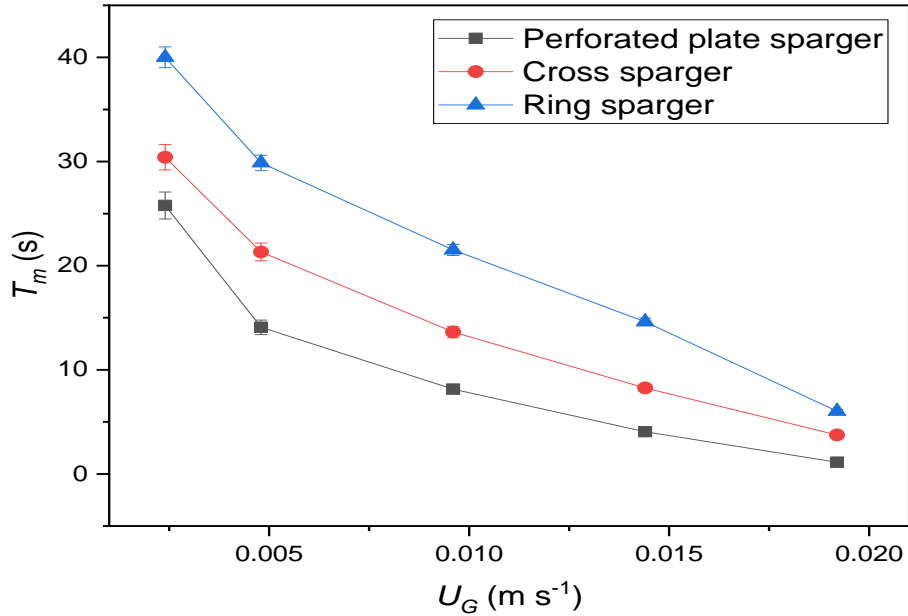
Figure 6. 6 Effect of superficial gas velocity on mixing time (T_m) for different types of sparger.

6.3.5 Influence of sparger type on Chlorella vulgaris growth

Figure 6.7 shows the *Chlorella vulgaris* cell density (cell mL^{-1}) over 10 days of cultivation time using three different types of gas sparger (perorated plate sparger, cross sparger, and ring sparger). *Chlorella vulgaris* showed good growth potential in primary wastewater (P_{ww}). The cell count of *Chlorella vulgaris* growth showed a rapid increase and recorded its maximum count 61.5×10^6 cell mL^{-1} for the perforated plate sparger over 10 days, while it was 39.35×10^6 and 35.31×10^6 cell mL^{-1} for the cross sparger and ring sparger, respectively. As shown in Figs. 6.2a, 6.2b, 6.3, 6.4a, 6.4b, 6.5, and 6.6, the perforated plate sparger showed higher gas hold-up, bubble arrival frequency, mixing time, and overall volumetric gas-liquid mass transfer coefficient distribution compared with the other spargers. Thus, the hydrodynamics (gas holdup, gas-liquid interfacial area, and bubble size) have a significant positive effect on the cell density of *Chlorella vulgaris* [214].
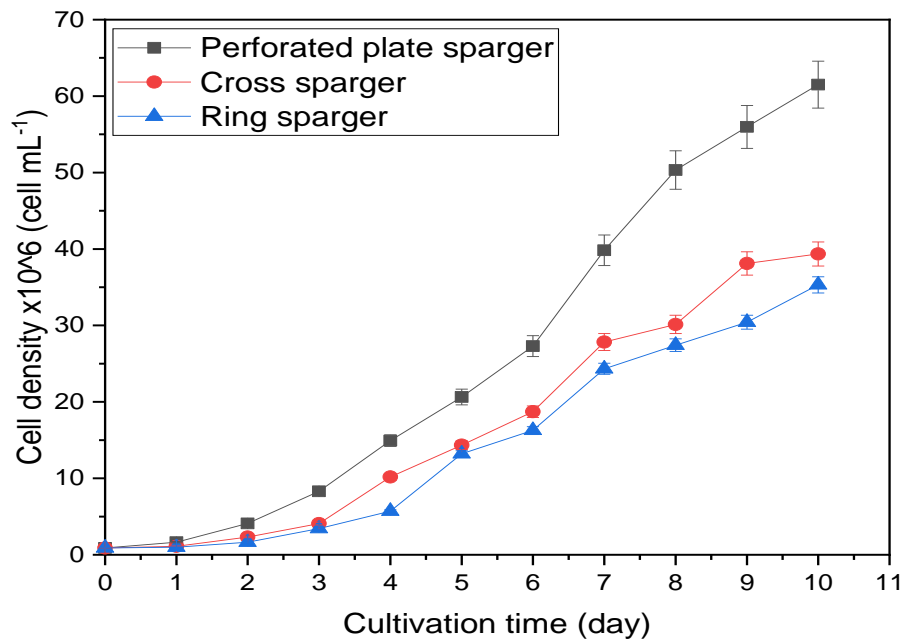
Figure 6. 7 Influence of sparger type on cell density.

6.3.6 Influence of sparger type on TN, TP, and COD removal efficiencies

Chlorella vulgaris showed a high capacity for utilizing and removing TN and TP from wastewater regardless of the type and configuration of the photobioreactor applied [198, 245, 257-259]. It will be interesting to see how the gas sparger type in a specific photobioreactor (in this case, the airlift photobioreactor) can impact the removal efficiency of TN and TP. Figures 6.8a and 6.8b show the daily TN and TP removal efficiencies from primary wastewater using different spargers (perforated plate sparger, cross sparger, and ring sparger). Both the TN and TP removal efficiencies increased with cultivation time for all the applied spargers with the highest value achieved at the end of the cultivation period (Day 10). The results show that when the perforated plate sparger was applied, the TN removal efficiency was 84.2%, while it was 70.6% and 48.2% for the cross sparger and ring sparger, respectively (Fig. 6.8a). A similar trend was observed for the TP removal efficiency, 99.4% TP removal was achieved on Day 10 of the cultivation using the perforated plate sparger, while for the cross sparger it was 84.4% and for the ring sparger it was 80.1%, (Fig.6.8b).
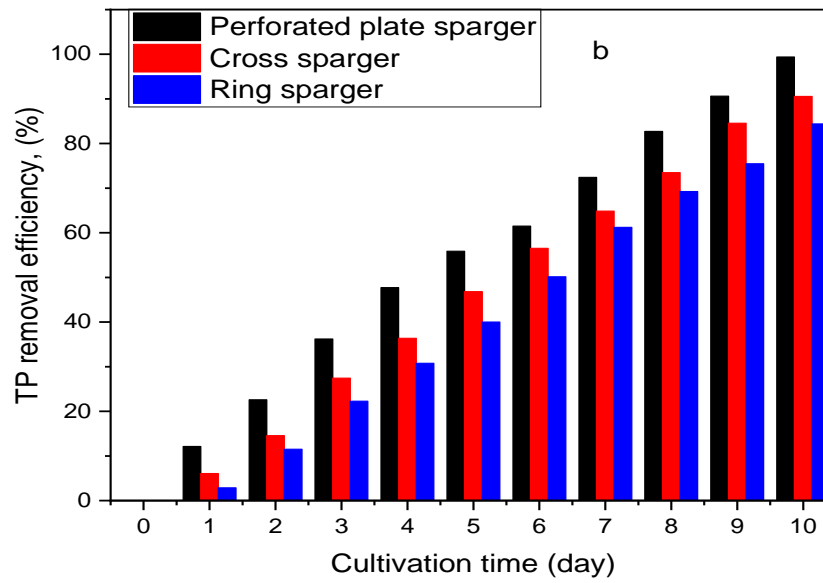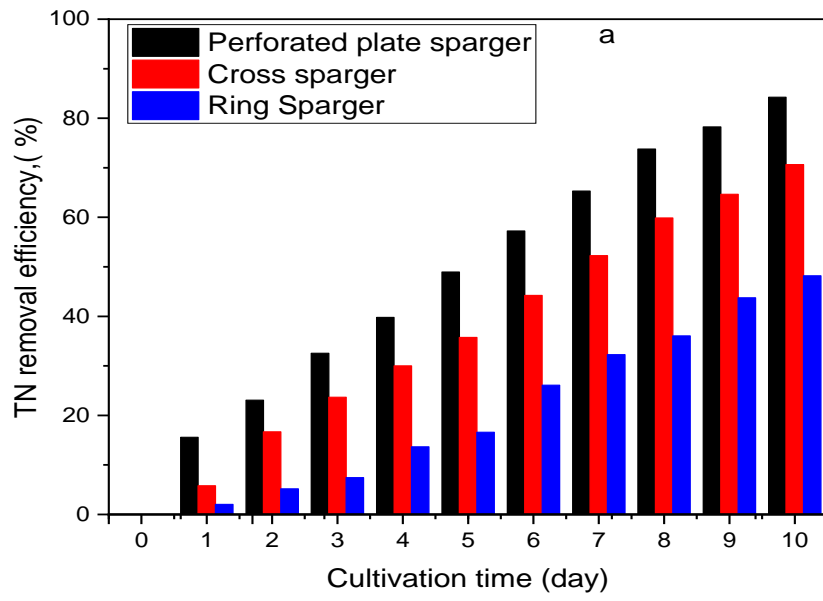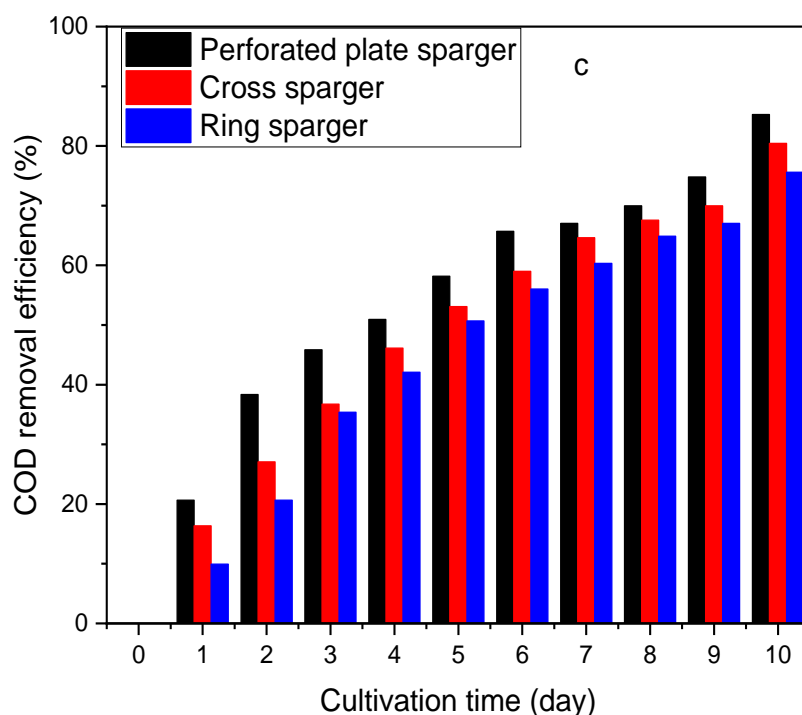
Figure 6. 8 Influence of sparger type on (a) TN removal, (b) TP removal efficiency and (c) COD removal.

Figure 6.8c, shows the daily COD removal efficiency using different gas spargers. The COD concentration decreased from 373 mg L^{-1} to 55 mg L^{-1} with 85.25% removal efficiency using the perforated plate sparger after 10 days of cultivation, while it was 80.4% and 75.6% for the cross sparger and ring sparger, respectively. Therefore, the hydrodynamics (gas hold up, bubble arrival frequency), K_La, and mixing time created by different applied gas spargers significantly affected the *Chlorella vulgaris* growth and consequently the TN and TP removal from the primary wastewater.

6.3.7 Calibration of the proposed model

Experimental data obtained under the following initial conditions (TP=6.6 mg L^{-1}, TN=30.6 mg L^{-1}, CO_2=2 %, I = 200 µmol m^{-2} s^{-1}, Q_G = 2 L min^{-1}) were applied to estimate the model parameters in Eq. (6.9). The estimated and the calculated parameters are listed in Table 6.1.

Table 6. 2 Estimated parameters used for the simulation

parameters	Unit	value	Notes
d_b	m	0.035	Calculated
μ_{max}	d^{-1}	0.355	Estimated, current study
K_N	gL^{-1}	0.0246	Estimated, current study
K_P	gL^{-1}	0.00453	Estimated, current study
K_C	gL^{-1}	0.2	Estimated, current study
K_I	$\mu mol\ m^{-2}\ s^{-1}$	10	Estimated, current study
Y_N	$g_N/g_{biomass}$	0.092	Calculated, current study
Y_P	$g_P/g_{biomass}$	0.356	Calculated, current study
Y_C	$g/g_{biomass}$	0.02	Calculated, current study
K_La	d^{-1}	0.5	Calculated, current study

These parameters were able to obtain good agreement between the experimental and simulated results as shown in Figures 6.9-6.13.
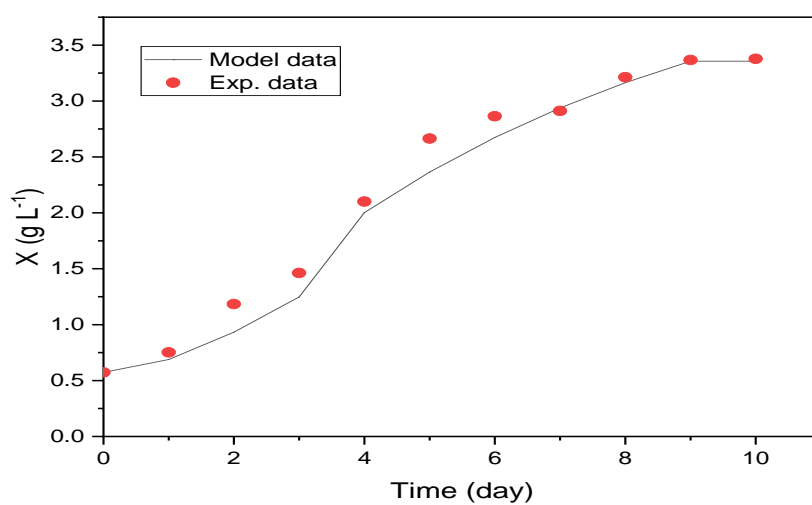
Figure 6. 9 Comparison of experimental data with model data for biomass concentration X

In addition, the proposed model was validated with experimental data from previous studies [246, 260] as shown in Figs 6.10 and 6.11. Zhu et al. [246], studied the cultivation of *Chlorella zofingiensis* in piggy wastewater for biodiesel production and wastewater treatment. They cultivated *Chlorella zofingiensis* in 1.37 L volume of photobioreactor, CO_2 concentration was 5-6%, and light intensity of 230 μmol m^{-2} s^{-1}. While, Huang et al.[260], studied the effect of gas sparger on CO_2 mass transfer to enhance *Chlorella pyrenoidosa* biomass production in 0.4 L of bioreactor volume, light intensity of 80 μmol m^{-2} s^{-1}, and CO_2 concentration 3-10%. The proposed model was developed depends on many factors such as gas holdup, bubble diameter, light intensity distribution, overall mass transfer coefficient, interfacial area, and half saturation constant for light intensity, total nitrogen, and total phosphorous. Therefore, there is a discrepancy between model data and experimental data, as shown in Figs 6.10 and 6.11.
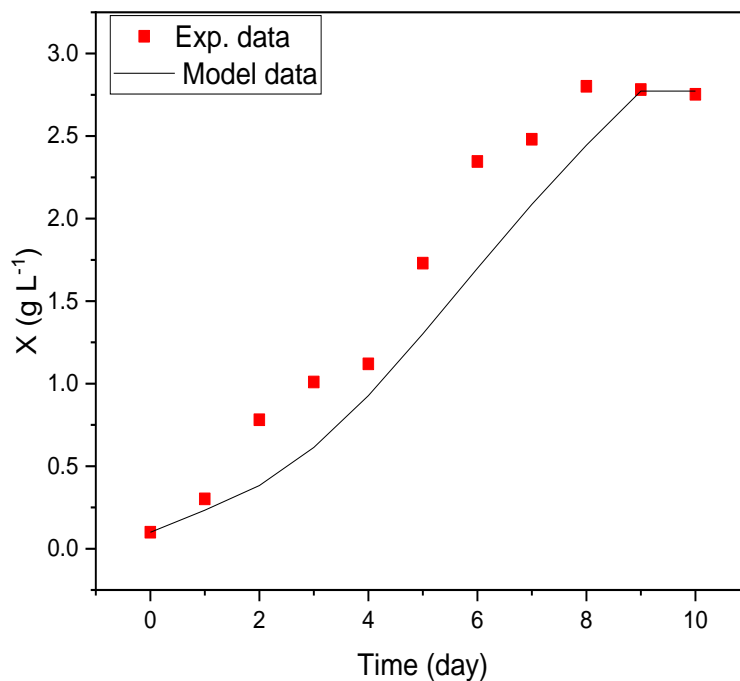
Figure 6. 10 Comparison of experimental data with model data for biomass concentration[246]
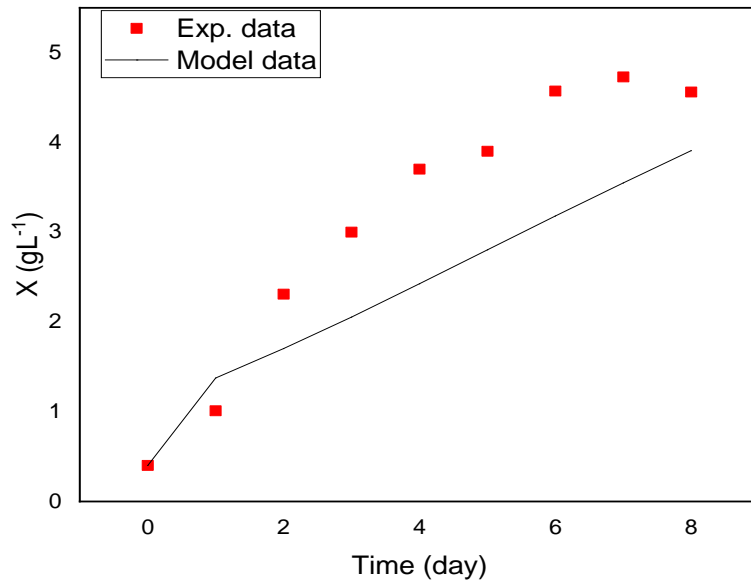
Figure 6. 11 Comparison of experimental data with model data for biomass concentration[68]
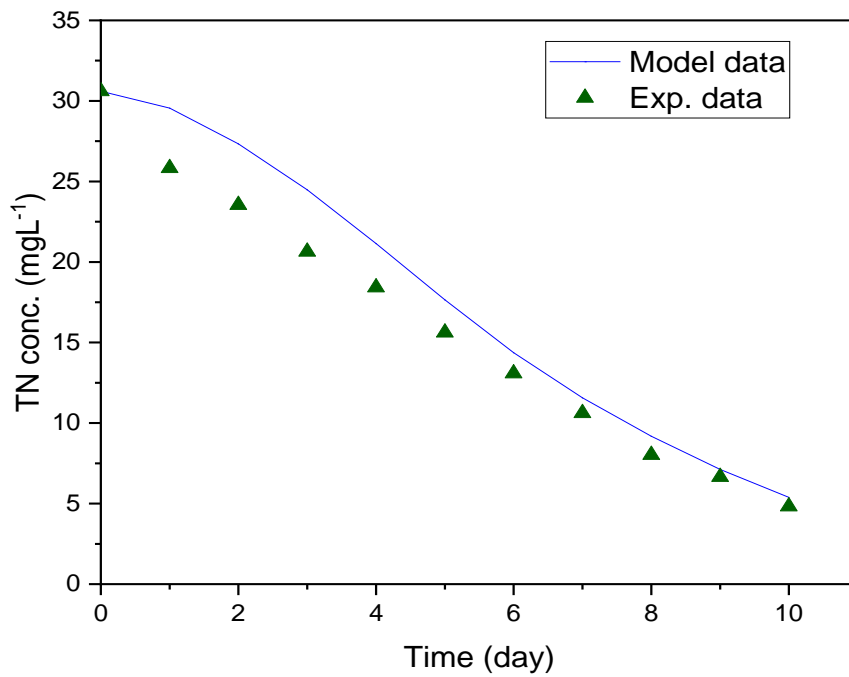
Figure 6. 12 Comparison of experimental data with model data for TN removal
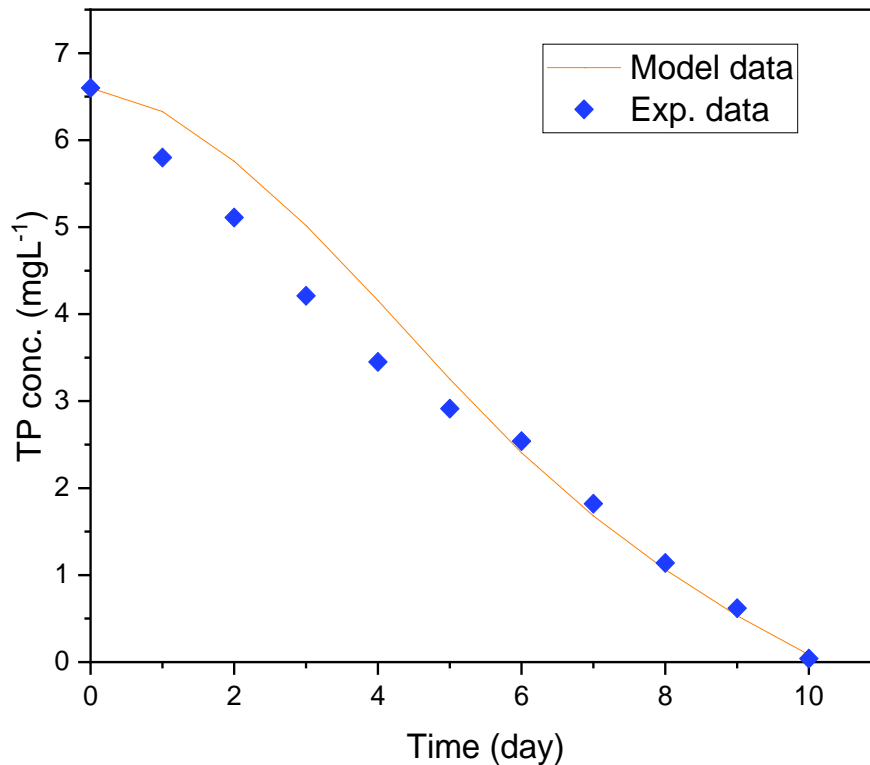
Figure 6. 13 Comparison of experimental data with model data for TP removal

Nutrient consumption transients showed rapid removal of TP to 100% removal, such that it became limited by around Day 6 to the lowest TP initial concentration of 6.6 mg/L., whilst the extracellular phosphorous was depleted rapidly in the cultivation medium, with the cells continuing to grow over the period of the experiment. The luxury uptake of nutrients and storage for later growth is a well-established phenomenon in phytoplankton [261], although this does not influence the P uptake rate. TN removal efficiencies of 80-99% were recorded after 10 days for TN initial concentrations of 30.6 mg/L. The model appears to adequately predict the dynamic depletion of TN and TP in the cultivation medium, along with algal biomass production over the ranges of initial nutrient concentration.
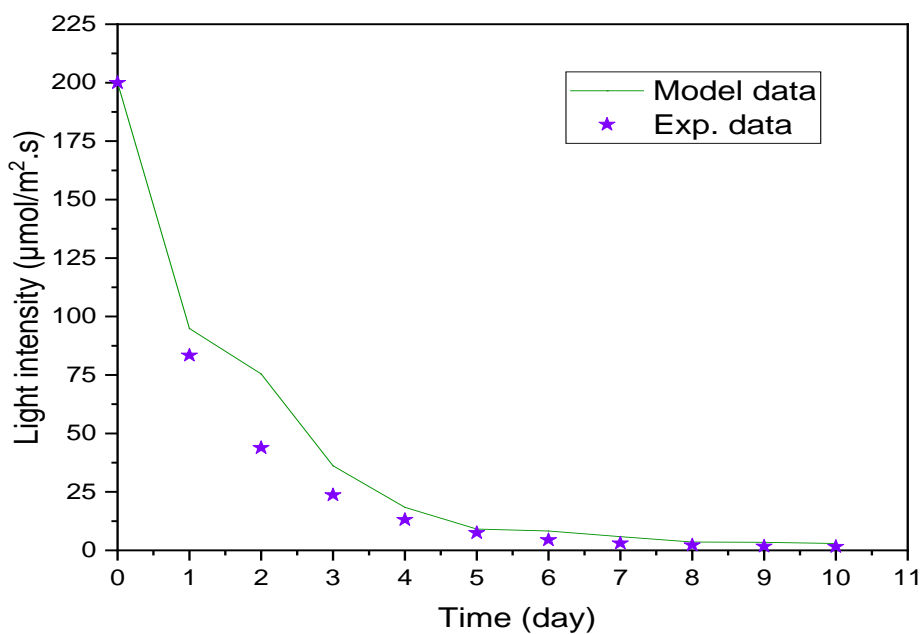
Figure 6. 14 Comparison of experimental data with model data for light intensity profile the centre of the reactor

To further validate the proposed model and the estimated parameters, the model was applied to simulate other experimental data obtained at different gas flow rates (1L min^{-1} and 5Lmin[-1]). Figures 6.15-6.18 clearly show the good agreement between the simulated and experimental light intensity distribution and biomass growth at both 1 and 5 L min^{-1}.
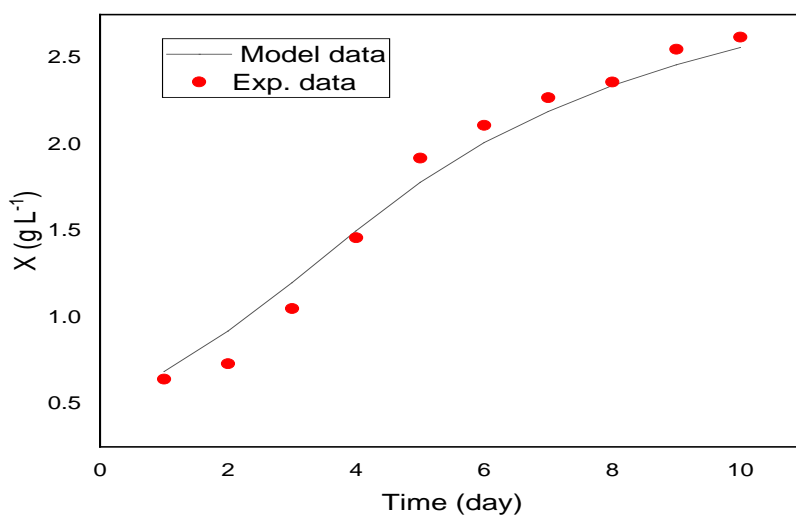
Figure 6. 15 model validation at flow rate of 1 L min^{-1}
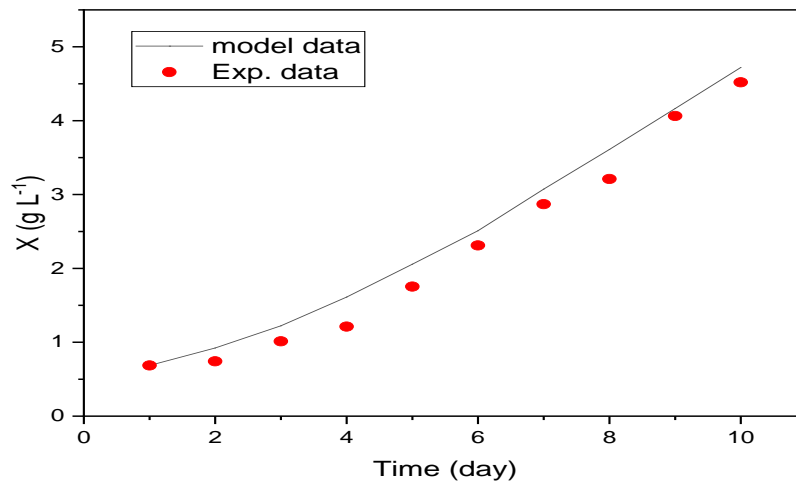
Figure 6. 16 model validation at gas flow rate of 5 L min^{-1}

It can be shown that the light intensity profile enhanced with increased gas flow rate. Therefore, it can be concluded that gas holdup is the limiting factor for light distribution inside the photobioreactor. In other words, the fluid dynamics in the photobioreactor determine the local light intensity that affects microalgae growth. The fluid dynamics depend on the gas flow rate which enhances the movement of liquid medium and algal cells [71]. As a result, increasing the gas flow rate impacts the distribution of gas holdup inside the photobioreactor which enhances the liquid movement and gas-liquid mass transfer. The comparison between predicted and measured data showed considerable agreement as shown in Figs 6.15 and 6.16.
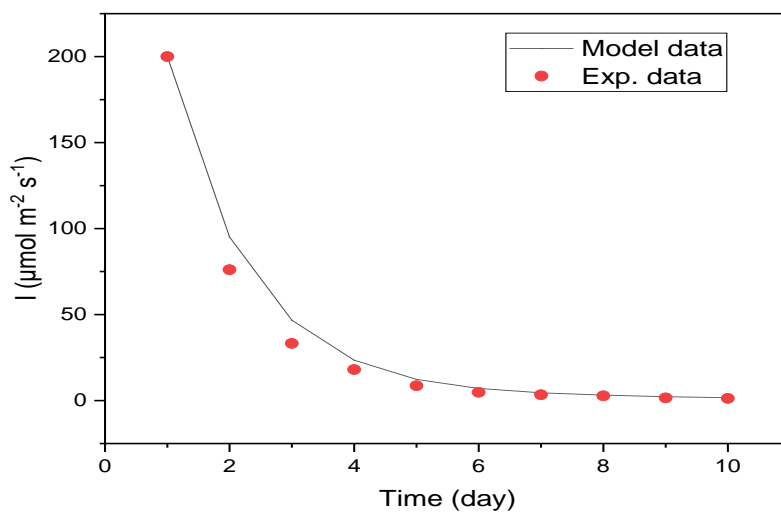
Figure 6. 17 comparison of predicted and experimental light intensity profile at gas flow rate (1 L min^{-1}) in the centre of the reactor
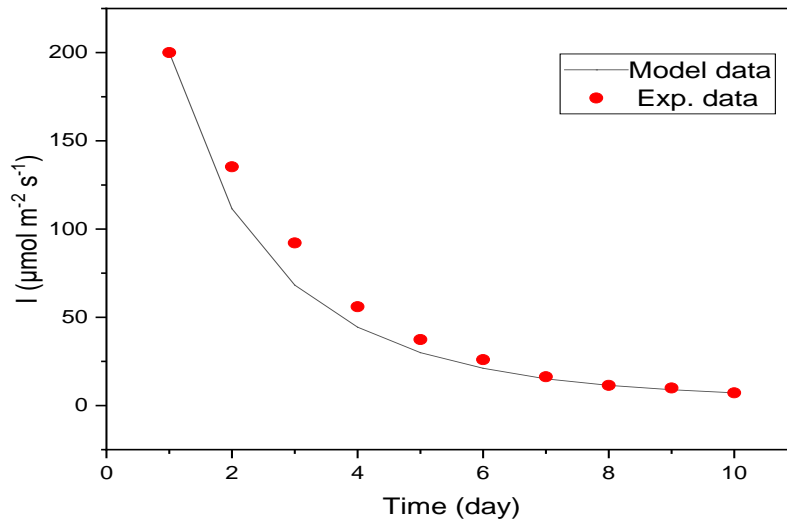
Figure 6. 18 comparison of predicted and experimental light intensity profile at gas flow rate (5L min^{-1}) in the centre of the reactor

6.3.8 Influence of variation of input parameters on biomass concentration X

The sensitivity of the biomass concentration profile to the variations parameters K_N, K_C, K_P, K_I and μ_{max}, k_La, and d_b were investigated for the conditions of $Cc,g = 2\%$, $T_N = 30.6$ mg L^{-1}, $T_P = 6.6$ mg L^{-1} and $I = 200$ µmol m^{-2} s^{-1}. The model parameters (Table 6.2) varied by $\pm 20\%$ to show their impact on biomass concentration (X). The mean predicted profile from four runs for each parameter is shown in Figs. 6.17 and 6.18 with the sensitivity coefficient ($\emptyset i$) calculated by Eq. (6.11), where high $\emptyset i$ indicates a more sensitive parameter on the response parameters (biomass concentration, X, in this case). According to the results in Figs 6.17 and 6.18, the maximum specific growth rate parameters μmax and the bubble diameter (d_b) have the highest $\emptyset i$, i.e, the most sensitive parameters on the biomass growth (X), with $\emptyset i$ of 1.57 and 1.815 respectively. Sensitivity to μmax has been previously reported [262] and reflects the importance of this parameter for the accuracy of model prediction. On the other hand, the parameters k_La and K_N are less sensitive to the biomass concentration (X), where $\emptyset i$ were 0.03 and 0.0024, respectively.
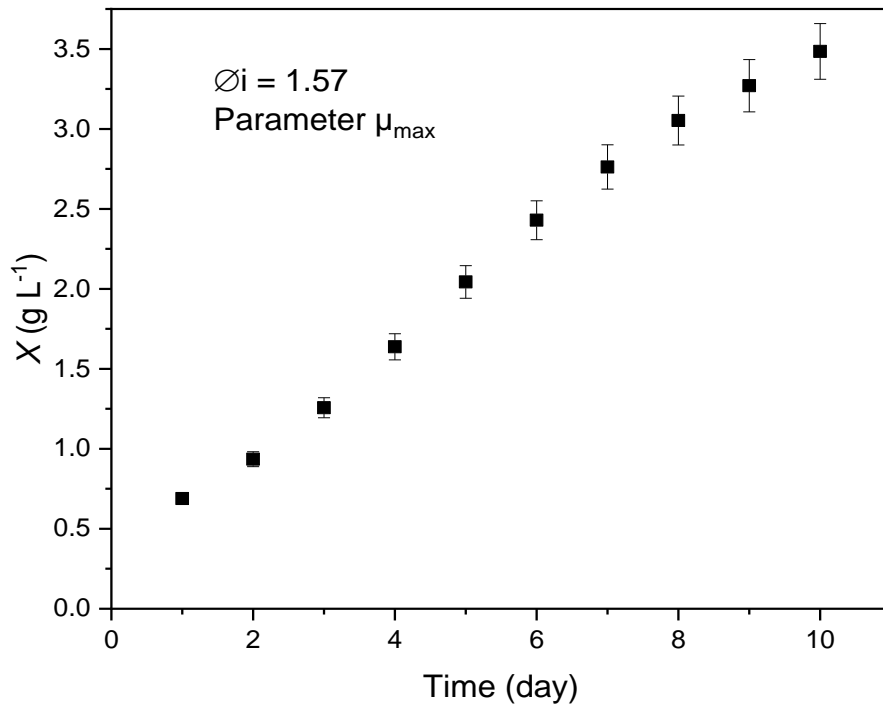
Figure 6. 19 Predicted mean X and its variation based on 20% change in μ_{max}
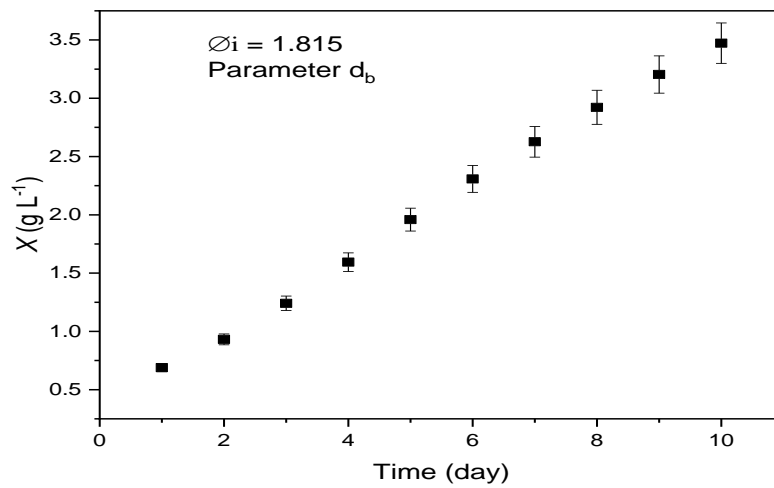
Figure 6. 20 Predicted mean X and its variation based on 20% change in d_b

6.4 summery

Influence of different types of gas spargers (perforated plate sparger, cross sparger, and ring sparger) on the hydrodynamics (gas holdup, liquid circulation, and mixing) and mass transfer coefficient ($K_L a$), on the cell density growth, TN, TP, and COD removal efficiencies were investigated using *Chlorella vulgaris* cultivated for 10 days in primary wastewater in an airlift photobioreactor. The results show the preference of the perforated plate sparger compared to the others (cross and ring spargers). The perforated plate sparger provided the adequate hydrodynamic conditions and high $K_L a$ which consequently improved the *Chlorella vulgaris* cells growth and their ability to utilize and remove TN, TP and COD after 10 days of cultivation. The TN, TP and COD removal efficiencies were 84.2%, 99.4%, and 85.25 %, respectively, with a cell density of 61.5×10^6 cell mL^{-1} when the perforated plate sparger was applied. Furthermore, a modified Monod kinetic model was proposed to consider the gas holdup and the bubble diameter in order to simulate the biomass growth, light distribution inside the airlift photobioreactors, and the TN and TP profiles during the cultivation period. The effect of four limiting factors (TN 30.6 mgL^{-1}, TP = 6.6 mgL^{-1}, CO_2 concentration 2%, and light intensity ($I = 200$ µmol m^{-2} s^{-1}) on microalgae cultivation were studied. The model was able to simulate the experimental results satisfactorily. The sensitivity analysis confirmed the importance of the maximum specific growth rate and bubble diameter on biomass growth.

Chapter seven
Synergistic impacts and optimization of gas flow rate, CO_2 concentration, and light intensity on CO_2 biofixation and nutrient removal from wastewater by *Chlorella vulgaris*

7.1 Introduction

Carbon dioxide (CO_2) mitigation and wastewater treatment have attracted significant attention due to the fact that CO_2 is one of the major causes of global warming. In addition, discharging wastewater with high concentration of P and N into the water bodies (lakes, rivers) without proper treatment will significantly impact the aquatic ecosystem and causes eutrophication [263]. Microalgae culture technology (MCT) have been extensively studied as a capable biotechnology for generating valuable products, mitigate CO_2, and wastewater treatment [7]. Microalgae fix CO_2 more efficiently compared with terrestrial plants [2] and can grow by utilizing the nutrients (P and N) in wastewater even at high concentrations [4]. Several studies have investigated the influence of light intensity, CO_2 concentration, and aeration rate on CO_2 biofixation as well as the ability of microalgae to remove nutrients from different types of wastewater [264].

CO_2 biofixation using microalgae is affected by the CO_2 concentration in the injected gas to the photobioreactor, light intensity, microalgae species, and photobioreactor configuration [265]. Naderi et al [197], studied the effect of light intensity on *Chlorella vulgaris* growth and CO_2 biofixation in a stirrer photobioreactor with 2% CO_2 concentration and a light intensity of 30-300 µmol $m^{-2} s^{-1}$. They achieved a maximum CO_2 biofixation rate of 0.45 $gCO_2.L^{-1}d^{-1}$ at a light intensity of 100 µmol $m^{-2} s^{-1}$. Cheng et al [85], investigated the influence of CO_2 concentration in the inlet gas at 0.05% to 1% on CO_2 biofixation using *Chlorella vulgaris* in an air lift reactor with a light intensity range from 23.6 to 236.4 µmol $m^{-2} s^{-1}$. They obtained 260 mg $L^{-1} h^{-1}$ biofixation rate at 1% CO_2 concentration and a light intensity of 157.6 µmol $m^{-2} s^{-1}$. The impact of gas flow rate on CO_2 biofixation rate in a raceway pond was studied by Cheng et al [266]. They found that gas flow rate had a significant influence on *Nannochloropsis oculata* growth and the biofixation rate of CO_2 increased from 26.3 to 31.9 g $m^{-2} d^{-1}$ with an increased gas flow rate from 50 to 150 $m^3 h^{-1}$. In another study by Yoo et al [267], the ability of *Botryococcus braunii, Chlorella vulgaris, and Scenedesmus* sp. were investigated for CO_2 biofixation at a light intensity of 150 µmol $m^{-2} s^{-1}$ and 10% CO_2 concentration. They reported

that *Scenedesmus sp.* was the most efficient species for CO_2 mitigation due to its having the highest biomass productivity and biofixation rate ability. Despite of considerable researches, optimum conditions for CO_2 biofixation have not yet been adequately established.

Algal wastewater treatment is achieved through the cultivation of microalgae by utilizing nutrients (nitrogen and phosphorus) and other pollutants in the wastewater. Wastewater treatment using microalgae offers advantages such as reduced heavy metal concentration, CO_2 emission through biofixation and processing costs, as well as generation of valuable products[268]. Microalgae can efficiently remove pollutants, toxic compounds, and accumulated heavy metals from industrial and municipal wastewater to produce a biomass which can be used for biofuel production [269]. Several studies by [270-275], have investigated the capability of microalgae for wastewater treatment.

Gas aeration is an important parameter that influences photobioreactor hydrodynamics, mixing performance and cell exposure to light, and prevents gradients of nutrients concentration inside the photobioreactor. Hence, aeration rate (gas flow rate and CO_2 concentration) is a crucial parameter for enhancing microalgae performance [276]. High aeration rate has shown a negative impact on the cost of the process, especially on large-scale of MCT [277]. Therefore, the aeration rate should be optimized for microalgae growth, CO_2 biofixation and nutrient removal. In this study, the synergistic influence of the aeration rate (gas flow rate and CO_2 concentration) and the light intensity on the CO_2 biofixation and nutrient (nitrogen and phosphorus) removal from wastewater by *Chlorella vulgaris* was investigated and optimized by applying Response Surface Methodology and Box-Behnken Design.

7.2 Materials and methods

7.2.1 Microalgae and culture conditions

Chlorella vulgaris (strain: CCAP 211/11B, CS-42) was used in this study. The microalgae cells were grown in an MLA medium [278]. The microalgae were cultivated in primary wastewater

for 10 days in a draft tube airlift photobioreactor, 100 cm in height and 10 cm in diameter, with a draft tube height of 60 cm and a diameter of 6 cm. CO_2-enriched air was bubbled into the photobioreactor through a perforated plate sparger.

7.2.2 Calculation of biomass productivity and CO₂ biofixation rate

Biomass productivity was calculated (P_X) using the following equation:

$$P_x = \frac{X_t - X_o}{t} \tag{7.1}$$

Where Px is biomass productivity (g $L^{-1}d^{-1}$), X_o is initial biomass concentration (gL^{-1}), X_t is biomass concentration at the end of the cultivation (gL^{-1}), and t is the cultivation time.

CO₂ biofixation rate was calculated as follows:

$$CO_2 \text{ biofixation rate } R_{CO_2} \ (gL^{-1}d^{-1}) = \%C \times P_x \times \frac{MW_{CO_2}}{MW_c} \tag{7.2}$$

Where *%C* is the percentage of carbon measured using an element analyser, P_x is biomass productivity (g$L^{-1}d^{-1}$), MW_{CO_2} is molar mass of CO_2, and MW_c is molar mass of carbon.

7.2.3 Experimental design and regression analysis

Box Behnken Design was employed to optimize the performance of the algal cultivation based on CO_2 biofixation and nutrient (total nitrogen and total phosphorus) removal. A multi-level, three-parameter matrix was utilized to investigate the synergistic influence between the three parameters (gas flow rate X_1, CO_2 concentration X_2, and light intensity X_3). To obtain these goals, 15 experiments will be accomplished by varying gas flow rate (Q), CO_2 concentration (% CO_2), and light intensity (I) as presented in Table 7.1

The ranges of these factors were chosen based on a literature search [85, 205, 264, 279].

The quadratic model used to predict the optimum response expressed as follows:

$$Y = \beta_o + \sum_{i-1}^{k} \beta_{ii} X_i^2 + \sum_{i-1}^{k} \sum_{j-1}^{k} \beta X_i + \varepsilon \tag{7.3}$$

Where Y is the response variable; i and j are the index numbers for the patterns; β_o is the constant coefficient; β_i, β_{ii} and β_{ij} are the regression coefficients for linear, quadratic, and

influence, respectively; x_i and x_j are the factors to be investigated, and the coded variables are defined as:

$$x_i = \frac{X_i - X_o}{\Delta X_i} \tag{7.4}$$

Where x_i is the coded value of the independent factors, X_i is the actual value of the independent factors, X_o is the actual value of the factor at the centre point, and ΔX_i is the step change value. The multi-level experimental design (minimum and maximum) used ranges of independent variables: gas flow rate (1-8 L min^{-1}), CO_2 concentration (0.03-7 %), and light intensity (150-400 µmol m^{-2} s^{-1}).

A total of 15 experiments, were randomly conducted in triplicate to minimize the influence of temporal errors to determine the 10 coefficients of the second order polynomial generated from Eq. (7.3). JMP statistical discovery software (SAS version 14.0.0) was employed to complete the regression analysis and to plot the 3D graphs and the contours. Equation (7.3) was also used to predict the optimum point and to identify the interaction among the variables within the specified experimental boundary conditions.

Table 7. 1 Experimental range of independent variables

Independent variable	Symbol	Range and level		
		-1	0	+1
Gas flow rate Q (L min^{-1})	X_1	1	4.5	8
CO_2 concentration (%)	X_2	0.03	3.5	7
Light intensity I (µmol m^{-2} s^{-1})	X_3	150	275	400

7.3 Results and discussion

7.3.1 Multiple regression analyses

Multiple regression analysis was used to determine the relationships between the three response parameters of CO_2 biofixation rate, total nitrogen and total phosphorus removal efficiency with respect to CO_2 concentration, gas flow rate, and light intensity, which generated second-order

polynomial equations from Box Behnken Design matrix of experimental data as shown in Table 7.2

Table 7. 2 Actual levels of Box Behnken Design matrix with experimental and predicted response values

Run	Independent variables			R_{CO_2} (g L^{-1}d^{-1})		TN removal efficiency (%)		TP removal efficiency (%)	
	X_1	X_2	X_3	Experimental	Predicted	Experimental	Predicted	Experimental	Predicted
1	1.0	0.03	275	0.425	0.393	58.6	57.6	81.4	80.4
2	1.0	7.00	275	0.625	0.6395	68.5	67.8	86.1	85.7
3	8.0	0.03	275	0.752	0.737	75.7	76.3	83.5	83.8
4	8.0	7.00	275	0.657	0.688	75.6	76.6	82.4	83.3
5	4.5	0.03	150	0.372	0.410	58.7	58.4	80.1	80.0
6	4.5	0.03	400	0.600	0.607	62.7	63.3	92.1	92.7
7	4.5	7.00	150	0.497	0.489	60.2	59.5	86.4	85.7
8	4.5	7.00	400	0.764	0.725	72.4	72.7	91.6	91.6
9	1.0	3.50	150	0.812	0.804	63.2	64.5	87.4	88.4
10	8.0	3.50	150	0.814	0.789	73.2	72.8	86.4	86.0
11	1.0	3.50	400	0.784	0.808	67.8	68.1	94.5	94.8
12	8.0	3.50	400	1.210	1.217	88.6	0.873	99.2	98.2
13	4.5	3.50	275	0.954	0.954	84.2	84.2	99.1	99.1
14	4.5	3.50	275	0.954	0.954	84.2	84.2	99.1	99.1
15	4.5	3.50	275	0.954	0.954	84.2	84.2	99.1	99.1

R_{CO_2}= CO$_2$ biofixation rate, TN= total nitrogen, TP= total phosphorus.

The results from the regression formulae were:

$$CO_2\ biofixation\ rate\ (g\ L^{-1}d^{-1}) = 0.945 + 0.098375x_1 + 0.04925x_2 + 0.107875x_3 -$$
$$0.07375x_1x_2 + 0.106x_1x_3 + 0.00975x_2x_3 + 0.00375x_1^2 -$$
$$0.343x_2^2 - 0.05275x_3^2 \hspace{2cm} (7.5)$$

$$TN\ removal\ efficiency\ (\%) = 0.842 + 0.06875x_1 + 0.02625x_2 + 0.4525x_3 -$$
$$0.025x_1x_2 + 0.027x_1x_3 + 0.0205x_2x_3 - 0.0245x_1^2 -$$
$$0.01215x_2^2 - 0.0855x_3^2 \tag{7.6}$$

$$TP\ removal\ efficiency\ (\%) = 0.991 + 0.002625x_1 + 0.01175x_2 + 0.046375x_3 -$$
$$0.0145x_1x_2 + 0.01425x_1x_3 - 0.017x_2x_3 -$$
$$0.057125x_1^2 - 0.100375x_2^2 - 0.015125x_3^2 \tag{7.7}$$

Where x_1, x_2, and x_3 are coded values calculated using Eq. (7.4), TN is total nitrogen and TP is total phosphorus. The determination coefficient (R^2) of the regression equations for CO_2 biofixation rate, and total nitrogen and total phosphorus removal efficiencies were 0.99, 0.99, and 0.99 respectively. Therefore, quadrative Eqs. (7.5 to 7.7) can appropriately represent the relationship between the variables and responses. The predicted values from Eqs. (7.5 to 7.7) were in good agreement with the data obtained experimentally as shown in Fig. 7.1.
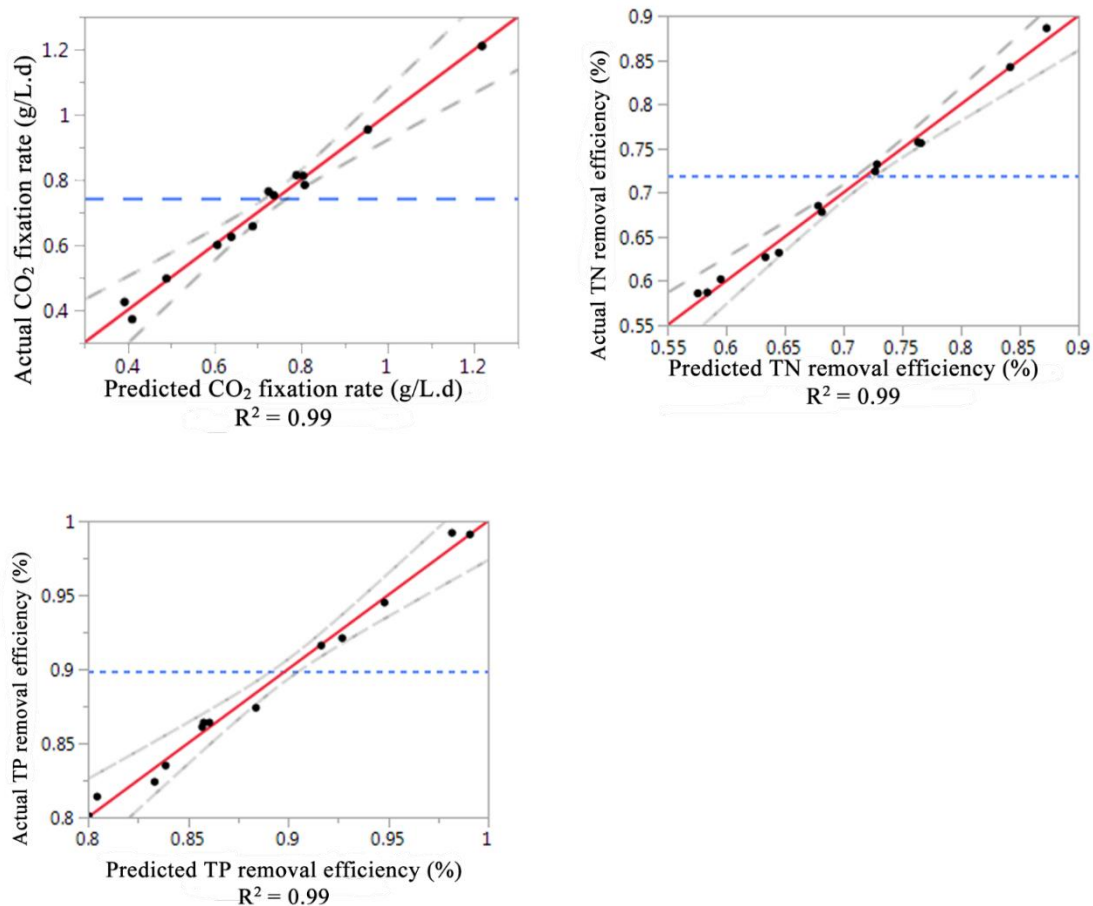
Figure 7. 1 Comparison between experimental and predicted data of CO_2 bio-fixation rate, total nitrogen and total phosphorus removal efficiencies, (**.**) experimental values, (– –_) confidence bands, and (——) fit line.

7.3.2 Analysis of variance (ANOVA)

Analysis of variance (ANOVA) was applied to determine the significance of each term (linear, interactive, and quadratic) of the second-order polynomial models as shown in Table 7.3. The *P*-value indicates the significance of each term (i.e. $p < 0.05$ indicates that the term is significant). Table 7.3 shows that the coefficients of the linear term (*% CO₂* and *I*), coefficients of quadratic term ($\%CO_2^2$ and I^2), and coefficients of interactive term (*Q. %CO₂* and *Q.I*) significantly influence the CO_2 biofixation rate, and total nitrogen and total phosphorus removal efficiencies. In addition, CO_2 biofixation rate and total nitrogen removal efficiency were significantly impacted by gas flow rate, CO_2 concentration, and light intensity with a *p*-value less than 0.05. However, for total phosphorus removal efficiency, the most significant factors were CO_2 concentration and light intensity followed by gas flow rate (Table 7.3). The results showed that the responses of CO_2 biofixation rate, and total nitrogen and total phosphorus removal efficiencies were significantly influenced by the synergistic effect of (*Q. %CO₂* and *Q.I*) with *p*-value <0.05, while (*% CO₂.I*) synergistic effect was less significant (*p*-value = 0.62) on CO_2 biofixation rate compared with total nitrogen and total phosphorus removal efficiencies.

7.3.3 Box Behnken Design analysis

The influences of gas flow rate (*Q*), CO_2 concentration (%CO₂), and light intensity (*I*) on CO_2 biofixation rate (*R_{CO2}*), TN and TP removal efficiencies are shown in Figs 7.2-7.4. These figures illustrate response surfaces (3D) and contours (2D) for CO_2 biofixation rate, TN removal, and TP removal efficiencies, respectively. These graphs clearly show the interfering impacts of all three variables on the responses. For all Figs. (7.2-7.4), one factor was fixed at level zero while changing the other two factors according to the experimental ranges. Increasing corresponding variables led to enhance responses to a certain level after which the responses decreased, although there was an increase in corresponding variables. This behaviour was aligned with the results of the ANOVA shown in Table 7.3, which demonstrated a significant influence of the quadratic terms of all three variables on CO_2 biofixation rate, and TN and TP removal efficiencies.

Figure 7.2a shows the impact of CO_2 concentration and gas flow rate on CO_2 biofixation rate. Increasing CO_2 concentration led to an increase in CO_2 biofixation rate due to the microalgae cells consuming CO_2 in order to store it and use it during times of nutrient deficiency [278].

Table 7. 3 ANOVA analysis from Box Behnken Design

Term	Estimate	Std Error	T-Value	P-Value
CO₂ biofixation rate				
Intercept	0.954000	0.021359	-	-
x_1	0.098375	0.013080	7.52	0.0007*
x_2	0.049250	0.013080	3.77	0.0131*
x_3	0.107875	0.013080	8.25	0.0004*
$x_1.x_2$	-0.07375	0.018498	-3.99	0.0105*
$x_1.x_3$	0.10600	0.018498	5.73	0.0023*
$x_2.x_3$	0.00975	0.018498	0.53	0.6207
x_1^2	0.00375	0.019253	0.19	0.8532
x_2^2	-0.34300	0.019253	-17.82	<.0001*
x_3^2	-0.05275	0.019253	-2.74	0.0408*
Total nitrogen removal efficiency				
Intercept	0.84200	0.007069	-	-
x_1	0.06875	0.004329	15.88	<.0001*
x_2	0.02625	0.004329	6.06	0.0018*
x_3	0.04525	0.004329	10.45	0.0001*
$x_1.x_2$	-0.0250	0.006122	-4.08	0.0095*
$x_1.x_3$	0.02700	0.006122	4.410	0.0070*
$x_2.x_3$	0.02050	0.006122	3.350	0.0204*
x_1^2	-0.0245	0.006372	-3.850	0.0121*
x_2^2	-0.1215	0.006372	-19.07	<.0001*
x_3^2	-0.0855	0.006372	-13.42	<.0001*
Total phosphorus removal efficiency				
Intercept	0.99100	0.005789	-	-
x_1	0.002625	0.003545	0.740	0.4923
x_2	0.011750	0.003545	3.310	0.0211*
x_3	0.046375	0.003545	13.08	<.0001*
$x_1.x_2$	-0.01450	0.005014	-2.890	0.0341*
$x_1.x_3$	0.014250	0.005014	2.840	0.0362*
$x_2.x_3$	-0.01700	0.005014	-3.39	0.0194*
x_1^2	-0.057125	0.005218	-10.95	0.0001*
x_2^2	-0.100375	0.005218	-19.23	<.0001*
x_3^2	-0.015125	0.005218	-2.900	0.0339*

Gas aeration rate had a significant influence on CO_2 biofixation rate due to its using aeration as a carbon source improved mixing that enhanced utilization of light by the cells [91]. CO_2 biofixation rate increased with increased gas aeration rate for all gas flow rates used in this study. As shown in Fig. 7.2a at CO_2 of 3.5% when gas flow rate increased from 1 to 8 Lmin^{-1}, R_{CO_2} increased from 0.784 to 1.21 g L^{-1}d^{-1}. However, Han et al [280] reported that a gas flow rate higher than 9 L min^{-1} caused damage to cells due to higher turbulence.

Figure 7.2c illustrates the influence of CO_2 concentration and light intensity on CO_2 biofixation rate. CO_2 biofixation rate (R_{CO_2}) increased from 0.814 g L^{-1}d^{-1} with increased light intensity from 150 to 400 µmol m^{-2} s^{-1} until it reached an optimal of 1.21 g L^{-1}d^{-1}. Cheah et al [281] concluded that the photosynthetic process was enhanced by using low and moderate light intensity due to photoinhibition by higher light intensity. Ho et al [282] studied the characterization and optimization of carbohydrate production using *Chlorella vulgaris*. They found that the optimal light intensity was 450 µmol m^{-2} s^{-1} and that any further increase in light intensity led to a drop-in biomass production. Present results are in agreement with these previous findings. The present results show that synergistic effect of CO_2 concentration, gas flow rate, and light intensity could enhance the CO_2 biofixation, and total nitrogen and total phosphorus removal.

Considerable interaction was indicated between *I* and CO_2 concentration in the case of TN removal efficiency as shown in Fig. 7.3c. As shown in Fig. 7.3c at ($Q_G = 8$ L min^{-1}) the TN removal efficiency increased from 73.2% to 88.6% when *I* increased from 275 µmol m^{-2} s^{-1} to 400 µmol m^{-2} s^{-1}. While TP removal efficiency increased from 94.2% to 99.5% when Q_G increased from 1 L min^{-1} to 8 L min^{-1} at CO_2 concentration of 3.5%.
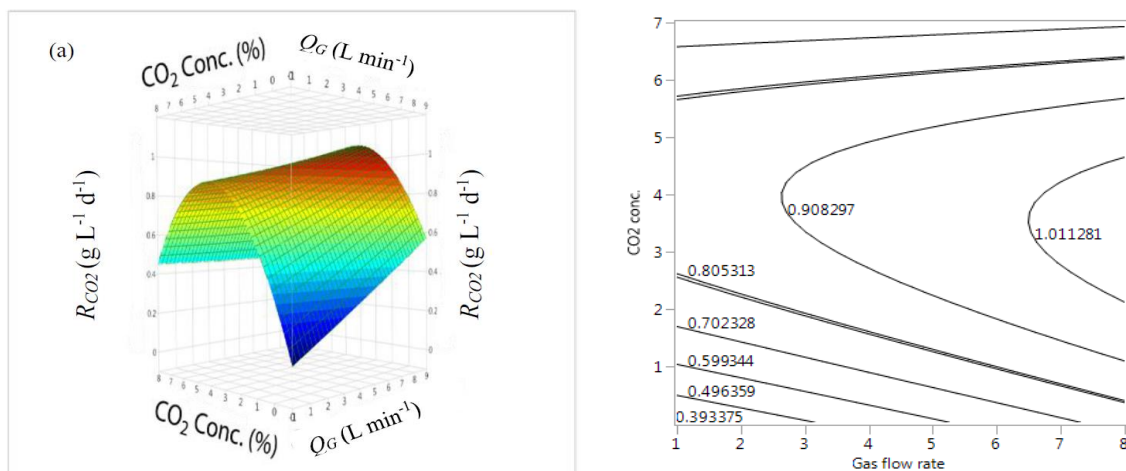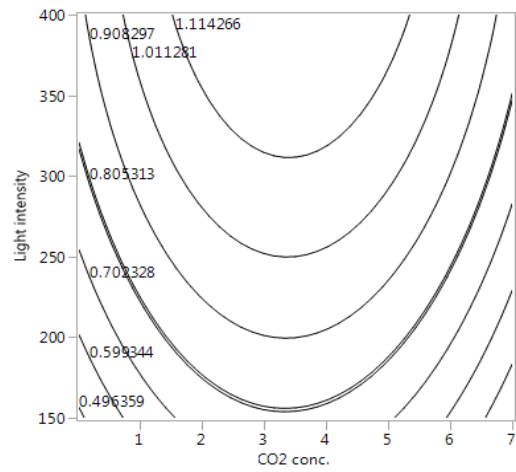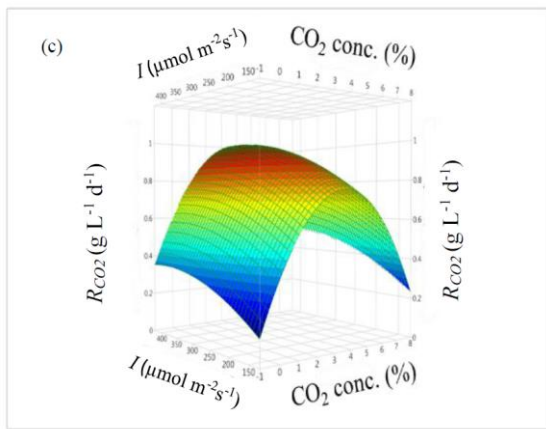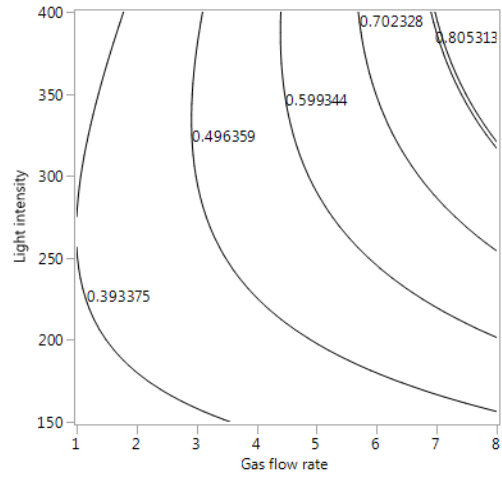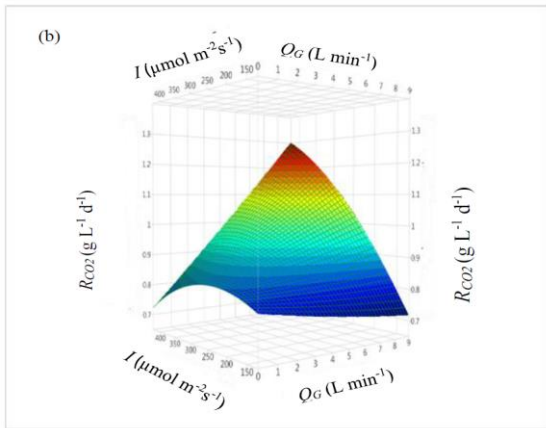
Figure 7. 2 3D response surface for CO_2 bio-fixation
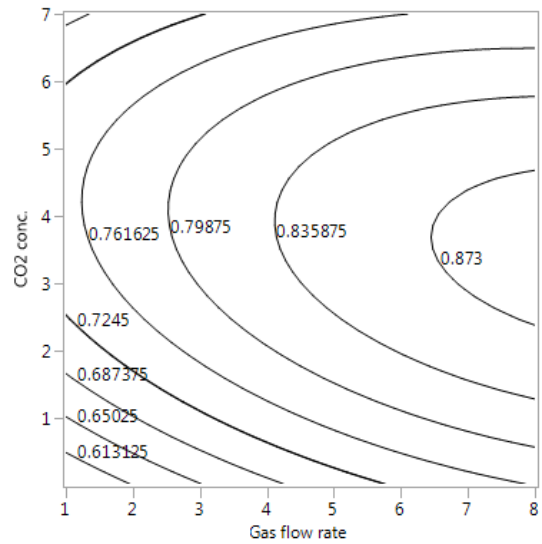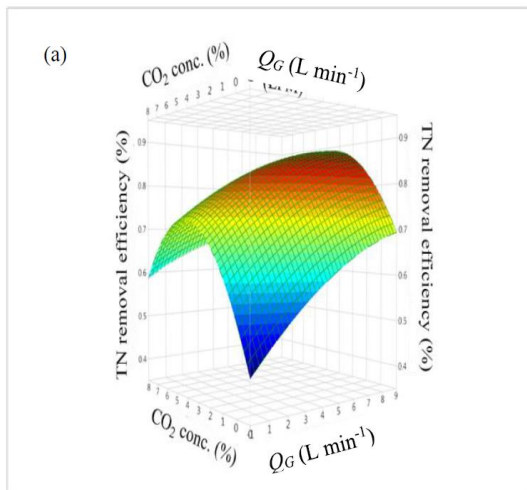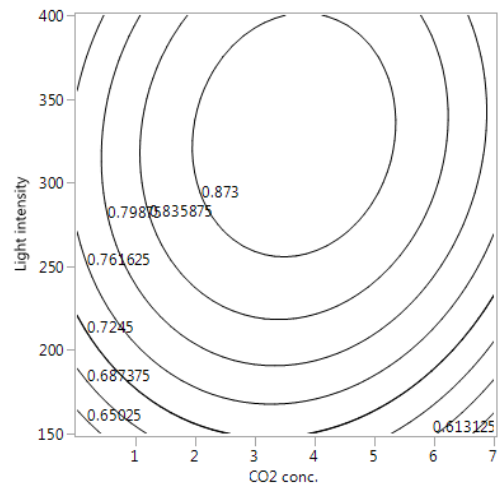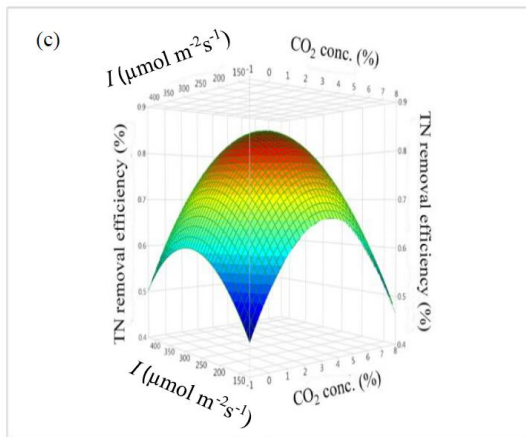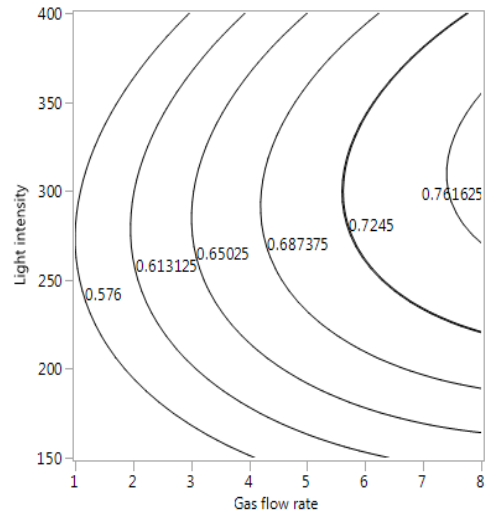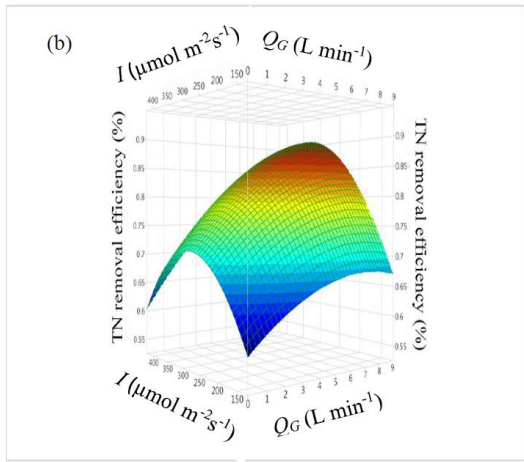
Figure 7. 3 3D response surface for total nitrogen removal efficiency
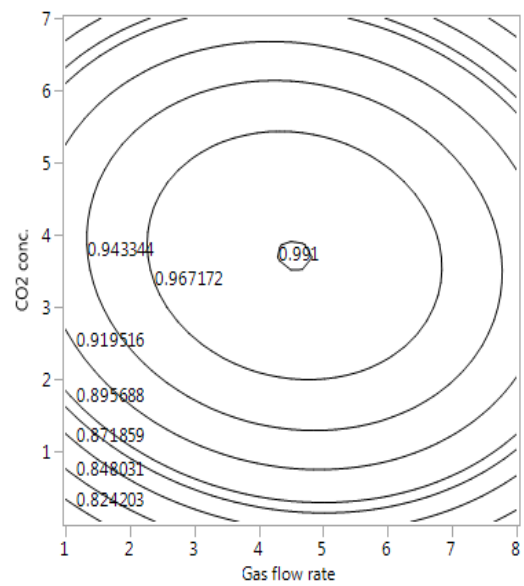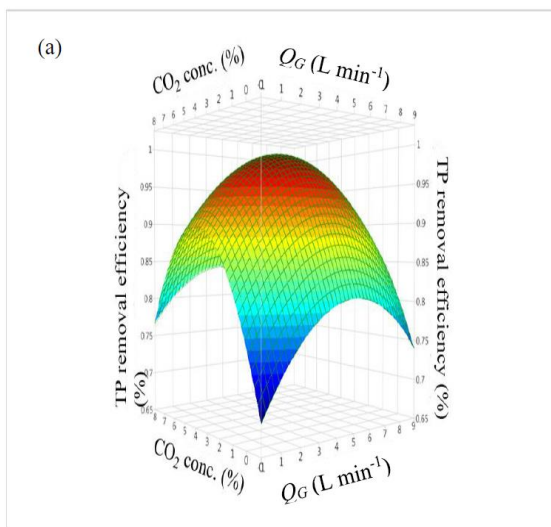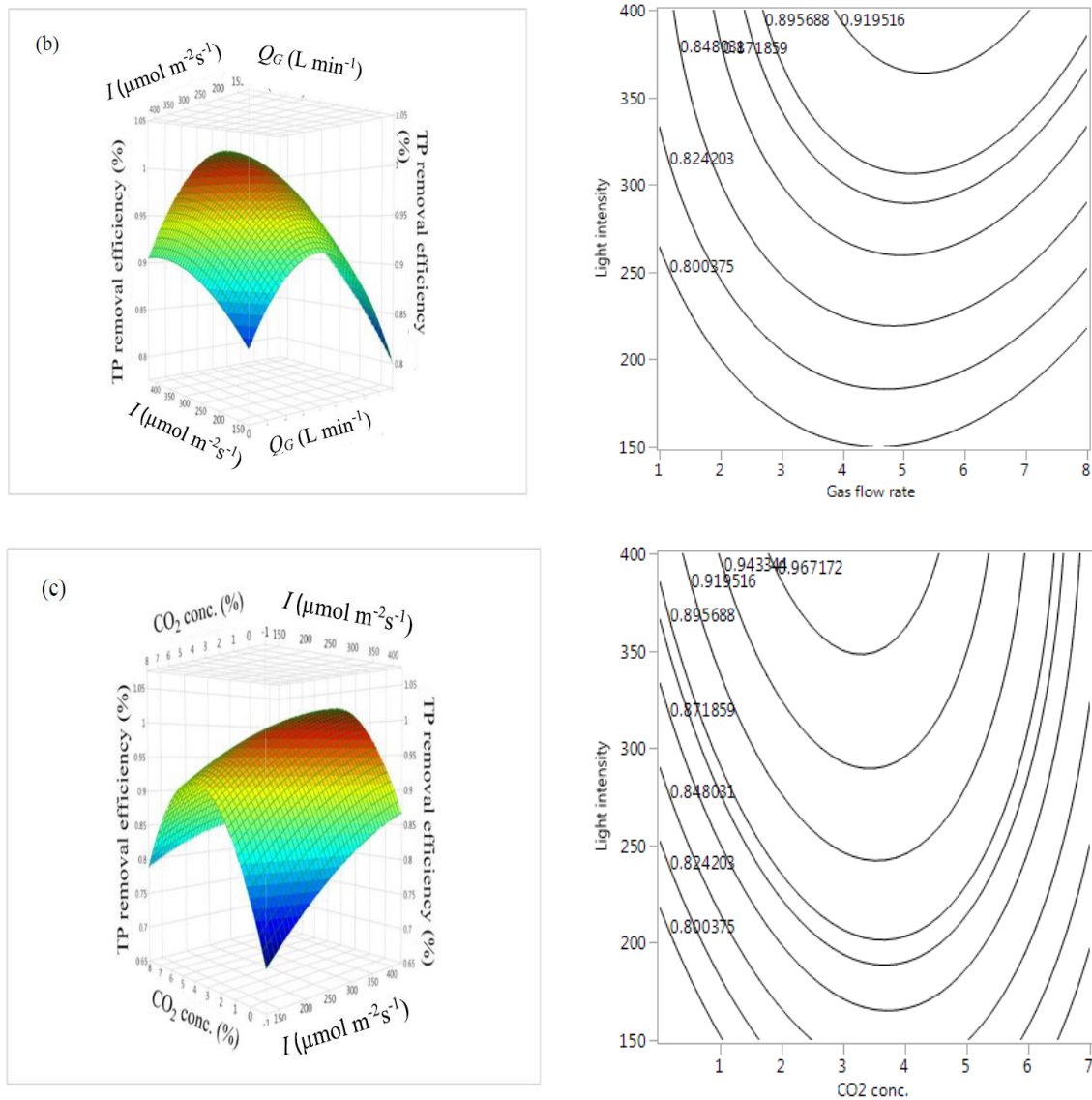
Figure 7. 4 3D response surface for total phosphorus removal efficiency

7.3.4 Model validation

Based on the Box Behnken Design results, the optimal value of gas flow rate, CO_2 concentration, and light intensity were 7.5 L min^{-1}, 3.5%, and 400 µmol m^{-2} s^{-1}, respectively with 0.904 desirability. The predicted values of R_{CO_2}, and TN and TP removal efficiencies based on the optimal value of the three independent factors were 1.186 g L^{-1} d^{-1}, 86.55%, and 99.5%, respectively. For model validation and accuracy, a typical experiment was conducted in triplicate under the optimal values of independent factors. The results were compared with the predicted values of the model as shown in Table 7.4.

Figure 7.5 shows the growth curve for *Chlorella vulgaris* and CO_2 biofixation rate. The adaption phase was observed from the beginning of the cultivation experiment until Day 4.

Table 7. 4 Comparison of experimental and predicted responses value at optimum conditions

Optimal condition		Response	Experimental	predicted	Error (%)
Gas flow rate, Q (L min^{-1})	7.5	R_{CO_2}	1.23	1.19	3.36
CO_2 conc. (%)	3.5	TN removal efficiency	83.9	86.6	3.12
I (µmol m^{-2} s^{-1})	400	TP removal efficiency	100	99.5	0.50

The *Chlorella vulgaris* started to grow exponentially up until Day 8, after which it entered the stationary phase. The maximum biomass concentration was 5.7 g L^{-1} and 1.23 g L^{-1} d^{-1} of CO_2 biofixation rate.

The findings of this study are comparable with those of Shabani [283] who investigated the ability of *Spirulina platensis and Chlorella vulgaris* for CO_2 biofixation under different CO_2 concentrations and salinity levels. They reported that value of 4.84 g L^{-1} and 0.95 g L^{-1} d^{-1} for biomass concentration and CO_2 biofixation rate, respectively. Assunção et al [284] studied the growth of three different microalgae species (*Scenedesmus obliquus*, *Chlorella vulgaris*, and *Chlorella protothecoides)* under different CO_2 concentrations (2.5-15%), light intensity of 74 µmol m^{-2} s^{-1} and gas flow rate of 1 vvm. They stated that higher biomass concentration and biofixation rate were achieved by cultivation of *Scenedesmus obliquus* under 15% CO_2 concentration. Kuo, et al. [139] investigated the growth performance of *Chlorella* sp. in aquaculture wastewater and boiler flue gas under different aeration rates from 0.05 to 0.3 vvm, CO_2 concentration of 2% and light intensity of 300 µmol m^{-2} s^{-1}. The higher biomass concentration was 2.46 g L^{-1}. The essential reasons for the different results are likely to be due to the different photobioreactor geometry, gas flow rate, and different light intensity used.
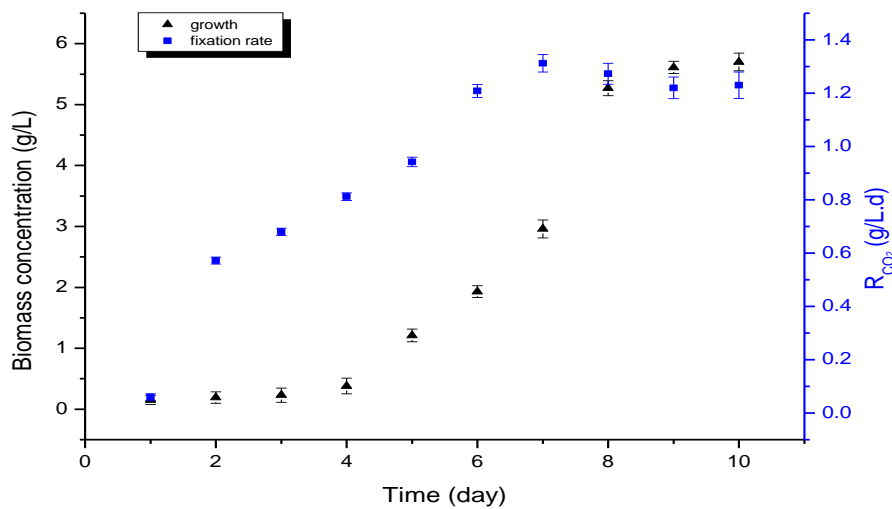
Figure 7. 5 *Chlorella vulgaris* growth and CO_2 biofixation rate at ($Q = 7.5$ L min^{-1} , % CO_2 = 3.5, and $I = 400$ µmol m^{-2} s^{-1})

7.4 Summery

Optimization and synergistic influence and of gas flow rate, CO_2 concentration, and light intensity on CO_2 biofixation rate, total nitrogen (TN) and total phosphorus (TP) removal efficiencies were studied using wastewater medium for *Chlorella vulgaris* cultivation. Gas flow rate range 1-8 L/min, CO_2 concentration range 0.03-7 %, and light intensity range 150-400 µmol/m^2.s were used. Response Surface Methodology and Box-Behnken experimental Design were utilized to specify the optimum values for gas flow rate, CO_2 concentration, and light intensity. The optimum values of gas flow rate, CO_2 concentration, and light intensity were 7.5 L/min, 3.5%, 400 µmol/m^2.s, while the desirability was 0.904. The maximum biomass concentration, CO_2 biofixation rate, TN and TP removal efficiencies at optimum conditions were 5.7 g/L, 1.23 gL^{-1}d^{-1}, 83.9% and 100%, respectively. The synergistic impact between gas flow rate and CO_2 concentration, and between gas flow rate and light intensity was significant on the three responses, while the effect between CO_2 concentration and light intensity was less significant on CO_2 biofixation rate. The results of this study could be very useful when using microalgae for CO_2 biofixation and nutrient removal from wastewater treatment.

Table 7. 5 Previous studies for biomass production, CO_2 biofixation, and nutrient removal

	Conditions			Microalgae	Biomass conc.(g/L)	R_{CO_2}	TN removal efficiency (%)	TP removal efficiency (%)	reference
Gas flow rate	CO_2 conc. (%)	I	medium						
0.03 L min^{-1}	15	4500 lux	Brostol's solution	*Chlorella PY-ZU1*	4.84	0.95	-	-	[241]
1.4 L min^{-1}	5	-	Municipal WW	*Chlorella vulgaris*	0.94	1.4	93.4	94.1	[283]
0.25 L min^{-1}	0.03-10	60 µmol m^{-2}s^{-1}	Domestic WW	*Scenedesmus* sp.	0.43	0.368	93.5	74.3	[285]
1 vvm	2.5-15	74 µmol m^{-2}s^{-1}	Bristol,s medium	*Scenedesmus obliquus*	2.51	0.47	-	-	[284]
0.3 L min^{-1}	0.04-30	450 µmol m^{-2}s^{-1}	Modified medium	*Tetraselmis*	0.72	0.111	-	-	[286]
0.05-0.3 vvm	2	300 µmol m^{-2}s^{-1}	Aquaculture WW	*Chlorella* sp.	2.46	-	90	99	[139]
0.2 L min^{-1}	3-10	163.5±9.4µmol m^{-2}s^{-1}	WW	*Chlorella vulgaris*	1.01	0.127±0.008	100	97.8±1.3	[287]
0.5 L min^{-1}	10	-	Brewery WW	*Scenedesmus obliquus*	0.95±0.07	-	88.5	40.8	[288]
7.5 L min^{-1}	3.5	400 µmol m^{-2}s^{-1}	Primary WW	*Chlorella vulgaris*	4.7 g L^{-1}	1.23	83.9	99.5	This study

R_{CO2} = CO_2 biofixation rate, TN = total nitrogen, TP = total phosphorus, WW = wastewater

Chapter Eight
Conclusions and Recommendations

8.1 Conclusions

This chapter provides the conclusions drawn from this PhD study and also the suggested recommendations for further research.

1. The two-phase system (gas-liquid) hydrodynamics in the bubble column were investigated in detail at various superficial gas velocities (0.48 - 4.8 cm s^{-1}) and when using different gas spargers. Gas holdup, interfacial area, and chord length had a linear relationship with superficial gas velocity. A new correlation for the gas holdup that considered the type of spargers in terms of Weber number (*We)* were developed. The highest gas holdup interfacial area, and chord length of 15.73%, A, and B respectively, were achieved using the perforated plate sparger. It will be crucial to understand and determine how the perforated plate sparger can enhance the performance of a bubble column photobioreactor in a three-phase system (microalgae culture) in terms of biomass productivity, CO_2 biofixation rate, specific growth rate, and lipid formation.

2. The influence of three different spargers (perforated plate, cross, and ring spargers) on the performance of the bubble column photobioreactors cultivating *Chlorella vulgaris* for 10 days was investigated. Higher mass transfer and better mixing efficiency was achieved by using the perforated plate sparger (PPS). Overall gas holdup decreased with increasing the biomass concentrations due to bubble coalescence. The perforated plate sparger was affected less than the others (ring and cross spargers). For all three spargers used, mass transfer coefficient increased linearly with the aeration rate (1-10 L min^{-1}). The highest K_La (0.0114 s^{-1}) was observed for the perforated plate sparger compared with the cross sparger (0.0062 s^{-1}) and ring sparger (0.00396 s^{-1}). The perforated plate sparger provided more small bubbles (higher surface areas and consequently higher mass transfer) than the other spargers. Sparger type had a significant effect on CO_2 biofixation, biomass productivity, and specific growth rate, while lipid content did not change significantly with sparger type. Sparger type had indirect effect on the light intensity distribution. The perforated plate sparger provided better light distribution in the region near to the photobioreactor wall even in the dense culture (Day 10). It provided a higher degree of mixing, and lower mixing time due to the higher orifices (open area) compared with the ring and cross spargers.

3. The influence of different types of gas spargers (perforated plate sparger, cross sparger, and ring sparger) on the hydrodynamics (gas holdup, liquid circulation, and mixing) and mass transfer coefficient (K_La), on cell density growth, TN, TP, and COD removal efficiencies were investigated using *Chlorella vulgaris* cultivated for 10 days in primary wastewater in another photobioreactor configuration (internal loop airlift). The results show the preference for the perforated plate sparger. After 10 days of cultivation, the TN, TP and COD removal efficiencies were 84.2%, 99.4%, 82.25%, respectively, with a cell density of 61.5×10^6 cell mL^{-1} when the perforated plate sparger was applied, while the ring sparger achieved only 48.2%, 80.1%, 75.6%, respectively, and with cell density of 35.31×10^6.

4. A modified Monod kinetic model was proposed to consider the gas holdup and the bubble diameter in order to simulate the biomass growth, light distribution inside the airlift photobioreactors, and the TN and TP profiles during the cultivation period. The model was able to simulate the experimental results satisfactorily. The sensitivity analysis confirmed the importance of the maximum specific growth rate and bubble diameter on biomass growth.

5. Optimization and synergistic influence of the gas flow rate (Q_G), CO_2 concentration (%CO_2), and light intensity (I) on CO_2 biofixation rate (R_{CO2}), total nitrogen (TN) and total phosphorus (TP) removal efficiencies were studied using a wastewater medium for *Chlorella vulgaris* cultivation. The predicted optimal conditions for Q_G, %CO_2, and I were 7.5 L min^{-1}, 3.5%, 400 µmol m^{-2} s^{-1}, respectively. Under these conditions the experimental responses of biomass concentration, CO_2 biofixation rate (R_{CO2}), total nitrogen (TN), and total phosphorus (TP) removal efficiencies were 5.7 g L^{-1}, 1.23 g $L^{-1}d^{-1}$, 83.9% and 100%, respectively. This was confirmed through experimental validation. The R_{CO2}, TN, and TP removal efficiencies appear to have been well described by quadratic models developed using BBD according to multiple linear regression analysis of the outputs, with ANOVA analysis confirming the relative importance of the different parameters.

6. The synergistic impact between gas flow rate and CO_2 concentration; and between gas flow rate and light intensity was significant for the three responses, while the effect between CO_2 concentration and light intensity was less significant on CO_2 biofixation

rate. The results of this study could be very useful when using microalgae for CO_2 biofixation and nutrient removal from wastewater treatment.

8.2 Recommendations

Based on the findings resulting from the current study, several recommendations for future research can be drawn:

1. Use a different technique for measuring bubble dynamics, such as Gamma Ray Computed Tomography (CT). The results of this study could be combined with the results obtained from CT experiments to provide a more complete picture of the gas-liquid interaction inside the bioreactor.

2. In this study, the author used only *Chlorella vulgaris*, but it would be very interesting to see the influence of other microalgae species on the hydrodynamics and gas-liquid mass transfer.

3. The influence of three different spargers on the performance of the bubble column and airlift photobioreactors was comprehensively investigated in this study. It should be further extended to consider other photobioreactor configurations (such as flat plate) and sparger types (such as tube sparger).

4. This study could be extended by using an outdoor cultivation photobioreactor, such as a horizontal type and raceway pond.

5. The proposed model presented has been successfully validated for the relatively small experimental dataset generated from this study across a range of nutrient and feed CO_2 concentrations. Its validity both for other operating conditions (in particular semi-batch and continuous) with other feedwater qualities and more extended operating conditions (such as light intensity, temperature, mixing, and the impact of accumulated O_2 gas) needs to be appraised and the sensitivities established. Of particular relevance is its robustness to scaling-up, since algal processes must necessarily be implemented on a very large scale to be viable.

6. Measurement of OD at 730 or 750 nm would be useful in order to further assess the growth of microalgae.

References

[1]   B. H. Davis, "Overview of reactors for liquid phase Fischer–Tropsch synthesis," *Catalysis Today,* vol. 71, no. 3-4, pp. 249-300, 2002.

[2]   J. Deswart and R. Krishna, "Influence of Particles Concentration on the Hydrodynamics of Bubble-Column Slurry Reactors," *Chemical engineering research & design,* vol. 73, no. 3, pp. 308-313, 1995.

[3]   B. Eisenberg, L. Ansell, R. Fiato, and R. Bauman, "Advanced gas conversion technology for remote natural gas utilization," in *PROCEEDINGS OF THE ANNUAL CONVENTION-GAS PROCESSORS ASSOCIATION*, 1994: GAS PROCESSORS ASSOCIATION, pp. 128-128.

[4]   B. Jager and R. Espinoza, "Advances in low temperature Fischer-Tropsch synthesis," *Catalysis Today,* vol. 23, no. 1, pp. 17-28, 1995.

[5]   K. Shollenberger, J. Torczynski, D. Adkins, T. O'hern, and N. Jackson, "Gamma-densitometry tomography of gas holdup spatial distribution in industrial-scale bubble columns," *Chemical Engineering Science,* vol. 52, no. 13, pp. 2037-2048, 1997.

[6]   K. Kumar, C. N. Dasgupta, B. Nayak, P. Lindblad, and D. Das, "Development of suitable photobioreactors for CO2 sequestration addressing global warming using green algae and cyanobacteria," *Bioresource technology,* vol. 102, no. 8, pp. 4945-4953, 2011.

[7]   J. Cheng, Y. Huang, J. Feng, J. Sun, J. Zhou, and K. Cen, "Improving CO2 fixation efficiency by optimizing Chlorella PY-ZU1 culture conditions in sequential bioreactors," *Bioresource technology,* vol. 144, pp. 321-327, 2013.

[8]   S.-H. Ho, C.-Y. Chen, D.-J. Lee, and J.-S. Chang, "Perspectives on microalgal CO2-emission mitigation systems—a review," *Biotechnology advances,* vol. 29, no. 2, pp. 189-198, 2011.

[9]   S. A. Razzak, M. M. Hossain, R. A. Lucky, A. S. Bassi, and H. de Lasa, "Integrated CO2 capture, wastewater treatment and biofuel production by microalgae culturing—a review," *Renewable and sustainable energy reviews,* vol. 27, pp. 622-653, 2013.

[10]   K. Larsdotter, "Wastewater treatment with microalgae-a literature review," *Vatten,* vol. 62, no. 1, p. 31, 2006.

[11]   I. S. Suh and C.-G. Lee, "Photobioreactor engineering: design and performance," *Biotechnology and Bioprocess Engineering,* vol. 8, no. 6, p. 313, 2003.

[12]   L. Xu, P. J. Weathers, X. R. Xiong, and C. Z. Liu, "Microalgal bioreactors: challenges and opportunities," *Engineering in Life Sciences,* vol. 9, no. 3, pp. 178-189, 2009.

[13]   T. M. Mata, A. A. Martins, and N. S. Caetano, "Microalgae for biodiesel production and other applications: a review," *Renewable and sustainable energy reviews,* vol. 14, no. 1, pp. 217-232, 2010.

[14]   S. A. Razzak, I. Al-Aslani, and M. M. Hossain, "Hydrodynamics and mass transfer of CO2 in water in a tubular photobioreactor," *Engineering in Life Sciences,* vol. 16, no. 4, pp. 355-363, 2016.

[15]   M. Chisti, K. Fujimoto, and M. Moo-Young, "Hydrodynamic and oxygen mass transfer studies in bubble columns and airlift bioreactors," in *Paper 117a presented at AICHE Annual Meeting, Miami Beach*, 1986.

[16]   J. C. Merchuk, M. Gluz, and I. Mukmenev, "Comparison of photobioreactors for cultivation of the red microalga Porphyridium sp," *Journal of Chemical Technology & Biotechnology: International Research in Process, Environmental & Clean Technology,* vol. 75, no. 12, pp. 1119-1126, 2000.

[17]   G. Li *et al.*, "Hydrodynamics, mass transfer and cell growth characteristics in a novel microbubble stirred bioreactor employing sintered porous metal plate impeller as gas sparger," *Chemical Engineering Science,* vol. 192, pp. 665-677, 2018.

[18]   K. A. Stone, M. V. Hilliard, Q. P. He, and J. Wang, "A mini review on bioreactor configurations and gas transfer enhancements for biochemical methane conversion," *Biochemical engineering journal,* vol. 128, pp. 83-92, 2017.

[19]   D. Wang *et al.*, "Improving mycelium-bound lipase production by aggregating Rhizopus chinensis on a draft tube in a modified stirred tank fermentor," *Process Biochemistry,* vol. 50, no. 12, pp. 2019-2028, 2015.

[20]   G. Hebrard, D. Bastoul, and M. Roustan, "Influence of the Gas Sparger on the Hydrodynamic Behavior of Bubble-Columns," *Chemical engineering research & design,* vol. 74, no. 3, pp. 406-414, 1996.

[21]   W. Bai, N. G. Deen, and J. Kuipers, "Numerical analysis of the effect of gas sparging on bubble column hydrodynamics," *Industrial & Engineering Chemistry Research,* vol. 50, no. 8, pp. 4320-4328, 2011.

[22]   R. Van der Lans, "Hydrodynamics of a bubble column loop reactor," TU Delft, Delft University of Technology, 1985.

[23]   J. S. Tan *et al.*, "A review on microalgae cultivation and harvesting, and their biomass extraction processing using ionic liquids," *Bioengineered,* vol. 11, no. 1, pp. 116-129, 2020.

[24]   K. G. Pavithra, P. S. Kumar, V. Jaikumar, K. H. Vardhan, and P. SundarRajan, "Microalgae for biofuel production and removal of heavy metals: a review," *Environmental Chemistry Letters,* pp. 1-19, 2020.

[25]   S.-Y. Chiu, C.-Y. Kao, C.-H. Chen, T.-C. Kuan, S.-C. Ong, and C.-S. Lin, "Reduction of CO2 by a high-density culture of Chlorella sp. in a semicontinuous photobioreactor," *Bioresource technology,* vol. 99, no. 9, pp. 3389-3396, 2008.

[26]   C. González, J. Marciniak, S. Villaverde, P. A. García-Encina, and R. Muñoz, "Microalgae-based processes for the biodegradation of pretreated piggery wastewaters," *Applied microbiology and biotechnology,* vol. 80, no. 5, pp. 891-898, 2008.

[27]   S. Sawayama, S. Inoue, Y. Dote, and S.-Y. Yokoyama, "CO2 fixation and oil production through microalga," *Energy Conversion and Management,* vol. 36, no. 6-9, pp. 729-731, 1995.

[28]   M. J. Barbosa, M. Albrecht, and R. H. Wijffels, "Hydrodynamic stress and lethal events in sparged microalgae cultures," *Biotechnology and bioengineering,* vol. 83, no. 1, pp. 112-120, 2003.

[29]   Y. Chisti, "Biodiesel from microalgae," *Biotechnology advances,* vol. 25, no. 3, pp. 294-306, 2007.

[30]   H. Znad, G. Naderi, H. Ang, and M. Tade, "CO2 biomitigation and biofuel production using microalgae: photobioreactors developments and future directions," *advances in Chemical Engineering,* pp. 230-244, 2012.

[31]   J. W. Lee, "Designer Photosynthetic Organisms for Photobiological Production of Ethanol from Carbon Dioxide and Water," in *Advanced Biofuels and Bioproducts*: Springer, 2013, pp. 405-445.

[32]   C.-C. A. Lai, D. E. Dietrich, and M. J. Bowman, "Global warming and the mining of oceanic methane hydrate," *Topics in catalysis,* vol. 32, no. 3-4, pp. 95-99, 2005.

[33]   B. Prézelin, "Light reactions in photosynthesis," *Physiological bases of phytoplankton ecology,* pp. 1-43, 1981.

[34]   J. Masojıdek, M. Koblızek, and G. Torzillo, "Photosynthesis in microalgae," *Handbook of microalgal culture: biotechnology and applied phycology,* p. 20, 2004.

[35]   C.-Y. Chen, K.-L. Yeh, R. Aisyah, D.-J. Lee, and J.-S. Chang, "Cultivation, photobioreactor design and harvesting of microalgae for biodiesel production: a critical review," *Bioresource technology,* vol. 102, no. 1, pp. 71-81, 2011.

[36]   J. Doucha and K. Lívanský, "Productivity, CO 2/O 2 exchange and hydraulics in outdoor open high density microalgal (Chlorella sp.) photobioreactors operated in a

Middle and Southern European climate," *Journal of Applied Phycology,* vol. 18, no. 6, pp. 811-826, 2006.

[37]   S. Boussiba *et al.*, "Outdoor cultivation of the marine microalga Isochrysis galbana in open reactors," *Aquaculture,* vol. 72, no. 3-4, pp. 247-253, 1988.

[38]   R. Hase, H. Oikawa, C. Sasao, M. Morita, and Y. Watanabe, "Photosynthetic production of microalgal biomass in a raceway system under greenhouse conditions in Sendai city," *Journal of bioscience and bioengineering,* vol. 89, no. 2, pp. 157-163, 2000.

[39]   C. Ugwu, H. Aoyagi, and H. Uchiyama, "Photobioreactors for mass cultivation of algae," *Bioresource technology,* vol. 99, no. 10, pp. 4021-4028, 2008.

[40]   R. Pate, G. Klise, and B. Wu, "Resource demand implications for US algae biofuels production scale-up," *Applied Energy,* vol. 88, no. 10, pp. 3377-3388, 2011.

[41]   B. Wang, C. Q. Lan, and M. Horsman, "Closed photobioreactors for production of microalgal biomasses," *Biotechnology advances,* vol. 30, no. 4, pp. 904-912, 2012.

[42]   J. P. Bitog *et al.*, "Application of computational fluid dynamics for modeling and designing photobioreactors for microalgae production: a review," *Computers and electronics in agriculture,* vol. 76, no. 2, pp. 131-147, 2011.

[43]   M. Barbosa, *Microalgal photobioreactors: scale-up and optimisation*. 2003.

[44]   Z. Yin *et al.*, "A comprehensive review on cultivation and harvesting of microalgae for biodiesel production: Environmental pollution control and future directions," *Bioresource Technology,* vol. 301, p. 122804, 2020.

[45]   N. T. Eriksen, "Production of phycocyanin—a pigment with applications in biology, biotechnology, foods and medicine," *Applied microbiology and biotechnology,* vol. 80, no. 1, pp. 1-14, 2008.

[46]   X. Chen, Q. Y. Goh, W. Tan, I. Hossain, W. N. Chen, and R. Lau, "Lumostatic strategy for microalgae cultivation utilizing image analysis and chlorophyll a content as design parameters," *Bioresource technology,* vol. 102, no. 10, pp. 6005-6012, 2011.

[47]   E. Ono and J. L. Cuello, "Design parameters of solar concentrating systems for CO2-mitigating algal photobioreactors," in *Greenhouse Gas Control Technologies-6th International Conference*, 2003: Elsevier, pp. 1503-1508.

[48]   C. Posten, "Design principles of photo-bioreactors for cultivation of microalgae," *Engineering in Life Sciences,* vol. 9, no. 3, pp. 165-177, 2009.

[49]   T. Maor and J. Appelbaum, "Horizontal Tubular Microalgae Photobioreactor Plant View Factors and Diffuse Radiation," *Journal of Solar Energy Engineering,* vol. 133, no. 2, p. 024503, 2011.

[50]   J. A. V. Costa, L. M. Colla, and P. F. Duarte Filho, "Improving Spirulina platensis biomass yield using a fed-batch process," *Bioresource Technology,* vol. 92, no. 3, pp. 237-241, 2004.

[51]   N. R. Moheimani, D. Parlevliet, M. P. McHenry, P. A. Bahri, and K. de Boer, "Past, present and future of microalgae cultivation developments," in *Biomass and biofuels from microalgae*: Springer, 2015, pp. 1-18.

[52]   F. Acién *et al.*, "Photobioreactors for the production of microalgae," in *Microalgae-based biofuels and bioproducts*: Elsevier, 2017, pp. 1-44.

[53]   Q. Hu, H. Guterman, and A. Richmond, "A flat inclined modular photobioreactor for outdoor mass cultivation of photoautotrophs," *Biotechnology and Bioengineering,* vol. 51, no. 1, pp. 51-60, 1996.

[54]   N. Zou and A. Richmond, "Effect of light-path length in outdoor fiat plate reactors on output rate of cell mass and of EPA in Nannochloropsis sp," in *Progress in Industrial Microbiology*, vol. 35: Elsevier, 1999, pp. 351-356.

[55]   P. L. Gupta, S.-M. Lee, and H.-J. Choi, "A mini review: photobioreactors for large scale algal cultivation," *World Journal of Microbiology and Biotechnology,* vol. 31, no. 9, pp. 1409-1417, 2015.

[56]   J. Joshi, "Computational flow modelling and design of bubble column reactors," *Chemical engineering science,* vol. 56, no. 21-22, pp. 5893-5933, 2001.

[57]   J. Merchuk, F. Garcia-Camacho, and E. Molina-Grima, "Photobioreactor design and fluid dynamics," *Chemical and biochemical engineering quarterly,* vol. 21, no. 4, pp. 345-355, 2007.

[58]   M. E. Díaz, F. J. Montes, and M. A. Galán, "Experimental study of the transition between unsteady flow regimes in a partially aerated two-dimensional bubble column," *Chemical Engineering and Processing: Process Intensification,* vol. 47, no. 9-10, pp. 1867-1876, 2008.

[59]   N. Kantarci, F. Borak, and K. O. Ulgen, "Bubble column reactors," *Process biochemistry,* vol. 40, no. 7, pp. 2263-2283, 2005.

[60]   S. Roy and J. Joshi, "CFD study of mixing characteristics of bubble column and external loop airlift reactor," *Asia-Pacific Journal of Chemical Engineering,* vol. 3, no. 2, pp. 97-105, 2008.

[61]   X. Su and T. J. Heindel, "Modeling Gas Holdup in Gas– Liquid– Fiber Semibatch Bubble Columns," *Industrial & engineering chemistry research,* vol. 44, no. 24, pp. 9355-9363, 2005.

[62]   M. J. Barbosa, M. Janssen, N. Ham, J. Tramper, and R. H. Wijffels, "Microalgae cultivation in air-lift reactors: modeling biomass yield and growth rate as a function of mixing frequency," *Biotechnology and bioengineering,* vol. 82, no. 2, pp. 170-179, 2003.

[63]   P. M. Doran, *Bioprocess engineering principles*. New York: Academic Press, 2013.

[64]   A. S. Miron, A. C. Gomez, F. G. Camacho, E. M. Grima, and Y. Chisti, "Comparative evaluation of compact photobioreactors for large-scale monoculture of microalgae," *Journal of Biotechnology,* vol. 70, no. 1-3, pp. 249-270, 1999.

[65]   S. Oncel and F. V. Sukan, "Comparison of two different pneumatically mixed column photobioreactors for the cultivation of Artrospira platensis (Spirulina platensis)," *Bioresource technology,* vol. 99, no. 11, pp. 4755-4760, 2008.

[66]   S. A. Razzak, S. A. M. Ali, M. M. Hossain, and H. deLasa, "Biological CO2 fixation with production of microalgae in wastewater–a review," *Renewable and Sustainable Energy Reviews,* vol. 76, pp. 379-390, 2017.

[67]   A. Richmond, E. Lichtenberg, B. Stahl, and A. Vonshak, "Quantitative assessment of the major limitations on productivity ofSpirulina platensis in open raceways," *Journal of Applied Phycology,* vol. 2, no. 3, pp. 195-206, 1990.

[68]   J. Fu, Y. Huang, Q. Liao, A. Xia, Q. Fu, and X. Zhu, "Photo-bioreactor design for microalgae: A review from the aspect of CO2 transfer and conversion," *Bioresource Technology,* vol. 292, p. 121947, 2019.

[69]   A. Kumar *et al.*, "Enhanced CO2 fixation and biofuel production via microalgae: recent developments and future directions," *Trends in biotechnology,* vol. 28, no. 7, pp. 371-380, 2010.

[70]   B. L. Gatamaneni, V. Orsat, and M. Lefsrud, "Factors affecting growth of various microalgal species," *Environmental Engineering Science,* vol. 35, no. 10, pp. 1037-1048, 2018.

[71]   D. Zhang, P. Dechatiwongse, and K. Hellgardt, "Modelling light transmission, cyanobacterial growth kinetics and fluid dynamics in a laboratory scale multiphase photo-bioreactor for biological hydrogen production," *Algal research,* vol. 8, pp. 99-107, 2015.

[72]   Z. Cui and L. Fan, "Turbulence energy distributions in bubbling gas–liquid and gas–liquid–solid flow systems," *Chemical Engineering Science,* vol. 59, no. 8-9, pp. 1755-1766, 2004.

[73]   E. M. Grima, F. G. Camacho, J. S. Perez, J. F. Sevilla, F. A. Fernández, and A. C. Gomez, "A mathematical model of microalgal growth in light-limited chemostat culture,"

Journal of Chemical Technology & Biotechnology: International Research in Process, Environmental AND Clean Technology, vol. 61, no. 2, pp. 167-173, 1994.

[74] J. A. Raven and R. J. Geider, "Temperature and algal growth," *New phytologist,* vol. 110, no. 4, pp. 441-461, 1988.

[75] O. Pulz, "Photobioreactors: production systems for phototrophic microorganisms," *Applied microbiology and biotechnology,* vol. 57, no. 3, pp. 287-293, 2001.

[76] A. W. Mayo, "Effects of temperature and pH on the kinetic growth of unialga Chlorella vulgaris cultures containing bacteria," *Water Environment Research,* vol. 69, no. 1, pp. 64-72, 1997.

[77] M. Ras, J.-P. Steyer, and O. Bernard, "Temperature effect on microalgae: a crucial factor for outdoor production," *Reviews in environmental science and bio/technology,* vol. 12, no. 2, pp. 153-164, 2013.

[78] L. Zhu *et al.,* "Nutrient removal and biodiesel production by integration of freshwater algae cultivation with piggery wastewater treatment," *Water research,* vol. 47, no. 13, pp. 4294-4302, 2013.

[79] B. Hu *et al.,* "Influence of exogenous CO 2 on biomass and lipid accumulation of microalgae Auxenochlorella protothecoides cultivated in concentrated municipal wastewater," *Applied biochemistry and biotechnology,* vol. 166, no. 7, pp. 1661-1673, 2012.

[80] J. W. Rachlin and A. Grosso, "The effects of pH on the growth ofChlorella vulgaris and its interactions with cadmium toxicity," *Archives of environmental contamination and toxicology,* vol. 20, no. 4, pp. 505-508, 1991.

[81] B. Chezeau and C. Vial, "Modeling and Simulation of the Biohydrogen Production Processes," in *Biohydrogen*: Elsevier, 2019, pp. 445-483.

[82] A. Juneja, R. M. Ceballos, and G. S. Murthy, "Effects of environmental factors and nutrient availability on the biochemical composition of algae for biofuels production: a review," *Energies,* vol. 6, no. 9, pp. 4607-4638, 2013.

[83] T. Cai, S. Y. Park, and Y. Li, "Nutrient recovery from wastewater streams by microalgae: status and prospects," *Renewable and Sustainable Energy Reviews,* vol. 19, pp. 360-369, 2013.

[84] B. Wang, Y. Li, N. Wu, and C. Q. Lan, "CO 2 bio-mitigation using microalgae," *Applied microbiology and biotechnology,* vol. 79, no. 5, pp. 707-718, 2008.

[85] L. Cheng, L. Zhang, H. Chen, and C. Gao, "Carbon dioxide removal from air by microalgae cultured in a membrane-photobioreactor," *Separation and purification technology,* vol. 50, no. 3, pp. 324-329, 2006.

[86] F. G. A. Fernández, C. González-López, J. F. Sevilla, and E. M. Grima, "Conversion of CO 2 into biomass by microalgae: how realistic a contribution may it be to significant CO 2 removal?," *Applied microbiology and biotechnology,* vol. 96, no. 3, pp. 577-586, 2012.

[87] P. J. McGinn, K. E. Dickinson, S. Bhatti, J.-C. Frigon, S. R. Guiot, and S. J. O'Leary, "Integration of microalgae cultivation with industrial waste remediation for biofuel and bioenergy production: opportunities and limitations," *Photosynthesis research,* vol. 109, no. 1-3, pp. 231-247, 2011.

[88] H. P. Luo and M. H. Al-Dahhan, "Analyzing and modeling of photobioreactors by combining first principles of physiology and hydrodynamics," *Biotechnology and bioengineering,* vol. 85, no. 4, pp. 382-393, 2004.

[89] A. S. Mirón, M.-C. C. García, F. G. Camacho, E. M. Grima, and Y. Chisti, "Mixing in bubble column and airlift reactors," *Chemical Engineering Research and Design,* vol. 82, no. 10, pp. 1367-1374, 2004.

[90] R. Ranjbar, R. Inoue, T. Katsuda, H. Yamaji, and S. Katoh, "High efficiency production of astaxanthin in an airlift photobioreactor," *Journal of Bioscience and Bioengineering,* vol. 106, no. 2, pp. 204-207, 2008.

[91] L. H. Fan, Y. T. Zhang, L. H. Cheng, L. Zhang, D. S. Tang, and H. L. Chen, "Optimization of carbon dioxide fixation by Chlorella vulgaris cultivated in a membrane-photobioreactor," *Chemical Engineering & Technology: Industrial Chemistry-Plant Equipment-Process Engineering-Biotechnology,* vol. 30, no. 8, pp. 1094-1099, 2007.

[92] J. Degen, A. Uebele, A. Retze, U. Schmid-Staiger, and W. Trösch, "A novel airlift photobioreactor with baffles for improved light utilization through the flashing light effect," *Journal of biotechnology,* vol. 92, no. 2, pp. 89-94, 2001.

[93] D. Frumento, A. A. Casazza, S. Al Arni, and A. Converti, "Cultivation of Chlorella vulgaris in tubular photobioreactors: a lipid source for biodiesel production," *Biochemical engineering journal,* vol. 81, pp. 120-125, 2013.

[94] M. Cuaresma, M. Janssen, C. Vílchez, and R. H. Wijffels, "Productivity of Chlorella sorokiniana in a short light-path (SLP) panel photobioreactor under high irradiance," *Biotechnology and bioengineering,* vol. 104, no. 2, pp. 352-359, 2009.

[95] W. Yee-keung and H. Kin-chung, "Optimization for cultivation of microalgae Chlorella vulgaris and lipid production in photobioreactor."

[96] G. Li, X. Yang, and G. Dai, "CFD simulation of effects of the configuration of gas distributors on gas–liquid flow and mixing in a bubble column," *Chemical Engineering Science,* vol. 64, no. 24, pp. 5104-5116, 2009.

[97] V. V. Buwa and V. V. Ranade, "Characterization of dynamics of gas–liquid flows in rectangular bubble columns," *AIChE journal,* vol. 50, no. 10, pp. 2394-2407, 2004.

[98] V. V. Ranade and Y. Tayalia, "Modelling of fluid dynamics and mixing in shallow bubble column reactors: influence of sparger design," *Chemical Engineering Science,* vol. 56, no. 4, pp. 1667-1675, 2001.

[99] A. R. Kommareddy and G. A. Anderson, "Mechanistic modeling of photobioreactor system," *ASABE Paper,* no. 057007, 2005.

[100] S. Becker, A. Sokolichin, and G. Eigenberger, "Gas—liquid flow in bubble columns and loop reactors: Part II. Comparison of detailed experiments and flow simulations," *Chemical Engineering Science,* vol. 49, no. 24, pp. 5747-5762, 1994.

[101] J. Lin, M. Han, T. Wang, T. Zhang, J. Wang, and Y. Jin, "Influence of the gas distributor on the local hydrodynamic behavior of an external loop airlift reactor," *Chemical Engineering Journal,* vol. 102, no. 1, pp. 51-59, 2004.

[102] R. D. Fraser and G. Hill, "Hydrodynamic characteristics of a spinning sparger, external loop airlift bioreactor," *The Canadian Journal of Chemical Engineering,* vol. 71, no. 3, pp. 419-425, 1993.

[103] R. Lau, W. S. B. Sim, and R. Mo, "Effect of gas distributor on hydrodynamics in shallow bubble column reactors," *The Canadian Journal of Chemical Engineering,* vol. 87, no. 6, pp. 847-854, 2009.

[104] G. Olivieri *et al.*, "Effects of photobioreactors design and operating conditions on Stichococcus bacillaris biomass and biodiesel production," *Biochemical engineering journal,* vol. 74, pp. 8-14, 2013.

[105] H. Qiang and A. Richmond, "Productivity and photosynthetic efficiency ofSpirulina platensis as affected by light intensity, algal density and rate of mixing in a flat plate photobioreactor," *Journal of Applied Phycology,* vol. 8, no. 2, pp. 139-145, 1996.

[106] M. R. Tredici and G. C. Zittelli, "Efficiency of sunlight utilization: tubular versus flat photobioreactors," *Biotechnology and bioengineering,* vol. 57, no. 2, pp. 187-197, 1998.

[107] I. Perner-Nochta and C. Posten, "Simulations of light intensity variation in photobioreactors," *Journal of Biotechnology,* vol. 131, no. 3, pp. 276-285, 2007.

[108] K. Loubiere, J. Pruvost, F. Aloui, and J. Legrand, "Investigations in an external-loop airlift photobioreactor with annular light chambers and swirling flow," *Chemical Engineering Research and Design,* vol. 89, no. 2, pp. 164-171, 2011.

[109]   A. M. Kliphuis, L. de Winter, C. Vejrazka, D. E. Martens, M. Janssen, and R. H. Wijffels, "Photosynthetic efficiency of Chlorella sorokiniana in a turbulently mixed short light-path photobioreactor," *Biotechnology progress,* vol. 26, no. 3, pp. 687-696, 2010.

[110]   L.-H. Fan, Y.-T. Zhang, L. Zhang, and H.-L. Chen, "Evaluation of a membrane-sparged helical tubular photobioreactor for carbon dioxide biofixation by Chlorella vulgaris," *Journal of Membrane Science,* vol. 325, no. 1, pp. 336-345, 2008.

[111]   J. Pruvost, G. Van Vooren, G. Cogne, and J. Legrand, "Investigation of biomass and lipids production with Neochloris oleoabundans in photobioreactor," *Bioresource technology,* vol. 100, no. 23, pp. 5988-5995, 2009.

[112]   P.-F. Wu, S.-C. J. Hwang, G.-Y. Lin, J.-T. Wu, and C. C.-Y. Hsieh, "Application of the Thin Flat-Plate Photo-Bioreactor to the Removal of Nitrate and Phosphate Using Marine Nannochloropsis oculata," *International Journal of Environmental Science and Development,* vol. 7, no. 1, p. 59, 2016.

[113]   F. Bahadori and R. Rahimi, "Simulations of gas distributors in the design of shallow bubble column reactors," *Chemical Engineering & Technology: Industrial Chemistry-Plant Equipment-Process Engineering-Biotechnology,* vol. 30, no. 4, pp. 443-447, 2007.

[114]   S. Sharaf, M. Zednikova, M. C. Ruzicka, and B. J. Azzopardi, "Global and local hydrodynamics of bubble columns–effect of gas distributor," *Chemical Engineering Journal,* vol. 288, pp. 489-504, 2016.

[115]   Y. Shen, "Carbon dioxide bio-fixation and wastewater treatment via algae photochemical synthesis for biofuels production," *RSC Advances,* vol. 4, no. 91, pp. 49672-49722, 2014.

[116]   M. Molazadeh, H. Ahmadzadeh, H. R. Pourianfar, S. Lyon, and P. H. Rampelotto, "The Use of Microalgae for Coupling Wastewater Treatment With CO2 Biofixation," *Frontiers in bioengineering and biotechnology,* vol. 7, 2019.

[117]   F. Almomani, S. Judd, R. R. Bhosale, M. Shurair, K. Aljaml, and M. Khraisheh, "Intergraded wastewater treatment and carbon bio-fixation from flue gases using Spirulina platensis and mixed algal culture," *Process Safety and Environmental Protection,* vol. 124, pp. 240-250, 2019.

[118]   M. Caporgno *et al.*, "Microalgae cultivation in urban wastewater: nutrient removal and biomass production for biodiesel and methane," *Algal Research,* vol. 10, pp. 232-239, 2015.

[119]   A. Kumari, A. Kumar, A. K. Pathak, and C. Guria, "Carbon dioxide assisted Spirulina platensis cultivation using NPK-10: 26: 26 complex fertilizer in sintered disk chromatographic glass bubble column," *Journal of CO2 Utilization,* vol. 8, pp. 49-59, 2014.

[120]   D. D.-W. Tsai, R. Ramaraj, and P. H. Chen, "Carbon dioxide bio-fixation by algae of high rate pond on natural water medium," *Ecological engineering,* vol. 92, pp. 106-110, 2016.

[121]   U. P. Veera and J. Joshi, "Measurement of gas hold-up profiles by gamma ray tomography: effect of sparger design and height of dispersion in bubble columns," *Chemical Engineering Research and Design,* vol. 77, no. 4, pp. 303-317, 1999.

[122]   S. M. Walke and V. Sathe, "Study on the Gas Holdup of Triangular Pitch and Square Pitch Sparger Geometry in Bubble Column," *International Journal of Fluid Mechanics Research,* vol. 39, no. 1, 2012.

[123]   X. Su and T. J. Heindel, "Effect of perforated plate open area on gas holdup in rayon fiber suspensions," *Journal of fluids engineering,* vol. 127, no. 4, pp. 816-823, 2005.

[124]   D. D. McClure, C. Wang, J. M. Kavanagh, D. F. Fletcher, and G. W. Barton, "Experimental investigation into the impact of sparger design on bubble columns at high superficial velocities," *Chemical Engineering Research and Design,* vol. 106, pp. 205-213, 2016.

[125] C. Vial, R. Laine, S. Poncin, N. Midoux, and G. Wild, "Influence of gas distribution and regime transitions on liquid velocity and turbulence in a 3-D bubble column," *Chemical engineering science,* vol. 56, no. 3, pp. 1085-1093, 2001.

[126] L. Han and M. H. Al-Dahhan, "Gas–liquid mass transfer in a high pressure bubble column reactor with different sparger designs," *Chemical engineering science,* vol. 62, no. 1-2, pp. 131-139, 2007.

[127] B. Ong, P. Gupta, A. Youssef, M. Al-Dahhan, and M. Dudukovic, "Computed tomographic investigation of the influence of gas sparger design on gas holdup distribution in a bubble column," *Industrial & Engineering Chemistry Research,* vol. 48, no. 1, pp. 58-68, 2009.

[128] M. Abraham, "Effect of sparger design on the hydrodynamics and mass transfer characteristics of a bubble column," *Ind. Chem. Eng.,* vol. 31, pp. 31-36, 1989.

[129] V. Michele and D. C. Hempel, "Liquid flow and phase holdup—measurement and CFD modeling for two-and three-phase bubble columns," *Chemical engineering science,* vol. 57, no. 11, pp. 1899-1908, 2002.

[130] R. P. Rastogi, A. Pandey, C. Larroche, and D. Madamwar, "Algal Green Energy–R&D and technological perspectives for biodiesel production," *Renewable and Sustainable Energy Reviews,* vol. 82, pp. 2946-2969, 2018.

[131] J. Liu and F. Chen, "Biology and industrial applications of Chlorella: advances and prospects," in *Microalgae biotechnology*: Springer, 2014, pp. 1-35.

[132] D. Bilanovic, A. Andargatchew, T. Kroeger, and G. Shelef, "Freshwater and marine microalgae sequestering of CO2 at different C and N concentrations–response surface methodology analysis," *Energy Conversion and Management,* vol. 50, no. 2, pp. 262-267, 2009.

[133] A. B. Fulke *et al.*, "Bio-mitigation of CO2, calcite formation and simultaneous biodiesel precursors production using Chlorella sp," *Bioresource technology,* vol. 101, no. 21, pp. 8473-8476, 2010.

[134] C. G. Borkenstein, J. Knoblechner, H. Frühwirth, and M. Schagerl, "Cultivation of Chlorella emersonii with flue gas derived from a cement plant," *Journal of applied phycology,* vol. 23, no. 1, pp. 131-135, 2011.

[135] B. Zhao and Y. Su, "Process effect of microalgal-carbon dioxide fixation and biomass production: a review," *Renewable and Sustainable Energy Reviews,* vol. 31, pp. 121-132, 2014.

[136] L. Wang *et al.*, "Cultivation of green algae Chlorella sp. in different wastewaters from municipal wastewater treatment plant," *Applied biochemistry and biotechnology,* vol. 162, no. 4, pp. 1174-1186, 2010.

[137] B. Wang and C. Q. Lan, "Biomass production and nitrogen and phosphorus removal by the green alga Neochloris oleoabundans in simulated wastewater and secondary municipal wastewater effluent," *Bioresource Technology,* vol. 102, no. 10, pp. 5639-5644, 2011.

[138] S. Heubeck, R. Craggs, and A. Shilton, "Influence of CO2 scrubbing from biogas on the treatment performance of a high rate algal pond," *Water Science and Technology,* vol. 55, no. 11, pp. 193-200, 2007.

[139] C.-M. Kuo *et al.*, "Simultaneous microalgal biomass production and CO2 fixation by cultivating Chlorella sp. GD with aquaculture wastewater and boiler flue gas," *Bioresource technology,* vol. 221, pp. 241-250, 2016.

[140] R. Chaudhary, A. K. Dikshit, and Y. W. Tong, "Carbon-dioxide biofixation and phycoremediation of municipal wastewater using Chlorella vulgaris and Scenedesmus obliquus," *Environmental Science and Pollution Research,* vol. 25, no. 21, pp. 20399-20406, 2018.

[141]   S. Aslan and I. K. Kapdan, "Batch kinetics of nitrogen and phosphorus removal from synthetic wastewater by algae," *Ecological engineering,* vol. 28, no. 1, pp. 64-70, 2006.

[142]   S. Chae, E. Hwang, and H.-S. Shin, "Single cell protein production of Euglena gracilis and carbon dioxide fixation in an innovative photo-bioreactor," *Bioresource technology,* vol. 97, no. 2, pp. 322-329, 2006.

[143]   H. Hsueh, W. Li, H. Chen, and H. Chu, "Carbon bio-fixation by photosynthesis of Thermosynechococcus sp. CL-1 and Nannochloropsis oculta," *Journal of Photochemistry and Photobiology B: Biology,* vol. 95, no. 1, pp. 33-39, 2009.

[144]   L. Xin, H. Hong-Ying, G. Ke, and S. Ying-Xue, "Effects of different nitrogen and phosphorus concentrations on the growth, nutrient uptake, and lipid accumulation of a freshwater microalga Scenedesmus sp," *Bioresource technology,* vol. 101, no. 14, pp. 5494-5500, 2010.

[145]   S. F. Baldia, "Growth characteristics of a blue-green alga Spirulina platensis for nitrogen utilization," 日本水産学会誌, vol. 57, no. 4, pp. 645-654, 1991.

[146]   N. Tam and Y. Wong, "Effect of ammonia concentrations on growth of Chlorella vulgaris and nitrogen removal from media," *Bioresource technology,* vol. 57, no. 1, pp. 45-50, 1996.

[147]   A. Smit, "Nitrogen uptake by Gracilaria gracilis (Rhodophyta): adaptations to a temporally variable nitrogen environment," *Botanica marina,* vol. 45, no. 2, pp. 196-209, 2002.

[148]   M. E. Martínez, F. Camacho, J. Jiménez, and J. Espinola, "Influence of light intensity on the kinetic and yield parameters of Chlorella pyrenoidosa mixotrophic growth," *Process Biochemistry,* vol. 32, no. 2, pp. 93-98, 1997.

[149]   D. Sasi, P. Mitra, A. Vigueras, and G. A. Hill, "Growth kinetics and lipid production using Chlorella vulgaris in a circulating loop photobioreactor," *Journal of Chemical Technology & Biotechnology,* vol. 86, no. 6, pp. 875-880, 2011.

[150]   K. Chojnacka and A. Zielińska, "Evaluation of growth yield of Spirulina (Arthrospira) sp. in photoautotrophic, heterotrophic and mixotrophic cultures," *World Journal of Microbiology and Biotechnology,* vol. 28, no. 2, pp. 437-445, 2012.

[151]   A. Yang, "Modeling and evaluation of CO2 supply and utilization in algal ponds," *Industrial & engineering chemistry research,* vol. 50, no. 19, pp. 11181-11192, 2011.

[152]   R. Filali, S. Tebbani, D. Dumur, A. Isambert, D. Pareau, and F. Lopes, "Growth modeling of the green microalga Chlorella vulgaris in an air-lift photobioreactor," *IFAC Proceedings Volumes,* vol. 44, no. 1, pp. 10603-10608, 2011.

[153]   E. Spijkerman, F. De Castro, and U. Gaedke, "Independent colimitation for carbon dioxide and inorganic phosphorus," *PLoS One,* vol. 6, no. 12, p. e28219, 2011.

[154]   N. C. D. Fré, A. L. d. Chagas, R. Rech, and N. R. Marcílio, "Kinetic modeling of Dunaliella tertiolecta growth under different nitrogen concentrations," *Chemical Engineering & Technology,* vol. 39, no. 9, pp. 1716-1722, 2016.

[155]   C. G. Khoo, M. K. Lam, and K. T. Lee, "Pilot-scale semi-continuous cultivation of microalgae Chlorella vulgaris in bubble column photobioreactor (BC-PBR): hydrodynamics and gas–liquid mass transfer study," *Algal research,* vol. 15, pp. 65-76, 2016.

[156]   D. Baquerisse, S. Nouals, A. Isambert, P. F. dos Santos, and G. Durand, "Modelling of a continuous pilot photobioreactor for microalgae production," *Journal of biotechnology,* vol. 70, no. 1-3, pp. 335-342, 1999.

[157]   A. Sánchez Mirón, F. Garcia Camacho, A. Contreras Gomez, E. M. Grima, and Y. Chisti, "Bubble-column and airlift photobioreactors for algal culture," *AIChE Journal,* vol. 46, no. 9, pp. 1872-1887, 2000.

[158]   J. Mendoza *et al.*, "Fluid-dynamic characterization of real-scale raceway reactors for microalgae production," *Biomass and Bioenergy,* vol. 54, pp. 267-275, 2013.

[159] M. Y. Chisti, *Airlift bioreactors*. Elsevier Applied Science London, 1989.

[160] E. G. Bligh and W. J. Dyer, "A rapid method of total lipid extraction and purification," *Canadian journal of biochemistry and physiology,* vol. 37, no. 8, pp. 911-917, 1959.

[161] O. N. Manjrekar, "Hydrodynamics and Mass Transfer in Bubble Columns," 2016.

[162] D. Chakraborty, G. S. R. Krishna, S. Chakraborty, and B. Meikap, "Hydrodynamic characteristics of a sparged gas– liquid contactor for fine bubble generation," *Industrial & Engineering Chemistry Research,* vol. 48, no. 24, pp. 11225-11229, 2009.

[163] E. Kadic and T. J. Heindel, *An introduction to bioreactor hydrodynamics and gas-liquid mass transfer*. John Wiley & Sons, 2014.

[164] G. Tirunehe and B. Norddahl, "The influence of polymeric membrane gas spargers on hydrodynamics and mass transfer in bubble column bioreactors," *Bioprocess and biosystems engineering,* vol. 39, no. 4, pp. 613-626, 2016.

[165] G. Besagni and F. Inzoli, "Comprehensive experimental investigation of counter-current bubble column hydrodynamics: Holdup, flow regime transition, bubble size distributions and local flow properties," *Chemical Engineering Science,* vol. 146, pp. 259-290, 2016.

[166] A. V. Kulkarni and J. B. Joshi, "Design and selection of sparger for bubble column reactor. Part I: Performance of different spargers," *Chemical engineering research and design,* vol. 89, no. 10, pp. 1972-1985, 2011.

[167] F. Möller *et al.*, "Performance comparison between different sparger plate orifice patterns: Hydrodynamic investigation using ultrafast X-ray tomography," *Chemical Engineering Journal,* vol. 316, pp. 857-871, 2017.

[168] D. Pjontek, V. Parisien, and A. Macchi, "Bubble characteristics measured using a monofibre optical probe in a bubble column and freeboard region under high gas holdup conditions," *Chemical Engineering Science,* vol. 111, pp. 153-169, 2014.

[169] H. Li and A. Prakash, "Influence of slurry concentrations on bubble population and their rise velocities in a three-phase slurry bubble column," *Powder Technology,* vol. 113, no. 1-2, pp. 158-167, 2000.

[170] K. Zhang, Y. Zhao, and B. Zhang, "Gas holdup characteristics in a tapered bubble column," *International Journal of Chemical Reactor Engineering,* vol. 1, no. 1, 2003.

[171] P. M. Wilkinson, A. P. Spek, and L. L. van Dierendonck, "Design parameters estimation for scale-up of high-pressure bubble columns," *AIChE Journal,* vol. 38, no. 4, pp. 544-554, 1992.

[172] M. Chisti, B. Halard, and M. Moo-Young, "Liquid circulation in airlift reactors," *Chemical Engineering Science,* vol. 43, no. 3, pp. 451-457, 1988.

[173] A. Kumar, T. Degaleesan, G. Laddha, and H. Hoelscher, "Bubble swarm characteristics in bubble columns," *The Canadian Journal of Chemical Engineering,* vol. 54, no. 5, pp. 503-508, 1976.

[174] H. Hikita and H. Kikukawa, "Liquid-phase mixing in bubble columns: Effect of liquid properties," *The Chemical Engineering Journal,* vol. 8, no. 3, pp. 191-197, 1974.

[175] I. Reilly, D. Scott, T. De Bruijn, A. Jain, and J. Piskorz, "A correlation for gas holdup in turbulent coalescing bubble columns," *The canadian journal of chemical engineering,* vol. 64, no. 5, pp. 705-717, 1986.

[176] H. Hikita, S. Asai, K. Tanigawa, K. Segawa, and M. Kitao, "Gas hold-up in bubble columns," *The Chemical Engineering Journal,* vol. 20, no. 1, pp. 59-67, 1980.

[177] G. Hughmark, "Holdup and mass transfer in bubble columns," *Industrial & Engineering Chemistry Process Design and Development,* vol. 6, no. 2, pp. 218-220, 1967.

[178] A. Mersmann, "Design and scale-up of bubble and spray columns," *Ger. Chem. Eng.,* vol. 1, pp. 1-11, 1978.

[179] H. Jin, Y. Qin, S. Yang, G. He, and Z. Guo, "Radial Profiles of Gas Bubble Behavior in a Gas-Liquid Bubble Column Reactor under Elevated Pressures," *Chemical Engineering & Technology,* vol. 36, no. 10, pp. 1721-1728, 2013.

[180] J. Xue, M. Al-Dahhan, M. Dudukovic, and R. Mudde, "Bubble velocity, size, and interfacial area measurements in a bubble column by four-point optical probe," *AIChE journal,* vol. 54, no. 2, pp. 350-363, 2008.

[181] A. Youssef, "Fluid dynamics and scale-up of bubble columns with internals," 2010.

[182] G. Kuncová and J. Zahradník, "Gas holdup and bubble frequency in a bubble column reactor containing viscous saccharose solutions," *Chemical Engineering and Processing: Process Intensification,* vol. 34, no. 1, pp. 25-34, 1995.

[183] M. O. O. Kagumba, "Heat transfer and bubble dynamics in bubble and slurry bubble columns with internals for Fischer-Tropsch synthesis of clean alternative fuels and chemicals," 2013.

[184] M. Kagumba and M. H. Al-Dahhan, "Impact of internals size and configuration on bubble dynamics in bubble columns for alternative clean fuels production," *Industrial & Engineering Chemistry Research,* vol. 54, no. 4, pp. 1359-1372, 2015.

[185] A. Ojha and M. Al-Dahhan, "Local gas holdup and bubble dynamics investigation during microalgae culturing in a split airlift photobioreactor," *Chemical Engineering Science,* vol. 175, pp. 185-198, 2018.

[186] K. H. CHOI and W. K. Lee, "Comparison of probe methods for measurement of bubble properties," *Chemical Engineering Communications,* vol. 91, no. 1, pp. 35-47, 1990.

[187] L. Sehabiague, "Modeling, scaleup and optimization of slurry bubble column reactors for Fischer-Tropsch synthesis," University of Pittsburgh, 2012.

[188] F. Hernandez-Alvarado, D. V. Kalaga, D. Turney, S. Banerjee, J. B. Joshi, and M. Kawaji, "Void fraction, bubble size and interfacial area measurements in co-current downflow bubble column reactor with microbubble dispersion," *Chemical Engineering Science,* vol. 168, pp. 403-413, 2017.

[189] C. Wu, *Heat transfer and bubble dynamics in slurry bubble columns for Fischer-Tropsch clean alternative energy*. Washington University in St. Louis, 2007.

[190] W. Luewisutthichat, A. Tsutsumi, and K. Yoshida, "Bubble characteristics in multi-phase flow systems: bubble sizes and size distributions," *Journal of chemical engineering of Japan,* vol. 30, no. 3, pp. 461-466, 1997.

[191] R. F. Mudde, "Gravity-driven bubbly flows," *Annu. Rev. Fluid Mech.,* vol. 37, pp. 393-423, 2005.

[192] O. N. Manjrekar, Y. Sun, L. He, Y. J. Tang, and M. P. Dudukovic, "Hydrodynamics and mass transfer coefficients in a bubble column photo-bioreactor," *Chemical Engineering Science,* vol. 168, pp. 55-66, 2017.

[193] X. Chai, X. Zhao, and W. Baoying, "Biofixation of carbon dioxide by Chlorococcum sp. in a photobioreactor with polytetrafluoroethene membrane sparger," *African Journal of Biotechnology,* vol. 11, no. 29, 2012.

[194] A. Sadeghizadeh, L. Moghaddasi, and R. Rahimi, "CO2 capture from air by Chlorella vulgaris microalgae in an airlift photobioreactor," *Bioresource technology,* vol. 243, pp. 441-447, 2017.

[195] Z. Chen, Z. Jiang, X. Zhang, and J. Zhang, "Numerical and experimental study on the CO2 gas–liquid mass transfer in flat-plate airlift photobioreactor with different baffles," *Biochemical engineering journal,* vol. 106, pp. 129-138, 2016.

[196] T. S. Chandra *et al.*, "Growth and biochemical characteristics of an indigenous freshwater microalga, Scenedesmus obtusus, cultivated in an airlift photobioreactor: effect of reactor hydrodynamics, light intensity, and photoperiod," *Bioprocess and biosystems engineering,* vol. 40, no. 7, pp. 1057-1068, 2017.

[197] G. Naderi, M. O. Tade, and H. Znad, "Modified photobioreactor for biofixation of carbon dioxide by Chlorella vulgaris at different light intensities," *Chemical Engineering & Technology,* vol. 38, no. 8, pp. 1371-1379, 2015.

[198] H. Znad, A. M. Al Ketife, S. Judd, F. AlMomani, and H. B. Vuthaluru, "Bioremediation and nutrient removal from wastewater by Chlorella vulgaris," *Ecological Engineering,* vol. 110, pp. 1-7, 2018.

[199] E. B. Sydney *et al.*, "Potential carbon dioxide fixation by industrially important microalgae," *Bioresource technology,* vol. 101, no. 15, pp. 5892-5896, 2010.

[200] M. E. Huntley and D. G. Redalje, "CO 2 mitigation and renewable oil from photosynthetic microbes: a new appraisal," *Mitigation and adaptation strategies for global change,* vol. 12, no. 4, pp. 573-608, 2007.

[201] E. Jacob-Lopes, L. M. C. F. Lacerda, and T. T. Franco, "Biomass production and carbon dioxide fixation by Aphanothece microscopica Nägeli in a bubble column photobioreactor," *Biochemical engineering journal,* vol. 40, no. 1, pp. 27-34, 2008.

[202] C. G. López, F. A. Fernández, J. F. Sevilla, J. S. Fernández, M. C. García, and E. M. Grima, "Utilization of the cyanobacteria Anabaena sp. ATCC 33047 in CO2 removal processes," *Bioresource technology,* vol. 100, no. 23, pp. 5904-5910, 2009.

[203] E. Ono and J. L. Cuello, "Carbon dioxide mitigation using thermophilic cyanobacteria," *Biosystems engineering,* vol. 96, no. 1, pp. 129-134, 2007.

[204] B. Zhao, Y. Zhang, K. Xiong, Z. Zhang, X. Hao, and T. Liu, "Effect of cultivation mode on microalgal growth and CO2 fixation," *Chemical engineering research and design,* vol. 89, no. 9, pp. 1758-1762, 2011.

[205] C. J. Hulatt and D. N. Thomas, "Productivity, carbon dioxide uptake and net energy return of microalgal bubble column photobioreactors," *Bioresource technology,* vol. 102, no. 10, pp. 5775-5787, 2011.

[206] J. De Swart, R. Van Vliet, and R. Krishna, "Size, structure and dynamics of "large" bubbles in a two-dimensional slurry bubble column," *Chemical Engineering Science,* vol. 51, no. 20, pp. 4619-4629, 1996.

[207] P. Mena, M. Ruzicka, F. Rocha, J. Teixeira, and J. Drahoš, "Effect of solids on homogeneous–heterogeneous flow regime transition in bubble columns," *Chemical Engineering Science,* vol. 60, no. 22, pp. 6013-6026, 2005.

[208] B. Gandhi, A. Prakash, and M. Bergougnou, "Hydrodynamic behavior of slurry bubble column at high solids concentrations," *Powder Technology,* vol. 103, no. 2, pp. 80-94, 1999.

[209] R. Reyna-Velarde, E. Cristiani-Urbina, D. J. Hernández-Melchor, F. Thalasso, and R. O. Cañizares-Villanueva, "Hydrodynamic and mass transfer characterization of a flat-panel airlift photobioreactor with high light path," *Chemical Engineering and Processing: Process Intensification,* vol. 49, no. 1, pp. 97-103, 2010.

[210] C.-Y. Tan, N. M. N. Sulaiman, S. K. Loh, and S.-M. Phang, "Chlorella biomass production in annular photobioreactor using palm oil mill effluent (POME): effect of hydrodynamics and mass transfer, irradiance, aeration rate and POME concentration," *Journal of Oil Palm Research,* vol. 28, no. 4, pp. 496-509, 2016.

[211] P. S. Kojić, I. M. Šijački, N. L. Lukić, D. Z. Jovičević, S. S. Popović, and D. L. Petrović, "Volumetric gas-liquid mass transfer coefficient in an external-loop airlift reactor with inserted membrane," *Chemical Industry and Chemical Engineering Quarterly,* vol. 22, no. 3, pp. 275-284, 2016.

[212] A. Pandit and Y. K. Doshi, "Mixing time studies in bubble column reactor with and without internals," *International Journal of Chemical Reactor Engineering,* vol. 3, no. 1, 2005.

[213] M. Ravinath, G. R. Kasat, and A. B. Pandit, "Mixing time in a short bubble column," *The Canadian Journal of Chemical Engineering,* vol. 81, no. 2, pp. 185-195, 2003.

[214]   D. J. Hernández-Melchor, R. O. Cañizares-Villanueva, J. R. Terán-Toledo, P. A. López-Pérez, and E. Cristiani-Urbina, "Hydrodynamic and mass transfer characterization of flat-panel airlift photobioreactors for the cultivation of a photosynthetic microbial consortium," *Biochemical Engineering Journal,* vol. 128, pp. 141-148, 2017.

[215]   R. Ramanan, K. Kannan, A. Deshkar, R. Yadav, and T. Chakrabarti, "Enhanced algal CO2 sequestration through calcite deposition by Chlorella sp. and Spirulina platensis in a mini-raceway pond," *Bioresource technology,* vol. 101, no. 8, pp. 2616-2622, 2010.

[216]   F.-F. Li *et al.*, "Microalgae capture of CO2 from actual flue gas discharged from a combustion chamber," *Industrial & engineering chemistry research,* vol. 50, no. 10, pp. 6496-6502, 2011.

[217]   A. Rinanti, K. Dewi, E. Kardena, and D. I. Astuti, "Biotechnology carbon capture and storage (CCS) by mix-culture green microalgae to enhancing carbon uptake rate and carbon dioxide removal efficiency with variation aeration rates in closed system photobioreactor," *Jurnal Teknologi,* vol. 69, no. 6, 2014.

[218]   U. Ramkrishnan, B. Bruno, and S. Swaminathan, "Sequestration of CO 2 by halotolerant algae," *Journal of Environmental Health Science and Engineering,* vol. 12, no. 1, p. 81, 2014.

[219]   R. Pandey, A. Sahu, and M. Premalatha, "Studies on light intensity distribution inside an open pond photo-bioreactor," *Bioprocess and biosystems engineering,* vol. 38, no. 8, pp. 1547-1557, 2015.

[220]   C. Wei, B. Xie, and H. Xiao, "Hydrodynamics in an Internal Loop Airlift Reactor with a Convergence-Divergence Draft Tube," *Chemical Engineering & Technology: Industrial Chemistry-Plant Equipment-Process Engineering-Biotechnology,* vol. 23, no. 1, pp. 38-45, 2000.

[221]   W. Yu, T. Wang, M. Liu, and Z. Wang, "Liquid backmixing and particle distribution in a novel multistage internal-loop airlift slurry reactor," *Industrial & Engineering Chemistry Research,* vol. 47, no. 11, pp. 3974-3982, 2008.

[222]   C. Cao, S. Dong, Q. Geng, and Q. Guo, "Hydrodynamics and Axial Dispersion in a Gas–Liquid–(Solid) EL-ALR with Different Sparger Designs," *Industrial & Engineering Chemistry Research,* vol. 47, no. 11, pp. 4008-4017, 2008.

[223]   I. M. Šijački *et al.*, "Sparger type influence on the hydrodynamics of the draft tube airlift reactor with diluted alcohol solutions," *Industrial & Engineering Chemistry Research,* vol. 50, no. 6, pp. 3580-3591, 2011.

[224]   J. Snape, J. Zahradnik, M. Fialova, and N. Thomas, "Liquid-phase properties and sparger design effects in an external-loop airlift reactor," *Chemical Engineering Science,* vol. 50, no. 20, pp. 3175-3186, 1995.

[225]   J. C. Merchuk, "Gas hold-up and liquid velocity in a two-dimensional air lift reactor," *Chemical engineering science,* vol. 41, no. 1, pp. 11-16, 1986.

[226]   T. Miyahara, H. Hamanaka, T. Umeda, and Y. Akagi, "Effect of plate geometry on characteristics of fluid flow and mass transfer in external-loop airlift bubble column," *Journal of chemical engineering of Japan,* vol. 32, no. 5, pp. 689-695, 1999.

[227]   B. Shankar, "Low-cost treatment for attenuation of nitrate from groundwater," *Journal of Engineering and Technology Research,* vol. 3, no. 1, pp. 16-21, 2011.

[228]   H.-J. Choi and S.-M. Lee, "Effects of microalgae on the removal of nutrients from wastewater: various concentrations of Chlorella vulgaris," *Environ Eng Res,* vol. 17, no. S1, pp. S3-S8, 2012.

[229]   C. Wang, X. Yu, H. Lv, and J. Yang, "Nitrogen and phosphorus removal from municipal wastewater by the green alga Chlorella sp," *Journal of Environmental Biology,* vol. 34, no. 2, pp. 421-425, 2013.

[230]   B. Wang, Y. Li, N. Wu, and C. Q. Lan, "CO2 bio-mitigation using microalgae," *Applied microbiology and biotechnology,* vol. 79, no. 5, pp. 707-718, 2008.

[231]   S. Van Den Hende, H. Vervaeren, and N. Boon, "Flue gas compounds and microalgae:(bio-) chemical interactions leading to biotechnological opportunities," *Biotechnology advances,* vol. 30, no. 6, pp. 1405-1424, 2012.

[232]   W. Mulbry, S. Kondrad, C. Pizarro, and E. Kebede-Westhead, "Treatment of dairy manure effluent using freshwater algae: algal productivity and recovery of manure nutrients using pilot-scale algal turf scrubbers," *Bioresource technology,* vol. 99, no. 17, pp. 8137-8142, 2008.

[233]   V. C. Eze, S. B. Velasquez-Orta, A. Hernández-García, I. Monje-Ramírez, and M. T. Orta-Ledesma, "Kinetic modelling of microalgae cultivation for wastewater treatment and carbon dioxide sequestration," *Algal research,* vol. 32, pp. 131-141, 2018.

[234]   F. A. Fernández, F. G. Camacho, J. S. Pérez, J. F. Sevilla, and E. M. Grima, "A model for light distribution and average solar irradiance inside outdoor tubular photobioreactors for the microalgal mass culture," *Biotechnology and bioengineering,* vol. 55, no. 5, pp. 701-714, 1997.

[235]   X. Guo, L. Yao, and Q. Huang, "Aeration and mass transfer optimization in a rectangular airlift loop photobioreactor for the production of microalgae," *Bioresource technology,* vol. 190, pp. 189-195, 2015.

[236]   K. J. Chavan, S. Chouhan, S. Jain, P. Singh, M. Yadav, and A. Tiwari, "Environmental factors influencing algal biodiesel production," *Environmental Engineering Science,* vol. 31, no. 11, pp. 602-611, 2014.

[237]   J. U. Grobbelaar, "Algal Nutrition–Mineral Nutrition," *Handbook of microalgal culture: biotechnology and applied phycology,* pp. 95-115, 2003.

[238]   D. Hoh, S. Watson, and E. Kan, "Algal biofilm reactors for integrated wastewater treatment and biofuel production: a review," *Chemical Engineering Journal,* vol. 287, pp. 466-473, 2016.

[239]   D. Hamby, "A review of techniques for parameter sensitivity analysis of environmental models," *Environmental monitoring and assessment,* vol. 32, no. 2, pp. 135-154, 1994.

[240]   J. Quinn, "Microalgae to biofuels evaluation through experimentally validated models," Citeseer, 2011.

[241]   R. Chaudhary, A. K. Dikshit, and Y. W. Tong, "Carbon-dioxide biofixation and phycoremediation of municipal wastewater using Chlorella vulgaris and Scenedesmus obliquus," *Environmental Science and Pollution Research,* pp. 1-8, 2017.

[242]   Z. Du *et al.*, "Cultivation of a microalga Chlorella vulgaris using recycled aqueous phase nutrients from hydrothermal carbonization process," *Bioresource technology,* vol. 126, pp. 354-357, 2012.

[243]   M.-s. Miao *et al.*, "Mixotrophic growth and biochemical analysis of Chlorella vulgaris cultivated with synthetic domestic wastewater," *International Biodeterioration & Biodegradation,* vol. 113, pp. 120-125, 2016.

[244]   R. Boonchai and G. Seo, "Microalgae membrane photobioreactor for further removal of nitrogen and phosphorus from secondary sewage effluent," *Korean Journal of Chemical Engineering,* vol. 32, no. 10, pp. 2047-2052, 2015.

[245]   H.-J. Choi, "Parametric study of brewery wastewater effluent treatment using Chlorella vulgaris microalgae," *Environmental Engineering Research,* vol. 21, no. 4, pp. 401-408, 2016.

[246]   L. Zhu *et al.*, "Scale-up potential of cultivating Chlorella zofingiensis in piggery wastewater for biodiesel production," *Bioresource technology,* vol. 137, pp. 318-325, 2013.

[247] S. Huo, Z. Wang, S. Zhu, W. Zhou, R. Dong, and Z. Yuan, "Cultivation of Chlorella zofingiensis in bench-scale outdoor ponds by regulation of pH using dairy wastewater in winter, South China," *Bioresource technology,* vol. 121, pp. 76-82, 2012.

[248] M. B. Johnson and Z. Wen, "Development of an attached microalgal growth system for biofuel production," *Applied microbiology and biotechnology,* vol. 85, no. 3, pp. 525-534, 2010.

[249] M. Blažej, M. Kiša, and J. Markoš, "Scale influence on the hydrodynamics of an internal loop airlift reactor," *Chemical Engineering and Processing: Process Intensification,* vol. 43, no. 12, pp. 1519-1527, 2004.

[250] A. Rengel, A. Zoughaib, D. Dron, and D. Clodic, "Hydrodynamic study of an internal airlift reactor for microalgae culture," *Applied microbiology and biotechnology,* vol. 93, no. 1, pp. 117-129, 2012.

[251] F. Gumery, F. Ein-Mozaffari, and Y. Dahman, "Characteristics of local flow dynamics and macro-mixing in airlift column reactors for reliable design and scale-up," *International Journal of Chemical Reactor Engineering,* vol. 7, no. 1, 2009.

[252] A. Ojha and M. Al Dahhan, "Investigation of local gas holdup and bubble dynamics using four-point optical probe technique in a split-cylinder airlift reactor," *International Journal of Multiphase Flow,* vol. 102, pp. 1-15, 2018.

[253] M. Chisti and M. Moo-Young, "Hydrodynamics and oxygen transfer in pneumatic bioreactor devices," *Biotechnology and bioengineering,* vol. 31, no. 5, pp. 487-494, 1988.

[254] E. Camarasa, C. Vial, S. Poncin, G. Wild, N. Midoux, and J. Bouillard, "Influence of coalescence behaviour of the liquid and of gas sparging on hydrodynamics and bubble characteristics in a bubble column," *Chemical Engineering and Processing: Process Intensification,* vol. 38, no. 4-6, pp. 329-344, 1999.

[255] A. Pirouzi, M. Nosrati, S. A. Shojaosadati, and S. Shakhesi, "Improvement of mixing time, mass transfer, and power consumption in an external loop airlift photobioreactor for microalgae cultures," *Biochemical engineering journal,* vol. 87, pp. 25-32, 2014.

[256] J. Merchuk, A. Contreras, F. Garcia, and E. Molina, "Studies of mixing in a concentric tube airlift bioreactor with different spargers," *Chemical Engineering Science,* vol. 53, no. 4, pp. 709-719, 1998.

[257] F. Gao, Z.-H. Yang, C. Li, G.-M. Zeng, D.-H. Ma, and L. Zhou, "A novel algal biofilm membrane photobioreactor for attached microalgae growth and nutrients removal from secondary effluent," *Bioresource technology,* vol. 179, pp. 8-12, 2015.

[258] L. Marbelia *et al.,* "Membrane photobioreactors for integrated microalgae cultivation and nutrient remediation of membrane bioreactors effluent," *Bioresource technology,* vol. 163, pp. 228-235, 2014.

[259] E. d. Sydney *et al.,* "Screening of microalgae with potential for biodiesel production and nutrient removal from treated domestic sewage," *Applied Energy,* vol. 88, no. 10, pp. 3291-3294, 2011.

[260] Y. Huang, S. Zhao, Y.-d. Ding, Q. Liao, Y. Huang, and X. Zhu, "Optimizing the gas distributor based on CO_2 bubble dynamic behaviors to improve microalgal biomass production in an air-lift photo-bioreactor," *Bioresource technology,* vol. 233, pp. 84-91, 2017.

[261] M. R. Droop, "25 years of algal growth kinetics a personal view," *Botanica marina,* vol. 26, no. 3, pp. 99-112, 1983.

[262] S. R. Ronda *et al.,* "A growth inhibitory model with SOx influenced effective growth rate for estimation of algal biomass concentration under flue gas atmosphere," *Bioresource technology,* vol. 152, pp. 283-291, 2014.

[263] W. Barclay and K. Apt, "Strategies for bioprospecting microalgae for potential commercial applications," *Handbook of microalgal culture: applied phycology and biotechnology, 2nd edn. Wiley-Blackwell, Chichester,* pp. 69-79, 2013.

[264] A. M. Al Ketife, S. Judd, and H. Znad, "Optimization of cultivation conditions for combined nutrient removal and CO2 fixation in a batch photobioreactor," *Journal of Chemical Technology & Biotechnology,* vol. 92, no. 5, pp. 1085-1093, 2017.

[265] S. Tebbani, R. Filali, F. Lopes, D. Dumur, and D. Pareau, *CO2 biofixation by Microalgae: automation process*. Wiley-ISTE, 2014.

[266] J. Cheng, Z. Yang, J. Zhou, and K. Cen, "Improving the CO 2 fixation rate by increasing flow rate of the flue gas from microalgae in a raceway pond," *Korean Journal of Chemical Engineering,* vol. 35, no. 2, pp. 498-502, 2018.

[267] C. Yoo, S.-Y. Jun, J.-Y. Lee, C.-Y. Ahn, and H.-M. Oh, "Selection of microalgae for lipid production under high levels carbon dioxide," *Bioresource technology,* vol. 101, no. 1, pp. S71-S74, 2010.

[268] L. Gouveia *et al.*, "Microalgae biomass production using wastewater: treatment and costs: scale-up considerations," *Algal Research,* vol. 16, pp. 167-176, 2016.

[269] J. P. Maity, J. Bundschuh, C.-Y. Chen, and P. Bhattacharya, "Microalgae for third generation biofuel production, mitigation of greenhouse gas emissions and wastewater treatment: Present and future perspectives–A mini review," *Energy,* vol. 78, pp. 104-113, 2014.

[270] L. E. De-Bashan, M. Moreno, J.-P. Hernandez, and Y. Bashan, "Removal of ammonium and phosphorus ions from synthetic wastewater by the microalgae Chlorella vulgaris coimmobilized in alginate beads with the microalgae growth-promoting bacterium Azospirillum brasilense," *Water research,* vol. 36, no. 12, pp. 2941-2948, 2002.

[271] G. Bayramoğlu, I. Tuzun, G. Celik, M. Yilmaz, and M. Y. Arica, "Biosorption of mercury (II), cadmium (II) and lead (II) ions from aqueous system by microalgae Chlamydomonas reinhardtii immobilized in alginate beads," *International Journal of Mineral Processing,* vol. 81, no. 1, pp. 35-43, 2006.

[272] J.-P. Hernandez, L. E. de-Bashan, and Y. Bashan, "Starvation enhances phosphorus removal from wastewater by the microalga Chlorella spp. co-immobilized with Azospirillum brasilense," *Enzyme and Microbial Technology,* vol. 38, no. 1-2, pp. 190-198, 2006.

[273] J. Park and R. Craggs, "Wastewater treatment and algal production in high rate algal ponds with carbon dioxide addition," *Water Science and Technology,* pp. 633-639, 2010.

[274] A. Beuckels, E. Smolders, and K. Muylaert, "Nitrogen availability influences phosphorus removal in microalgae-based wastewater treatment," *Water research,* vol. 77, pp. 98-106, 2015.

[275] A. Hodges, Z. Fica, J. Wanlass, J. VanDarlin, and R. Sims, "Nutrient and suspended solids removal from petrochemical wastewater via microalgal biofilm cultivation," *Chemosphere,* vol. 174, pp. 46-48, 2017.

[276] M. Anjos, B. D. Fernandes, A. A. Vicente, J. A. Teixeira, and G. Dragone, "Optimization of CO2 bio-mitigation by Chlorella vulgaris," *Bioresource technology,* vol. 139, pp. 149-154, 2013.

[277] K. Zhang, N. Kurano, and S. Miyachi, "Optimized aeration by carbon dioxide gas for microalgal production and mass transfer characterization in a vertical flat-plate photobioreactor," *Bioprocess and biosystems engineering,* vol. 25, no. 2, pp. 97-101, 2002.

[278] S. Kasiri, S. Abdulsalam, A. Ulrich, and V. Prasad, "Optimization of CO2 fixation by Chlorella kessleri using response surface methodology," *Chemical Engineering Science,* vol. 127, pp. 31-39, 2015.

[279] S. Chinnasamy, B. Ramakrishnan, A. Bhatnagar, and K. Das, "Biomass production potential of a wastewater alga Chlorella vulgaris ARC 1 under elevated levels of CO2 and temperature," *International journal of molecular sciences,* vol. 10, no. 2, pp. 518-532, 2009.

[280] F. Han, H. Pei, W. Hu, M. Song, G. Ma, and R. Pei, "Optimization and lipid production enhancement of microalgae culture by efficiently changing the conditions along with the growth-state," *Energy Conversion and Management,* vol. 90, pp. 315-322, 2015.

[281] W. Y. Cheah, P. L. Show, J.-S. Chang, T. C. Ling, and J. C. Juan, "Biosequestration of atmospheric CO2 and flue gas-containing CO2 by microalgae," *Bioresource technology,* vol. 184, pp. 190-201, 2015.

[282] S.-H. Ho, S.-W. Huang, C.-Y. Chen, T. Hasunuma, A. Kondo, and J.-S. Chang, "Characterization and optimization of carbohydrate production from an indigenous microalga Chlorella vulgaris FSP-E," *Bioresource Technology,* vol. 135, pp. 157-165, 2013.

[283] M. Shabani, "CO2 bio-sequestration by Chlorella vulgaris and Spirulina platensis in response to different levels of salinity and CO2," *Proceedings of the International Academy of Ecology and Environmental Sciences,* vol. 6, no. 2, p. 53, 2016.

[284] J. Assunção *et al.*, "CO2 utilization in the production of biomass and biocompounds by three different microalgae," *Engineering in Life Sciences,* vol. 17, no. 10, pp. 1126-1135, 2017.

[285] M. Nayak, A. Karemore, and R. Sen, "Performance evaluation of microalgae for concomitant wastewater bioremediation, CO2 biofixation and lipid biosynthesis for biodiesel application," *Algal Research,* vol. 16, pp. 216-223, 2016.

[286] M. A. Kassim and T. K. Meng, "Carbon dioxide (CO2) biofixation by microalgae and its potential for biorefinery and biofuel production," *Science of the Total Environment,* vol. 584, pp. 1121-1129, 2017.

[287] A. L. Gonçalves, C. M. Rodrigues, J. C. Pires, and M. Simões, "The effect of increasing CO2 concentrations on its capture, biomass production and wastewater bioremediation by microalgae and cyanobacteria," *Algal research,* vol. 14, pp. 127-136, 2016.

[288] A. Ferreira *et al.*, "Scenedesmus obliquus mediated brewery wastewater remediation and CO2 biofixation for green energy purposes," *Journal of cleaner production,* vol. 165, pp. 1316-1327, 2017.

Appendix A

Synergistic Impacts and Optimization of Gas Flow Rate, Concentration of CO_2, and Light Intensity on CO_2 Biofixation in Wastewater Medium by Chlorella vulgaris. International Journal of Biotechnology and Bioengineering, 13(10), 260-266.

Authors	Conception and design	Acquisition of data and method	Data conditioning and manipulation	Analysis & statistical method	Interpretation & discussion	Final Approval
Dr. Hussein Znad					X	X
I acknowledge that these represent my contribution to the above research output Singed.						
Dr. Ranjeet Utikar						X
I acknowledge that these represent my contribution to the above research output Singed. *RU*						

Optical probe calibration report

Probe ref. :	226-T3-1C				
Customer :	**Curtin University**				
Calibration parameters					
Cal. Ref	Et1-071015	Velocity range :	0.2<V<4.3 m/s	Nb of points :	142
Rise time thresholds	V = Ls. Tm^b		Comments		
	Ls	b			
10% - 80%	21	-1			

Probe details:					
Optical cable length	Stainless steel tube diameter	Tube length	Probe shape		
4.0 m	3 mm	mm	Custom		
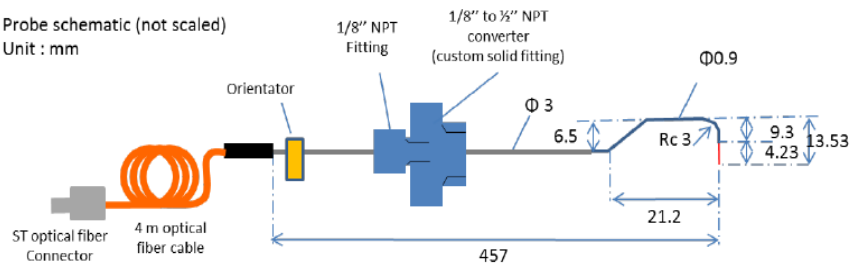
Typical signature	Tip picture

VIASENSOR

CO$_2$ ANALYSIS
G110

SPECIALIST CONTROLLED
ATMOSPHERE MONITORING

⊞ Features

- CO$_2$ 0 – 100%
- Options for:
  - O$_2$ 0 – 100%
  - Dual temperature probes
    32°F – 122°F (0°C – 50°C)
  - Humidity Sensor 0 – 100%
  - Data storage and download

⊞ Applications

- Food Processing
- Research
- Brewing
- Medical

⊞ Key Benefits

- High accuracy on CO$_2$ readings
- Quick verification of CO$_2$ levels
- Time saving with dual temperature probes
- Large data storage with software
- Easy to read large well-lit display
- Built in gas moisture removal

TECHNICAL SPECIFICATIONS:

Gas Ranges

Gases Measured	CO$_2$	By custom dual wavelength infra-red sensor with reference channel
	O$_2$ (Optional)	By internal electrochemical cell
Oxygen cell lifetime	Approximately 3 years in air	
Range	CO$_2$	0-100%
	O$_2$	0-100%
Measurement Accuracy*	Gas	
	CO$_2$	± 1% of range after calibration
	O$_2$	± 1% of range after calibration
Response time, T^{90}	CO$_2$	≤20 seconds
	O$_2$	≤60 seconds

* plus accuracy of calibration gas used

Pump

Flow	100cc/min typically

Facilities

Temperature (Optional)	X2 using optional probes, range 32°F to 122°F (0°C to +50.0°C)
Temperature accuracy, typical	±0.2°C
Barometric pressure	800-1,200 mbar
RH measurement (Optional)	RH Probe 0-100% RH non condensing
RH accuracy	±1.5% RH across the range
Visual and audible alarm	User selectable CO$_2$ and O$_2$ alarm levels
Communications	USB type B mini-connect, HID device class
Data Storage	1,000 reading sets + 270 events

Environmental Conditions

Operating temperature	32°F - 122°F (0°C – 50°C)
Relative humidity	0 - 95% non condensing
Barometric pressure	±201 H$_2$O from calibration pressure, (±500mbar)

Power Supply

| Battery type	Li Ion
Battery life	10 Hours (8 hours with pump)
Battery charger	5v DC external power supply and internal charging circuit
Charge time	3 Hours
Alternative power	USB connector DC power supply

Physical

Weight	1.1 lbs (495 grams)
Size	L 6.5 in, W 3.9 in, D 2.2 in (L 165mm, W100mm, D55mm)
Case Material	ABS / Polypropylene with Silicone Rubber Inserts
Keys	17 Resin capped Silicone rubber keys
Display	Liquid crystal display, 128 x 64 pixel With RGB LED back-light
Gas sample filters	Built-in gas dryer tube to remove moisture User replaceable PTFE water trap filter

3081 Elm Point Industrial Dr.
St. Charles, MO 63301
Phone +1-888-223-6763
Fax +1 (314) 638-3200

✍ Note:
Due to Viasensor's continuous program of improvement, this specification is subject to change without prior notice.

www.bcgroupintl.cc
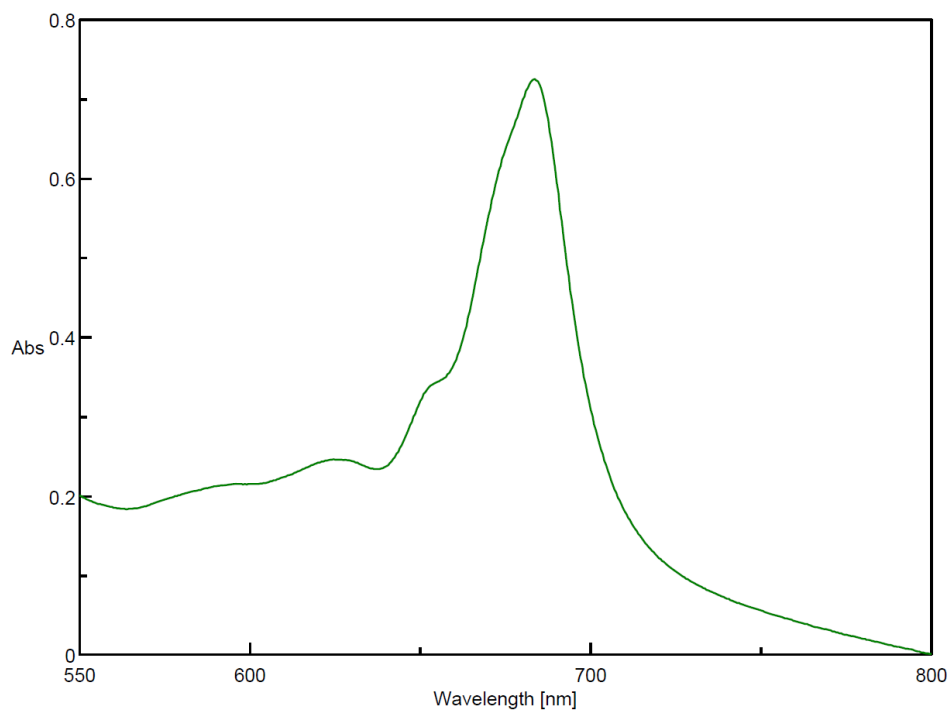
[Comment]
Sample Name   0%
Comment
User   HUS
Division
Company   Curtin University of Technology

[Measurement Information]
Instrument Name   Jasco
Model Name   V-670
Serial No.   A024361154

Photometric Mode   Abs
Measurement range   800 - 550 nm
Data pitch   0.5 nm
Band width(UV/Vis)   2.0 nm
Band width(NIR)   8.0 nm
Response   Fast
Scanning speed   400 nm/min
Source Change   340 nm
Grating Change   850 nm
Light Source   D2/WI
Filter Exchange   Step
Correction   Baseline

[Data Information]
Creation Date   28/04/2017 1:45 PM
Data array type   Linear data array
Horizontal   Wavelength [nm]
Vertical   Abs
Start   800 nm
End   550 nm
Data pitch   0.5 nm
Data points   501